2009

Novel Allosteric Inhibitors of Thrombin

Bijoy Desai
Virginia Commonwealth University

NOVEL ALLOSTERIC INHIBITORS OF THROMBIN

A thesis submitted in partial fulfillment of the requirements for the degree of Master of Science at Virginia Commonwealth University.

by

BIJOY JATIN DESAI
B.Pharm, Tamil Nadu Dr. MGR Medical University, 2006, India

Director: UMESH R. DESAI
PROFESSOR, DEPARTMENT OF MEDICINAL CHEMISTRY
Co-Director: H. TONIE WRIGHT
PROFESSOR, DEPARTMENT OF BIOCHEMISTRY & MOLECULAR BIOLOGY

Virginia Commonwealth University
Richmond, Virginia
July 2009

Acknowledgement

I would start by thanking my advisor Dr. Umesh Desai for giving me a chance to work in the lab and constantly encouraging us to do good science. I am greatly indebted to my co-advisor Dr. Tonie Wright for introducing me to the science of x-ray crystallography, and for his constant guidance and patience. I would also like to convey my gratitude to Dr. Neel Scarsdale for guiding me through crystallographic structure refinement. His suggestions and tips have been extremely helpful. I would like to thank Dr. Faik Musayev for his constant help in troubleshooting with the Raxis and for teaching some of the "tricks of the trade" in the x-ray lab. Working with Dr. Desai's research group has been a tremendous learning experience and all the lab members have contributed in making it one. I would especially like to thank Dr. Aiye Liang and Jay Thakkar who have been very helpful. Jay synthesized the FDs used in the competitive experiments. I am grateful to Dr. Philip Mosier for his tips on working with linux-based operating-systems.

Good research environment is critical for learning and innovating. The Institute of Structural Biology and Drug Discovery at VCU is a very good example of such an interdisciplinary environment. I would like to thank members of the Institute for their help, support and comradeship. I would like to acknowledge Michelle Craighead for her help. Finally, I would like to thank my family and friends for their love, unconditional support and encouragement.

Table of Contents

Page

Acknowledgements iii

List of Tables vi

List of Figures vii

Chapter

1 Introduction 1

1.1 Physiological Role of Thrombin 1

1.2 Overview of Thrombin Structure 4

1.3 Active Site Interactions 11

1.4 Interaction of Anion-binding Exosite I 15

1.5 Interactions of Anion-binding Exosite-II 18

1.6 Interactions at the Na^+ Binding Site 26

1.7 Sulfated Dehydro-polymers: Novel Allosteric Inhibitors of Thrombin Acting via Exosite-II 35

1.8 Specific Aims of the Research 41

2 Crystallographic Analysis of 4AS-Soaked Native Bovine Thrombin Crystals and Human PPACK Thrombin-4AS Co-Crystals 42

2.1 Introduction 42

2.2 Results 45

2.3 Experimental 55

2.4 Discussion 61

3 Biophysical and Biochemical Characterization of Thrombin-Sucrose Octasulfate Interaction 66

3.1 Introduction 66

3.2 Determination of Equilibrium Dissociation Constant (K_D) and Salt Dependence for Thrombin-Sucrose Octasulfate Interaction 67

3.3 Competitive Enzyme Inhibition Assays of DHPs in Presence of Sucrose Octasulfate 70

3.4 Crystal Structure Determination of Thrombin-Sucrose Octasulfate Complex 74

3.5 Discussion 81

3.6 Conclusion and Significance of Work 86

3.7 Future Directions 87

List of References 89

List of Tables

Page

Table 1:Substrate sequences interacting with the active site of thrombin……..……..15

Table 2:Fast and slow structures submitted in the PDB and their respective Cα RMSD as compared to 1PPB……...32

Table 3:IC_{50} values of inhibition of Thormbin, fXa, fIXa and fVIIa by various DHPs……40

Table 4: Result summary of optimization trials for native bovine thrombin crystals…..…46

Table 5:Preliminary diffraction data of native bovine thrombin, bovine thrombin-4AS soak and human PPACK thrombin-4AS co-crystals……...50

Table 6:Refined model statistics for native bovine thrombin, bovine thrombin-4AS soak, and human PPACK thrombin crystal form-I...……....51

Table 7:Different conditions used to optimize the crystallization of native bovine thrombin crystals. pH under all conditions was 6.2……56

Table 8:Data collection protocol…….…….59

Table 9:Molecular replacement summary……..……..…….60

Table 10:K_{Dobs} values of sucrose octasulfate-thrombin interaction at different salt concentrations…..…….69

Table 11:IC_{50} values of FDs for thrombin in presence of various concentrations of SOS……..72

Table 12:Preliminary diffraction data of bovine thrombin-SOS co-crystals……..…….75

Table 13:Preliminary diffraction data for bovine thrombin-SOS co-crystals exchanged in bis-tris…….…….80

Table 14:Comparison of $IC_{50measured}$ measured experimentally and IC_{50calc}. calculated using Dixon-Webb relationship…….84

List of Figures

Page

Figure 1:Role of thrombin in blood coagulation…….……...3

Figure 2:Activation of Prethrombin…….……..5

Figure 3:Sequence alignment of H chain: human thrombin, bovine thrombin and bovine chymotrypsin……7

Figure 4:Stereo-view of human α-thrombin shown in standard orientation……..9

Figure 5:Stereo-view of human α-thrombin shown in standard orientation……10

Figure 6:Schechter and Berger nomenclature of specificity regions in substrate and their corresponding specificity pockets in the active site cleft around the scissile peptide bond …….……..…….…..11

Figure 7:Interaction of PPACK with human α-thrombin……..……...14

Figure 8:Electrostatic potential surface of thrombin centered on anion-binding exosite-I……...17

Figure 9:Stereo-view of anion binding exosite-II represented by semi-transparent electrostatic surface……....20

Figure 10:The structures of the major and minor repeating sequences of heparin …….…….…….....21

Figure 11:Mechanism of heparin induced inhibition of thrombin by AT-III…….….22

Figure 12:Crystal structure of thrombin bound to heparin……....……...24

Figure 13:Schematic representation of the two heparin chains interacting with two thrombin monomers in the crystal structure of thrombin bound to heparin…...25

Figure 14:Structure of sucrose octasulfate……...26

Figure 15:Environment of Na^+ binding site in relation to S1 specificity pocket…….……28

Figure 16:Chemoenzymatic synthesis of DHPs……...……38

Figure 17:Direct inhibition of fXa and Thrombin by CDs……..……..39

Figure 18:Structure of 4AS……..40

Figure 19:Crystals of native bovine thrombin under previously reported conditions……..47

Figure 20:Crystals of native bovine thrombin obtained under optimized conditions……..47

Figure 21: Human PPACK thrombin-4AS co-crystals……48

Figure 22:SDS polyacrylamide gel of native bovine thrombin crystals of different age and the corresponding mother liquor solution in which they were grown……49

Figure 23:Ramachandran plot of refined native bovine thrombin structure……....52

Figure 24:Ramachandran plot of refined bovine thrombin-4AS soak structure……..53

Figure 25:Ramachandran plot of refined human ppack thrombin form-I structure……..…54

Figure 26:Asymmetric unit of bovine thrombin-4AS soak structure shown along with neighboring symmetry related molecules……..62

Figure 27:$2F_o$-F_c omit map overlaid on FPR fragment in human PPACK thrombin crystal form structure.....63

Figure 28:Overlay of protein backbone of bovine thrombin from 1MKX and solved structure……..64

Figure 29:The catalytic triad of L and H chain of 1MKX superposed on the solved native bovine thrombin structure……..……....65

Figure 30:Binding isotherm of sucrose octasulfate for thrombin at 50 mM NaCl……..68

Figure 31:Binding isotherm of sucrose octasulfate for thrombin at 150 mM NaCl…….....68

Figure 32:Binding isotherm of sucrose octasulfate for thrombin at 250 mM NaCl…...….69

Figure 33:Inhibition of thrombin by FDs in absence and presence of SOS…...……..70

Figure 34:Inhibition of thrombin activity by SOS ..……...….71

Figure 35:Ramachandran plot of the refined structure of bovine thrombin-SOS co-crystals……...…..……76

Figure 36:Interaction of two SOS molecules with two thrombin monomers in the asymmetric unit……78

Figure 37:Thrombin residues in interacting distance of the two SOS molecule……79

Figure 38:Salt dependence plot of thrombin-sucrose octasulfate interaction……...…...83

Figure 39:Graph of $IC_{50measured}$ measured experimentally at different concentrations of SOS and IC_{50calc} calculated using Dixon-webb relationship……..……84

Figure 40:Interaction of sucrose octasulfate molecule SCR2 with thrombin monomer…….86

Abstract

NOVEL ALLOSTERIC INHIBITORS OF THROMBIN

By Bijoy J. Desai, M.S.

A Thesis submitted in partial fulfillment of the requirements for the degree of Masters of Science at Virginia Commonwealth University.

Virginia Commonwealth University, 2009

Major Director: Umesh R. Desai
Professor, Department of Medicinal Chemistry
Co-Director: H. Tonie Wright
Professor, Department of Biochemistry & Molecular Biology

Thrombin is a critical enzyme involved in blood coagulation and haemostasis. For this reason the study of its interactions with substrates, inhibitors and modulator is essential. It is also a unique enzyme in the serine protease family because unlike enzymes like trypsin and chymotrypsin its activity is modulated by various endogenous and exogenous ligands. This is due to the presence of "exosites" on the thrombin surface. Exosite II, unlike exosite-I, has not been characterized for its allosteric effect. In order to understand the structural basis of interaction and inhibition of inhibitor 4AS, which possibly interacts with exosite-II, native bovine thrombin crystals and human thrombin

crystals grown in presence of 4-AS were prepared. X-ray diffraction data was collected on 4AS soaks of native bovine thrombin as well as human thrombin crystals. The data were phased by molecular replacement using appropriate search models. The structures were refined to R factors of 0.24 and 0.27 for native bovine thrombin-4AS soaks and human thrombin-4AS co-crystals respectively. Examination of a $2F_o$-F_c electron density map revealed no density for 4-AS. Low affinity of the inhibitor may be the reason for its absence in the solved structures. In the process of solving these structures, unliganded native bovine thrombin in a new crystal form, previously unreported in literature, was solved. The structure shows an overall topology similar to that found in previously published thrombin molecules. Examination of the crystal packing shows that the exosite-II is solvent exposed. This crystal form can be used in the future to study interaction of exosite-II ligands.

To characterize the interaction of sucrose octasulfate with thrombin, which may interact with thrombin exosite-II, fluorimetric equilibrium binding titrations were performed using the active site fluorescent probe para-amino benzamidine. At physiological salt concentrations, the K_D was found to be ~22 μM, which is lower than heparin fragment of corresponding length. The higher affinity was attributed to the high charge density of the ligand. Measurement of K_D at different salt concentrations showed a significant amount of contribution to the binding energy from ionic interactions. Based on the salt dependence experiments, the number of charged interactions per sucrose octasulfate molecule interacting with thrombin was found to be 3.5. Competitive

experiments of sucrose octasulfate with FDs (a sulfated dehydro-polymer being investigated in the lab for its anticoagulant properties) for inhibition of thrombin activity showed competitive effects that did not appear to follow Dixon-Webb competitive phenomenon. It was found that sucrose octasulfate itself is a weak inhibitor of thrombin. To investigate the mode of interaction, co-crystals of sucrose-ocasulfate complexed with thrombin were prepared. High resolution data (2.2 Å) was collected. The structure solved using this data showed weak density for two sucrose octasulfate molecules. Sucrose octasulfate was modeled into this density and refined. The refined structure shows that two sucrose octasulfate molecules bind to two thrombin monomers of the asymmetric unit at exosite-II. One of the sucrose octasulfate molecules interacts with both monomers, and could be present as an artifact of crystal packing. The second molecule interacts with exosite-II of only one of the thrombin monomers. The key residues involved in the interaction are Lys236, His91, Arg93 and Arg101.

The thrombin-sucrose octasulfate structure does not show any major deviation from unliganded structure. It is possible that the conformational change may have been masked due to crystal packing. Characterization of this novel interaction mode of sucrose octasulfate interaction with thrombin adds one more candidate to the list of compounds that interact with exosite-II in a manner very similar to heparin, but unlike heparin can inhibit thrombin activity.

CHAPTER 1 INTRODUCTION

1.1 Physiological Role of Thrombin

Thrombin (fIIa) is the ultimate trypsin-like serine protease produced as a result of upstream activation of blood coagulation cascade. Vascular injury triggers this cascade, which is now understood to be brought about by two convergent pathways: intrinsic pathway and extrinsic pathway.[1, 2] Both pathways converge to generate fXa, which complexes with factor Va (fVa), tissue factor (TF) and calcium on platelet cell. surface to form the prothrombinase complex.[3-7] This major complex catalyzes the formation of thrombin from its zymogen, prothrombin (fII).[8] fII is biosynthesized in liver in a Vitamin K dependent manner.[9-15]

Thrombin serves pivotal function in hemostatis, thrombosis and cell differentiation (**Figure 1**).[16-19] In a sodium-dependent manner, thrombin catalyzes the conversion of fibrinogen to fibrin monomers.[20] The fibrin monomers so formed rapidly polymerizes to form a clot, which is stabilized by covalent cross-linking of lysine and glutamine residues through a reaction catalyzed by transglutaminase action of factor XIIIa (fXIIIa).

Thrombin also activates a metal-dependent carboxypeptidase, thrombin-activable fibrinolysis inhibitor (TAFI) to TAFIa.[21-23] TAFIa removes lysine residues recognized by fibrinolytic enzymes from cross-linked fibrin clot. In addition to the above stated direct pro-coagulant actions, thrombin can also activate factors V, VII and VIII, in effect enhancing its own production.[5, 24-28] A group of receptors on platelets called proteinase-activated receptors (PARs) 1, 3 and 4 have been identified, which are proteolytically activated by thrombin. This activation has been reported to cause platelet aggregation, degranulation and surface expression of procoagulant phospholipids.[29-32] The activation of PARs is significantly enhanced by surface glycoproteins GPIbα.[33] In contrast to its pro-coagulant activities, the presence of thrombomodulin (TM), an integral membrane protein in intact vascular endothelium, converts thrombin into an anti-coagulant, which can activate protein C (PC). Activated protein C proteolytically deactivates factor VIIIa (fVIIIa) and fVa. TM is an integral membrane protein in intact vascular endothelium. The anticoagulant property of thrombin in presence of TM ensures that there is no undue formation of thrombus.[34, 35]

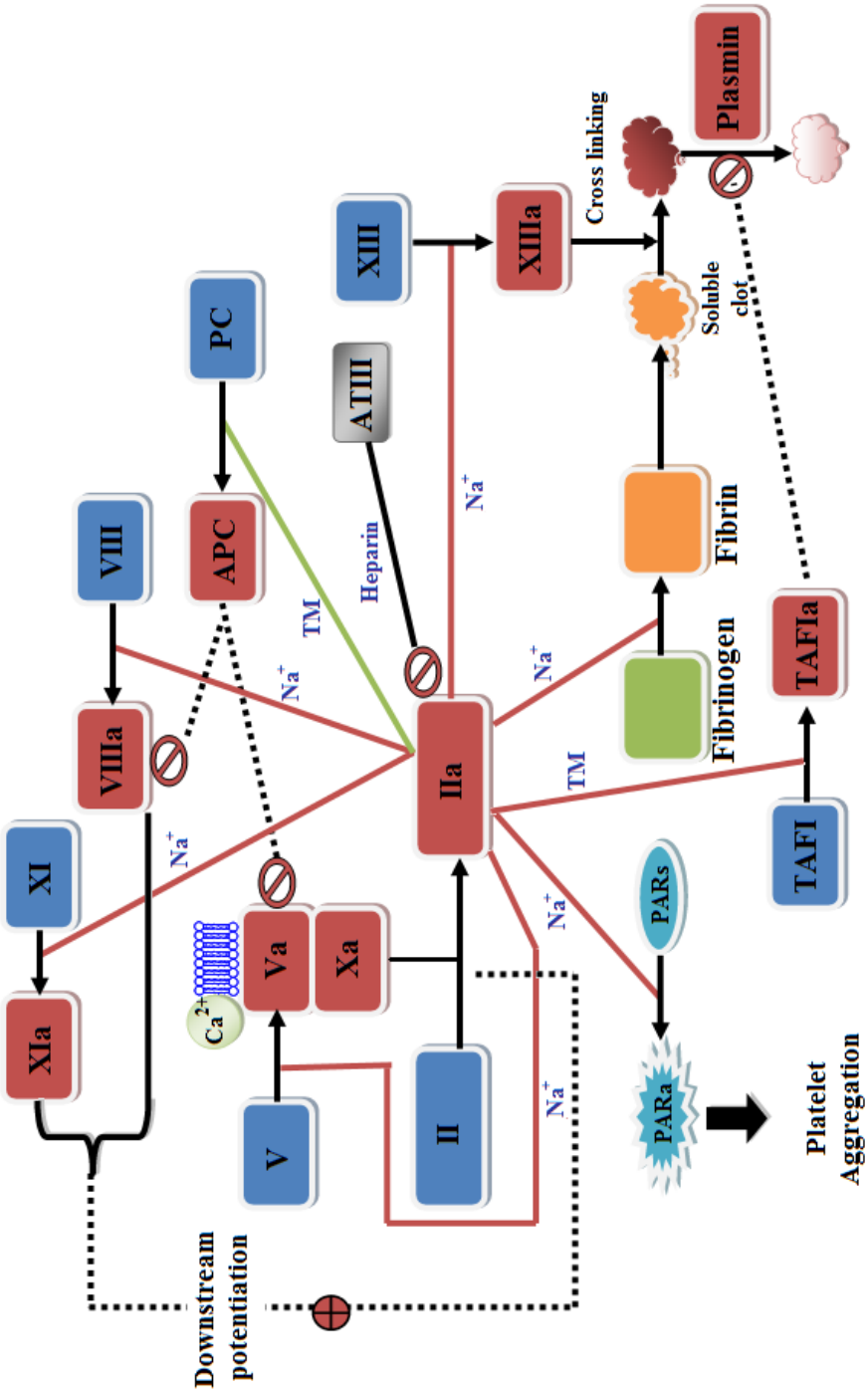

Figure 1. Role of thrombin in blood coagulation. Procoagulant and anticoagulant actions of thrombin are shown in red and green lines respectively. Cofactors (if any) for the reactions are written in blue above the lines. Bold lines and arrows show conversion.red (\) sign indicates inhibition and (+) indicates potentiation.

Thrombin activity is regulated by irreversible serine proteinase inhibitors (SERPINS) antithrombin-III (ATIII) in blood and heparin cofactor (HCII) in extra-vascular tissue. Their activity is greatly enhanced by sulfated glycosaminoglycans (GAGs) heparin sulfate and heparan sulfate.[36-38]

1.2 Overview of Thrombin Structure

Thrombin (EC 3.4.21.5, MEROPS classification peptidase S01.217 of family S1A, clan PA(S)[39]) is a serine protease belonging to the trypsin family. Like trypsin, it employs the same chemical mechanism for proteolysis. However, in contrast to trypsin, thrombin is highly selective for its substrate and its activity can be modulated by cofactors and inhibitors. This property can be attributed to the presence of a series of insertion loops which bind to cofactors and inhibitors. Thrombin and other serine proteases like trypsin, chymotrypsin, plasmin and kalikrein have evolved to perform specialized functions from the same ancestral protein through divergent evolution.[40-42]

The formation of thrombin from prothrombin occurs by the cleavage of two peptide bonds viz. R320-I321 and R272-T273 (prothrombin numbering) due to the action of prothrombinase complex.[8] Kinetic studies suggest that there is no particular preference for the order in which these bonds are broken.[43] The products of each of these cleavages are: membrane-bound, catalytically-active, meizothrombin and catalytically inactive prethrombin + prothrombin fragment 1.2 respectively. There is an additional cleavage of R284-T285 in human prothrombin which does not occur in bovine prothrombin.

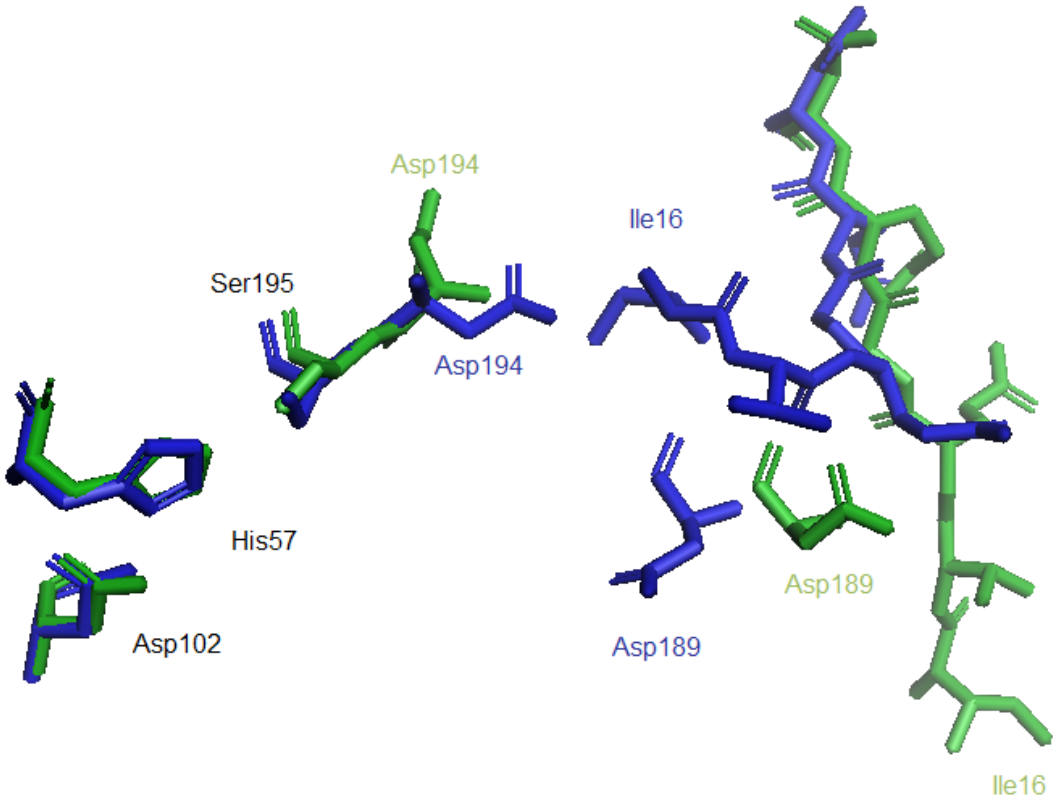

Figure 2: Activation of Prethrombin. Prethrombin (green) is superposed on thrombin(blue). Important changes associated with activation involve flipping of Ile-16 and Asp194 to form a salt bridge and movement of Asp189, a residue important for determining substrate specificity. The model was taken from PDB (PDB ID 1MKX)[44] and superposed using superpose utility of CCP4 0.6.2. The figure was generated using PyMol using PDB coordinates of 1MKX. 1MKX is a co-crystal structure of bovine thrombin and prethrombin.

The cleavage of R320-I321 is critical for thrombin activation. Crystallographic analysis of structures of prethrombin and thrombin reveal that the cleavage of the arginine-isoleucine bond leads to an outside-in flipping of the new amino terminal isoleucine residue and reorientation of D194 (thrombin numbering[45, 46]) side chain,

enabling them to form a salt bridge (**Figure 2**). This leads to a conformational change making the active site functional and more accessible to the substrate.[44, 47]

The primary structure of thrombin consists of two polypeptide chains: a short L chain and a large H chain, covalently linked together by a single disulfide linkage (**Figure 4**). H chain resembles the trypsin domain and consists of two β-barrel motifs at the junction of which are the catalytic residues Ser195, His57 and Asp102 which form the charge relay system.[45] Although the L chain is not involved in any of the major interaction with substrate or inhibitor, its presence is important for the structural stability and functioning of the enzyme. This also explains why genetic mutations to important L chain residues cause severe bleeding disorders.[48]

Figure 4 and **5.** Show the thrombin molecule in standard orientation.[45] Thrombin is a globular protein with a roughly ellipsoid shape. The active site cleft passes equatorially, bisecting the two β-barrel motifs in a perpendicular fashion. At the centre of the cleft is the catalytic triad. In contrast to trypsin, the extended nature of the cleft allows the specificity of the substrate to extend much beyond the P1 specificity position (see section 1. 1.3).

The entrance to the active site is restricted by two large insertion loops. The first is a relatively flexible loop called the "149 loop/autolysis loop/γ loop", named so for its observed ex-vivo autolysis.[49] The second is the rigid "60 loop". This loop is highly conserved in thrombin of all vertebrate species and contains a rigid –YPPW- hairpin β-turn (see **Figure 3**).

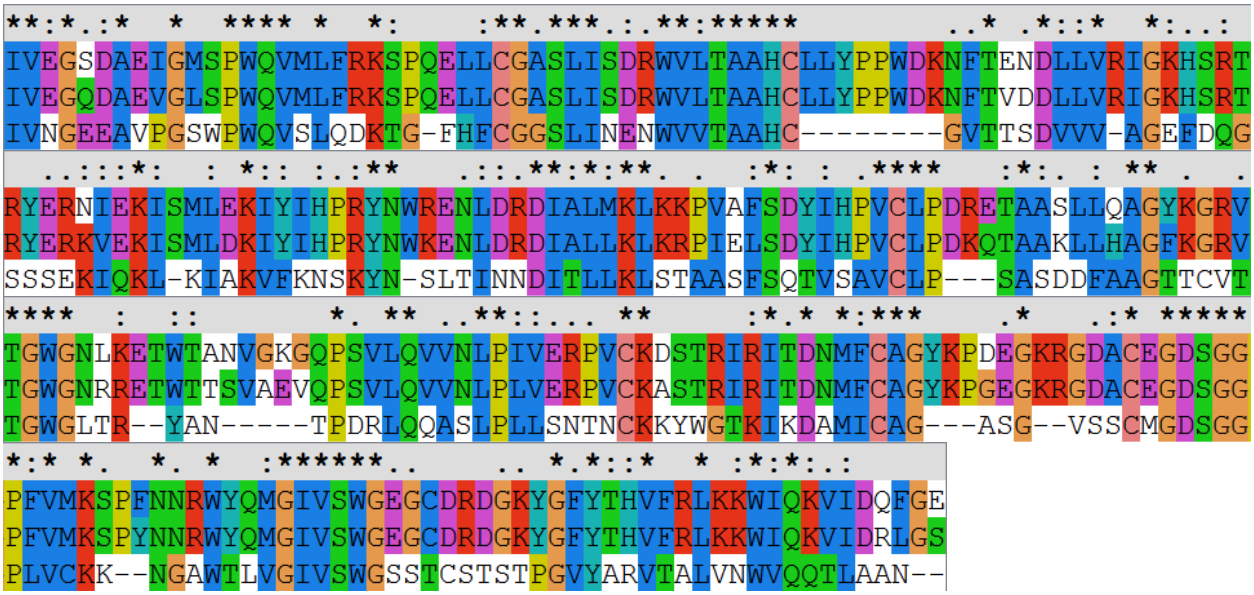

Figure 3. Primary sequence alignment of H chain(top to bottom): human thrombin, bovine thrombin and bovine chymotrypsin. The alignment was performed using CLUSTAL-X. The coloring is based on the chemical nature of residue side chains. Conserved regions are indicated by (*), conserved regions with homologous mutations are indicated by (:) and semi-conserved regions are indicated by (.).

An examination of electrostatic surface potentials of thrombin reveals the presence of a polarized surface charge distribution. Three contiguous surface patches, one of negative potential and two of positive potential, have been identified to be crucial in cofactor/inhibitor binding and substrate recognition. The first positively charged surface patch is convex in shape and extends from where the active site cleft levels off (**Figure 5**, lower right). This site makes additional interactions with fibrinogen when it binds to thrombin and hence is termed as “fibrinogen recognition exosite” or “anion-binding exosite-I”.[50] The second, more strongly positively charged surface patch extends from the

intermediate portion of the C-terminus helix of the H chain (**Figure 5**, upper left). Due to its interaction with heparin this site is termed as "heparin binding site" or "anion-binding exosite II".[51] A third site which lies near to the S1 specificity pocket consists of a small positively charged cavity with many ordered water molecules. This site is known to bind to Na^+ ion, which is an allosteric effector of thrombin. Upon binding it converts thrombin to a kinetically distinct form called "fast" form. The unbound form of thrombin is called "slow" form. This transitioning from slow to fast form and vice-versa has been shown to be important for regulation of anticoagulant and procoagulant functions of thrombin.[52-57]

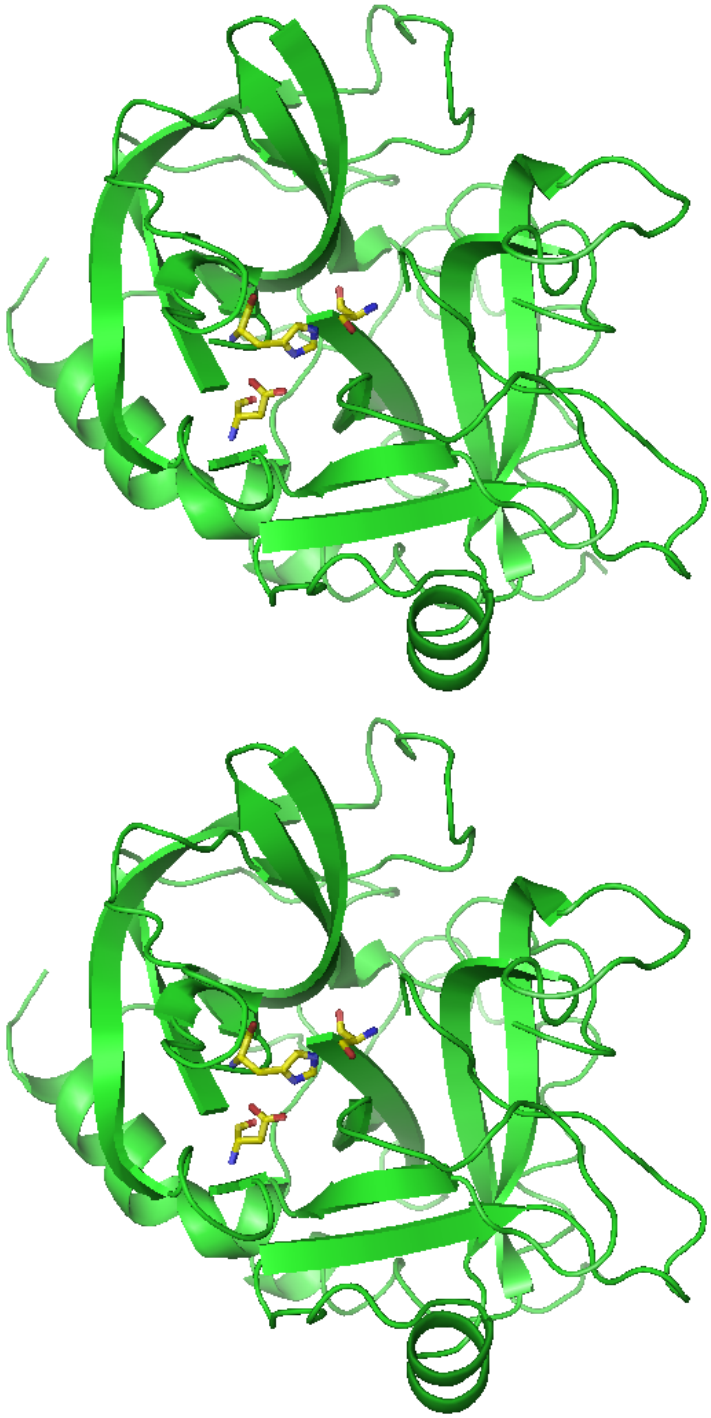

Figure 4. Stereo view of human α-thrombin shown in standard orientation (cartoon representation). Catalytic triad is shown in stick . The figure was created using PyMOL0.99.

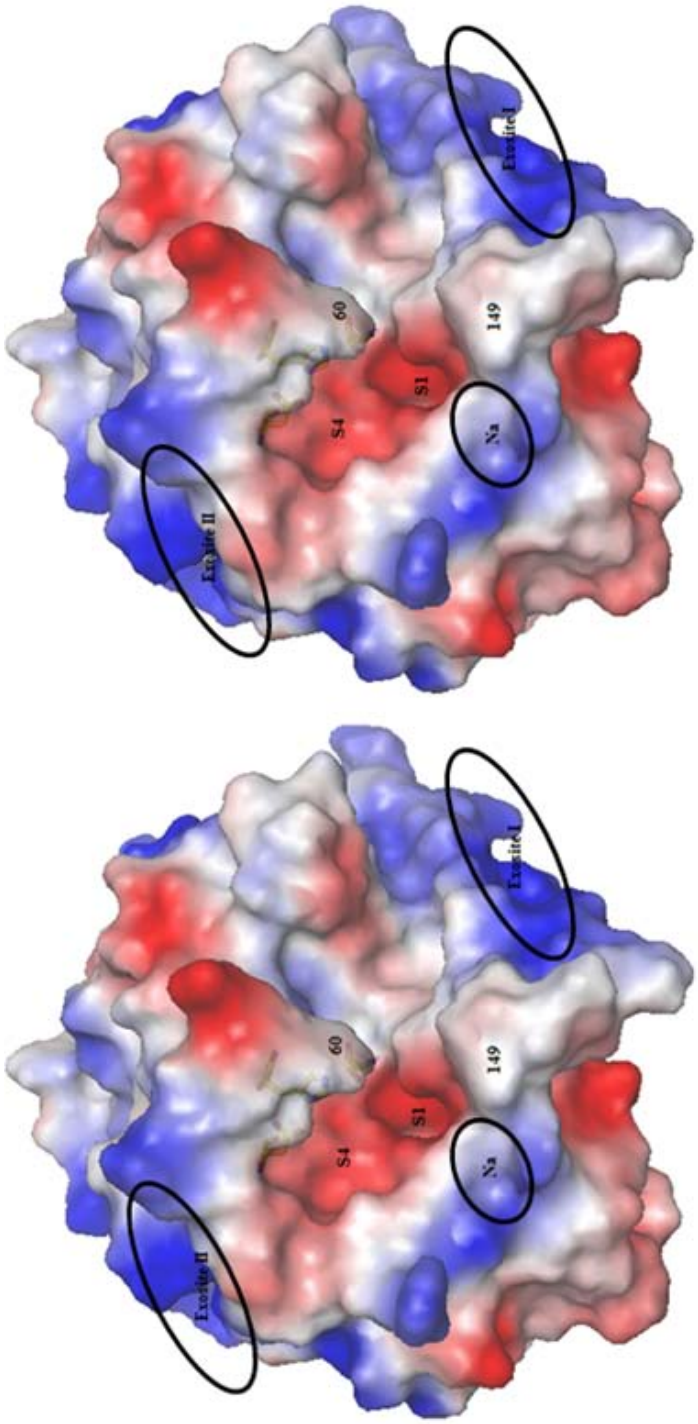

Figure 5. Stereo view of human α-thrombin shown in standard orientation (Electrostatic surface representation). Catalytic triad is shown in stick representation (Hidden behind the 60 loop). Important loops are circled.

1.3 Active Site Interactions

The center of the active site cleft contains the catalytic triad which divides the active site cleft into two parts. The interaction of regions in these two halves with the substrate determines the substrate specificity. The regions are termed "specificity pockets". The regions of the active site cleft that interact with the residues of the substrate before the scissile bond are indicated as S1, S2, S3…Sn, S1 being the region that interacts with the residue immediately preceding the scissile bond. The corresponding residues of the substrates are indicated by P1, P2, P3,….,Pn. The regions of the active site cleft that interact with the residues of the substrate after the scissile bond are indicated as S1',S2',S3',…,Sn'; S1' being the region that interacts with the residue immediately after the scissile bond. The corresponding residues of the substrate are indicated by P1',P2',P3',…,Pn' (see **Figure 6**). (Note that Pn to Pn' are by definition contiguous in primary sense in N-terminal to C-terminal direction.)

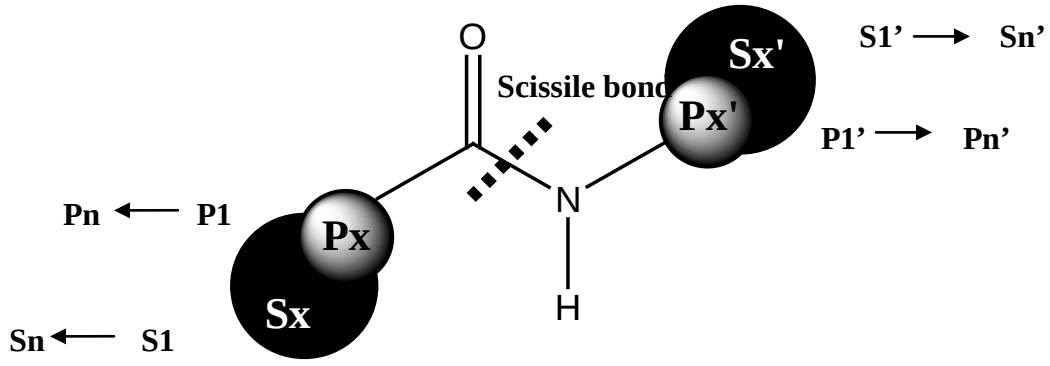

Figure 6. Schechter and Berger nomenclature of specificity regions in substrate (P) and their corresponding specificity pockets in the active site cleft (S) around the scissile peptide bond (CO-NH).

Like trypsin, the S1 pocket in thrombin (**Figure 7**) contains acidic residue Asp189 (thrombin numbering)* at its bottom. Due to this there is a strong preference for basic P1 residue like arginine for binding in this site. However, unlike trypsin, the pocket in thrombin contains the less bulky residue Ala190. This allows accommodation of more hydrophobic/uncharged P1 groups. At the entrance to S1 pocket there is an acidic residue Glu192, which is important in determining specificity of substrate and inhibitor.[45, 58-60] On the top of the S1 binding pocket extends a hydrophobic region, the base of which is formed by Trp215 indole moiety. This region is subdivided into S2 cavity and the aryl binding S4 groove.

The S1' pocket is limited in size by Lys60*f* residue of the 60 loop and can only accept P1' residues with small polar side chains. The S2' region is made up of less bulky; hydrophobic residues and hence can accept P2' residues with bulky and hydrophobic side chains. S3' region is wide, slightly acidic and prefers basic P3' residues.

1.3.1 PPACK-thrombin Interaction

PPACK (D-Phenylalanyl-L-prolyl-L-arginyl-chloromethyl ketone) is an irreversible covalent inhibitor of thrombin.[61] Its crystal structure illustrates the role of specificity pockets in binding peptidyl substrates (**Figure 8**). The three residue peptidyl moiety of PPACK fits snugly in the active site pocket; making three hydrogen bonds with the extended thrombin segment Ser214 to Glu217 in a twisted anti-parallel manner.

*Footnote: The thrombin numbering system is based on topological equivalence of residues to chymotrypsin residues.

The C-terminal P1-R carbonyl group covalently links to Ser195 Oγ and His57 Nε2 via the tetrahedral hemiketal and methylene group. The side chain of the P1-R group fits into the S1 specificity pocket, forming a charged hydrogen bond with Asp189, Gly219 and a buried water molecule. The P2-Pro of PPACK fits into S2 cavity. The benzyl side chain of D-Phe moiety extends into the wide S4 aryl-binding site. With natural substrates, this site is occupied by P4 L-amino acyl side chain. The P3 side chain for substrates usually points away from the active site cleft. By comparing various substrates sequences that interact with the active site cleft, an optimal consensus sequence of FXPRSFR corresponding to P4 P3 P2 P1 P1' P2' P3', has been deduced (**Table 1**).[62-67] This sequence has been extremely useful for designing active site directed reversible inhibitors. As seen in **Table 1** some substrates do not make optimal interactions with the active site. These substrates usually utilize additional binding sites distant from the active site cleft viz. Na^+ binding site, anion-binding exosite-I or anion binding exosite-II.

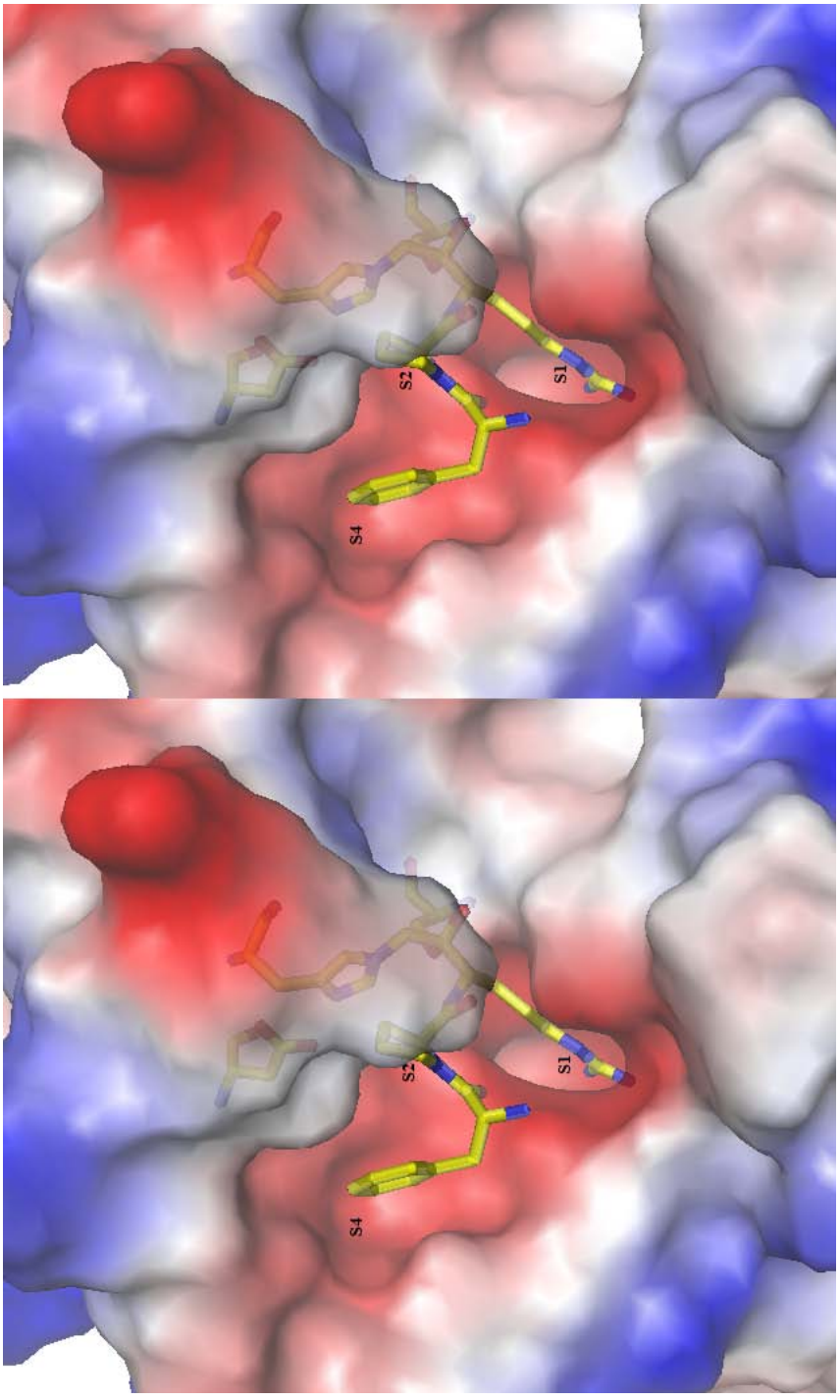

Figure 7. Interaction of PPACK with human α-thrombin. P1-Arg-CH_2, P2-Pro, P4-Phe and the catalytic triad (hidden behind the 60 loop) are shown in stick representation.

Table 1. Substrate sequences interacting with the active site of thrombin. The scissile bond is indicated by ( ). This figure was modified from Reference 17.

Substrate	P3 P4 P2 P1 P1'P2'P3'
Fibrinogen Aα	GGVRGPR
Fibrinogen Bβ	FSARGHR
Factor V	LGIRSFR
Factor V	LSPRTFH
Factor V	WYLRSNN
Factor VIII	IQIRSVA
Factor VIII	IEPRSFS
Factor XI	IKPRIVG
Factor XIII	VVPRGVN
PAR 1	LDPRSFL
Protein C	VDPRLID
TAFI	VSPRASA
AT III	IAGRSLN
HC II	FMPLSST
Consensus sequence	FXPRSFR

1.4 Interactions of Anion-binding Exosite I

Exosite I is a surface depression which starts at the end of the P' side of the active site cleft approximately 20 Å away from the catalytic triad. It is mainly formed by insertion loops 70 to 80 (equivalent to the calcium binding loop of trypsin but the Ca^{2+} ion replaced by Lys70 amine group[68]) with some bordering residues from 37 loop and Lys-109, Lys-110 side chains. The base of this depression is formed by the exposed hydrophobic side chains of Tyr-76 and Ile-82 which is surrounded by cationic side chains of lysines : 149E, 36, 109, 110, 81 and 70, and arginines 77A, 75, 67, and 73 (see **Figure 8**).[45, 68, 69] Exosite I is known to interact with fibrinogen, PARs, fV, fVIII, fXI, HCII, hirudin, TM and staphylocoagulase. [32, 70, 71]

1.4.1 Thrombin-Hirudin Interaction: A Prototypic Exosite I interaction

Hirudin is a 65 amino acid protein which was discovered in salivary secretions of European leech *Hirudo medicinalis.*[72, 73] It is one of the most potent and selective thrombin inhibitor with a K_D in femto-molar range. Since it was one of the first thrombin inhibitor investigated for binding to both exosite-I and the active site, it became a model for interaction of thrombin with thrombomodulin, PARs and fibrinogen.

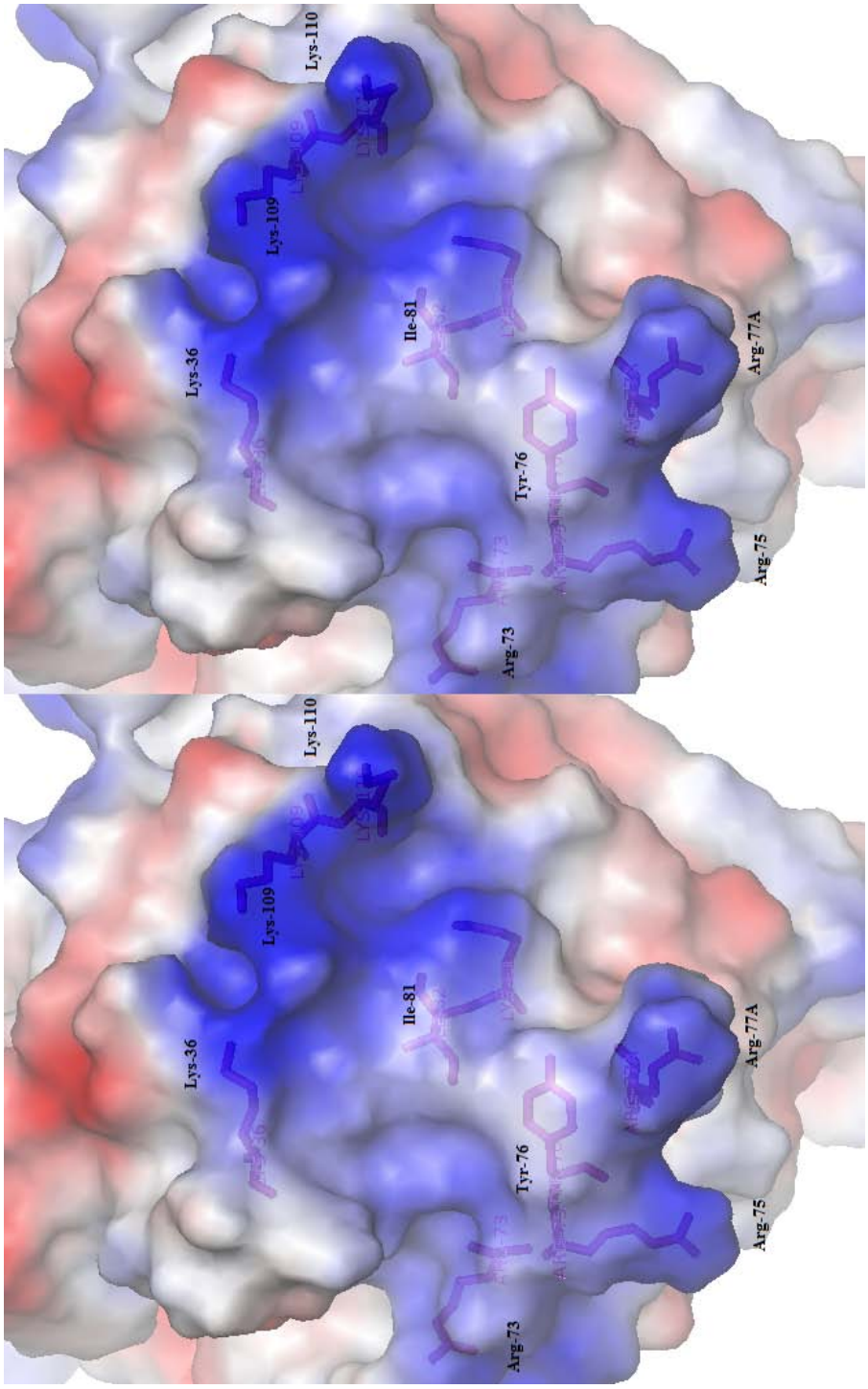

Figure 8. Electrostatic potential surface of thrombin centered on anion-binding exosite-I. mportant residues comprising the exosite are labeled and shown in stick representation.

The crystal structure of thrombin-hirudin complex shows that the C-terminal domain of the inhibitor interacts extensively with exosite I by both hydrophobic and electrostatic interactions, accounting for high specificity of the inhibitor.[74, 75] The N-terminal domain binds to the active site, making several non-polar contacts in the active site cleft.[76, 77] Mutagenesis studies by Stone et. al. show that substitution of acidic residues on the C-terminal domain reduces the association rate of complex formation and decrease the affinity. A similar lowering of affinity is observed when hydrophobic residues are substituted.[78]

Comparison of the NMR structure of free hirudin with the thrombin bound form shows that in free form the N-terminal end of hirudin is disordered, and upon binding to thrombin adopts a 3_{10}-helical form.[74, 79, 80] This gives rise to a large change in heat capacity. An unusually large change in heat capacity and an entropy deficit associated with the formation of an ordered structure when hirudin binds to thrombin suggests an induced-fit mechanism of binding. This mechanism has been supported by kinetic studies.[81, 82] A binding model based on initial recognition by electrostatic steering by complementary charged interactions followed by change in inhibitor structure to make optimum hydrophobic interaction has been proposed.

1.5 Interactions of Anion-binding Exosite-II

The mapping of heparin binding exosite-II was done using a combination of site-directed mutagenesis and functional studies of heparin induced AT-III inhibition of thrombin. Exosite-II covers an area of approximately 200 $Å^2$. (upper left corner of

Figure5) It is located near the C-terminus of the H-chain of thrombin, centered on the groove formed by Leu234 and surrounded by basic side-chains of Arg93, Arg101, Arg165, Arg233, Arg126, Lys236, Lys235, Lys240 and His91. (see **Figure 9**) The charges of most of these basic residues are not compensated by acid residues and therefore exosite-II has the highest charge density on the thrombin surface. The kringle-2 domain of prothrombin forms a non-covalent adduct with exosite-II, indicating that it is not solvent exposed in the zymogen.

Besides heparin, many ligands interacting with exosite-II have been identified. Platelet receptor GpIbα, which acts as a cofactor for activation of PARs, interacts with thrombin utilizing exosite-II. Prothrombin fragment 1.2, CS moiety of TM and fVIII interact with thrombin via exosite-II. Many exogenous natural inhibitors like Haemadin form *Haemadipsa sylvestris* leech, interacts with thrombin via exosite II and the active site. Due to their polyanionic nature, many DNA and RNA aptamers have been designed to interact with exosite-II.[83, 84] Recently, Suramin was shown to inhibit thrombin by binding to exosite-II.[85]

1.5.1 Thrombin-heparin interaction

Naturally occurring heparin is a sulfated GAG composed of repeating iduronic acid and N-acetyl glucosamine units with variable sulfation pattern and chain length. As a result heparin is inherently polydisperse. It is primarily composed of a major (~75-95%) trisulfated disaccharide repeating unit consisting of 2-O-sulfo-α-L-iduronic acid 1→4 linked to 6-O-sulfo-N-sulfo-α-D-glucosamine (→4]IdoA2S(1→4)GlcNS6S[1→) along

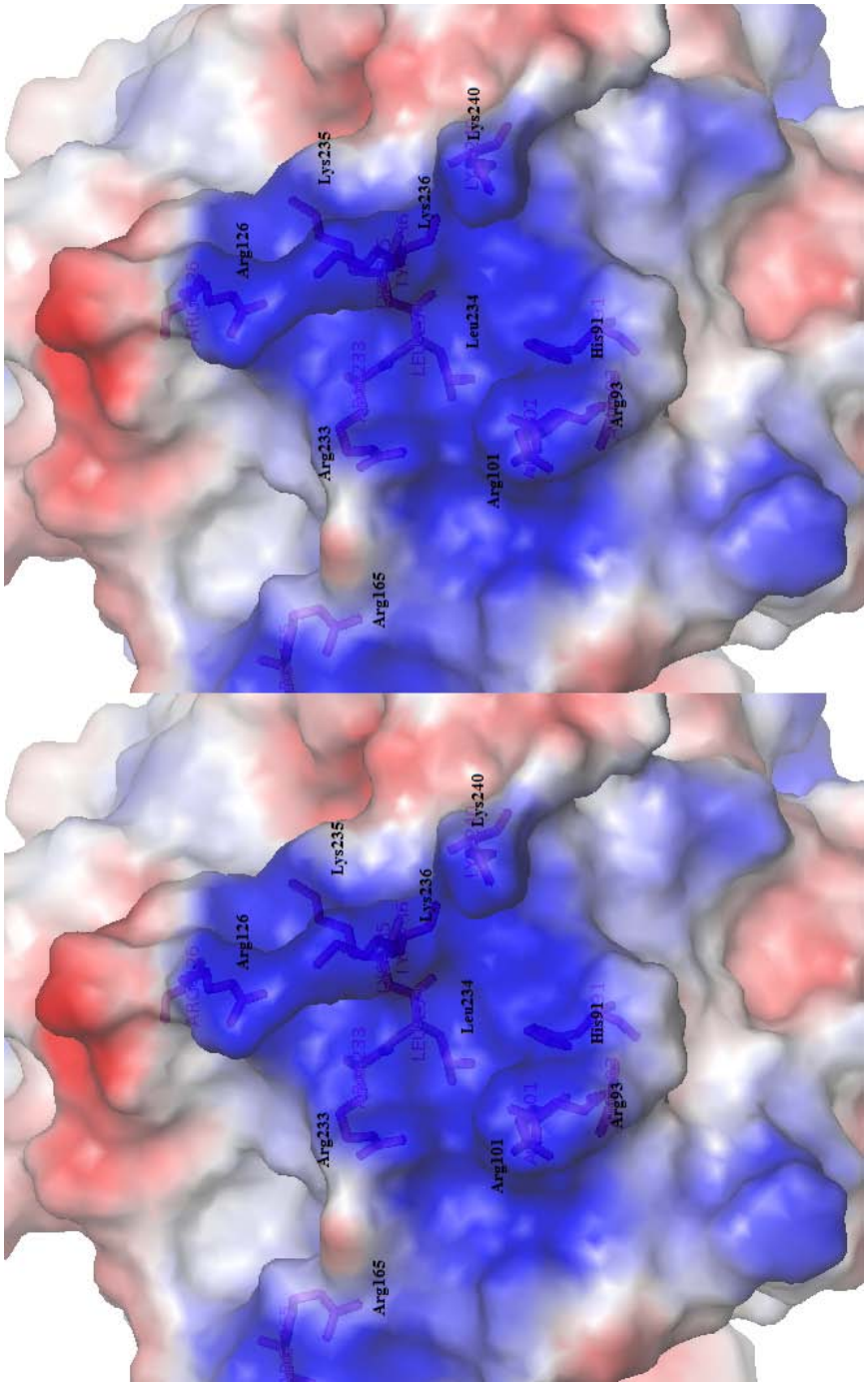

Figure 9. Stereoview of anion binding exosite-II represented by semi-transparent electrostatic surface. Red and blue indicate electropositive and electronegative regions respectively. Important residues are labeled and represented in stick overlaid with semi-transparent electrostatic surface.

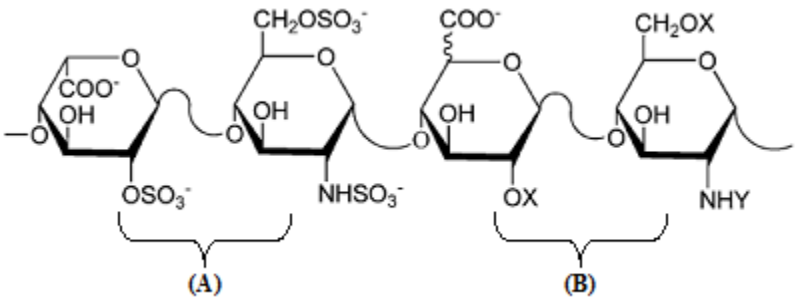

Figure 10. The structures of the major (A) and minor (B) repeating sequences of heparin. X = SO_3^- or H and Y = SO_3^- or COCH3.

with a number of additional minor disaccharide structures corresponding to its variable sequence (**Figure 10**). There is a unique sequence combination that makes specific interaction with AT-III, called the pentasaccharide sequence. It is composed of GlcNAc/NS6S → GlcA → GlcNDS3S,6S → IdoA2S → GlcNS6S.

Heparin enhances AT-III mediated inhibition of thrombin by two mechanisms. Binding of pentasaccharide sequence to AT-III induces an allosteric change in the conformation of AT-III, making it more reactive towards thrombin. If the heparin chain is sufficiently long, sequence distal to the pentasaccharide binding site interacts with exosite-II of thrombin, effectively bridging the two molecules and thereby increasing their effective concentrations. (see **Figure 11**) In combination, these two mechanisms enhance thrombin-ATIII reaction more than 1000 fold. The ternary complex of antithrombin-thrombin-heparin complex has been independently solved by two groups.[86,87]

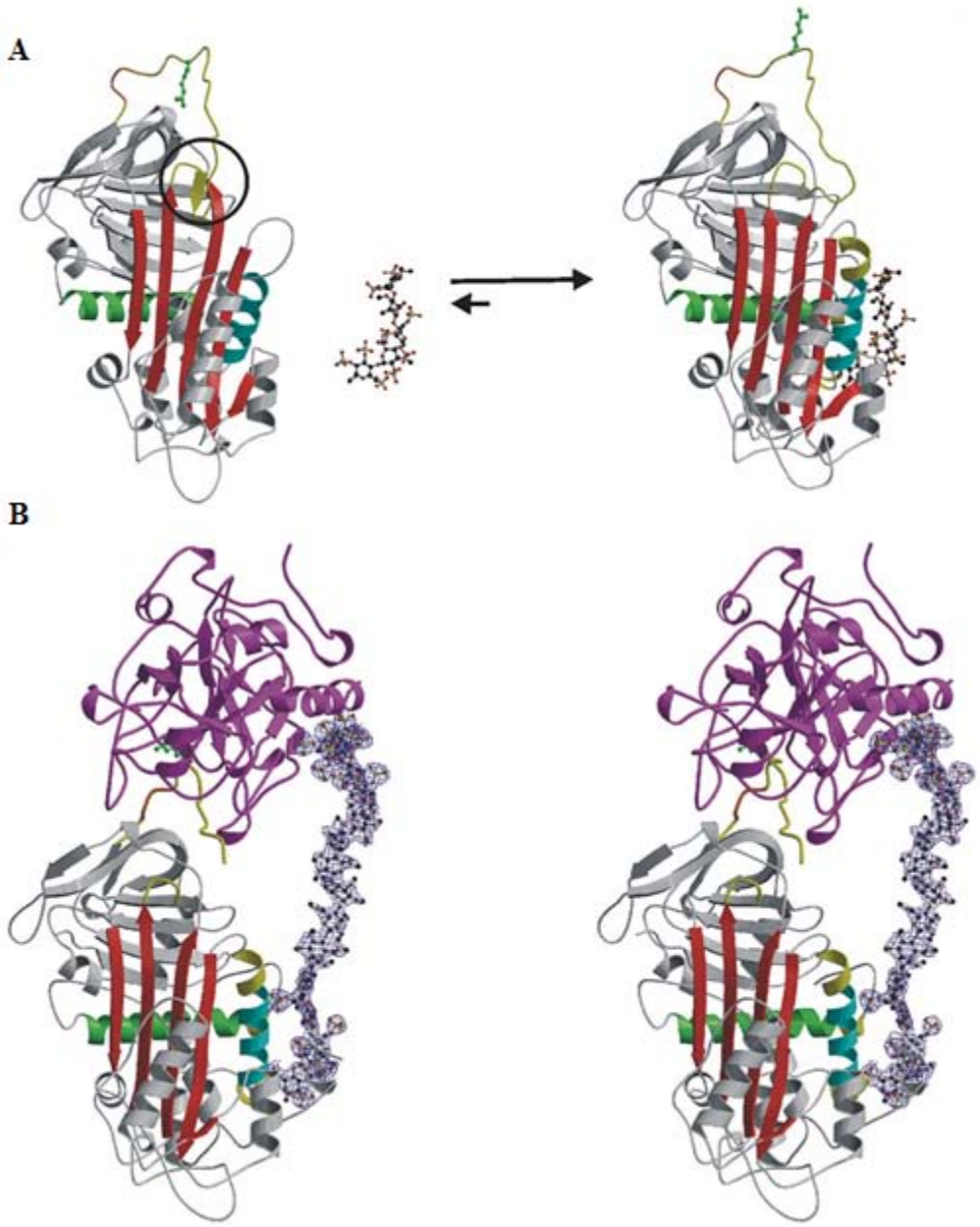

Figure 11. Mechanism of heparin induced inhibition of thrombin by AT-III. (A) Pentasachharide sequence (ball and stick) of heparin binds to AT-III (cartoon representation) and induces allosteric unfolding of reactive centre loop (circled) making it more flexible. (B) Ternary complex of thrombin (cartoon representation colored pink)-antithrombin(cartoon representation in multiple coloring)-heparin (ball and stick representation with 2Fo-Fc electron density contoured at 1σ shown in blue). PDB code: 1TB6. This figure is taken form Reference 87.

Thermodynamic studies of thrombin-heparin interaction show that binding of heparin to thrombin is non-specific and depends on heparin chain length. High salt dependence of K_D indicates that a major component contributing to the binding energy is ionic. The crystal structure of PPACK-thrombin bound to heparin (1XMN) is consistent with this hypothesis. The structure consists of two heparin octasaccharides, each sandwiched between two thrombin molecules. Both heparin sequences interact differently with each of the thrombin molecules (through exosite-II), but in both the cases, the heparin chain makes extensive contacts with one and fewer contacts with the other thrombin molecules, indicating that the latter interactions are just to compensate the residual charge. Exosite residues that interact with heparin are R93, H91, R101, R126, R165, H230, R233, W237 and K240.[51] (see **Figure 12** and **13**)

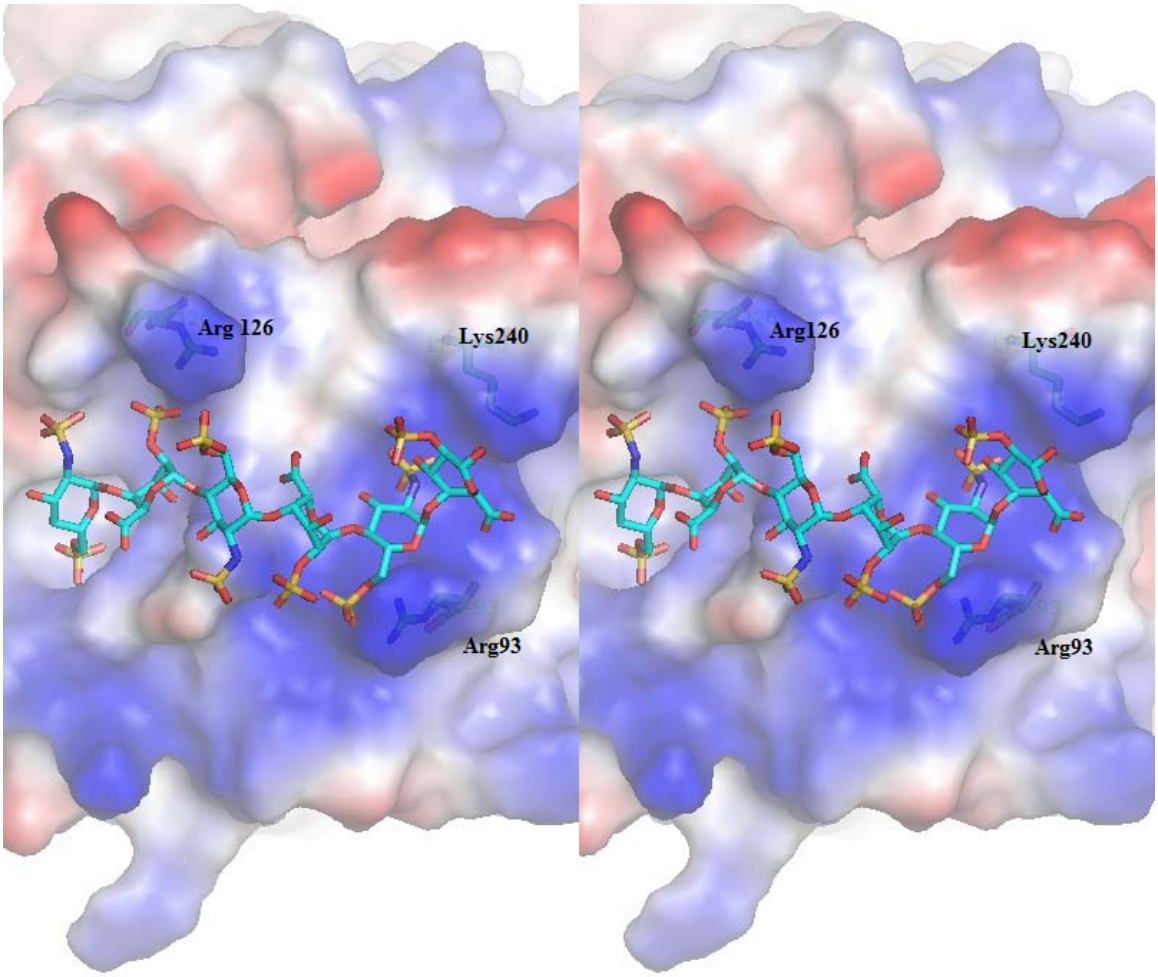

Figure 12. Crystal structure of thrombin bound to heparin (PDB ID:1XMN). The thrombin monomer (monomer AB) making extensive contacts with heparin is shown by semitransparent electrostatic surface potential (red is negative and blue is positive). Heparin is shown in ball and stick representation.

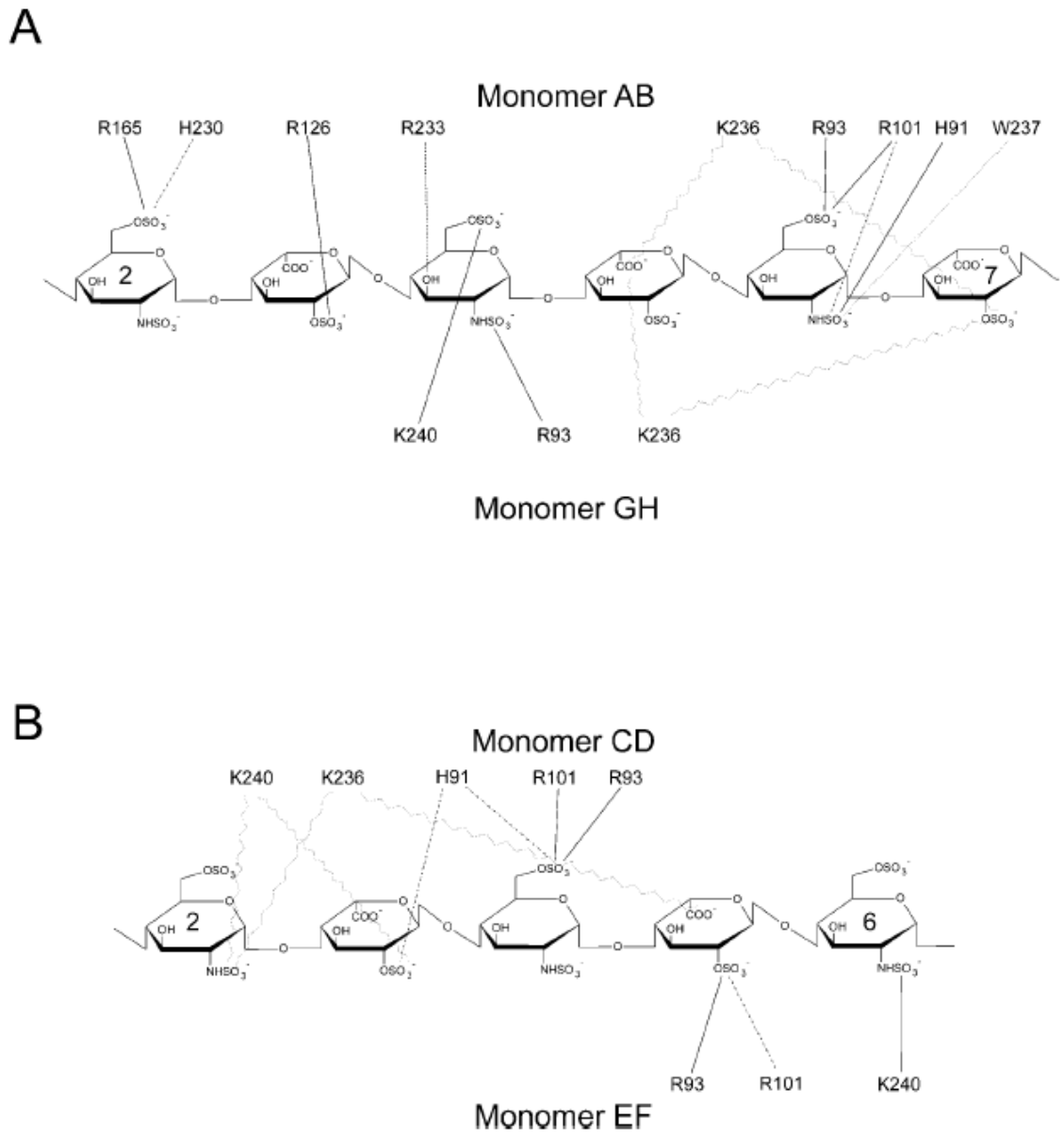

Figure 13. Schematic representation of the two heparin chains interacting with two thrombin monomers (A) AB and GH and (B) CD and EF respectively in the crystal structure of thrombin bound to heparin (PDB ID:1XMN). Ionic interactions are indicated by solid lines, dashed lines indicate hydrogen bonds, solvent mediated hydrogen bonds are shown by dotted-dashed line and jagged dotted line indicates potential ionic interaction for incompletely built side-chains. This figure was taken from Reference 51.

1.5.2 Sucrose Octasulfate: A Heparin Mimic?

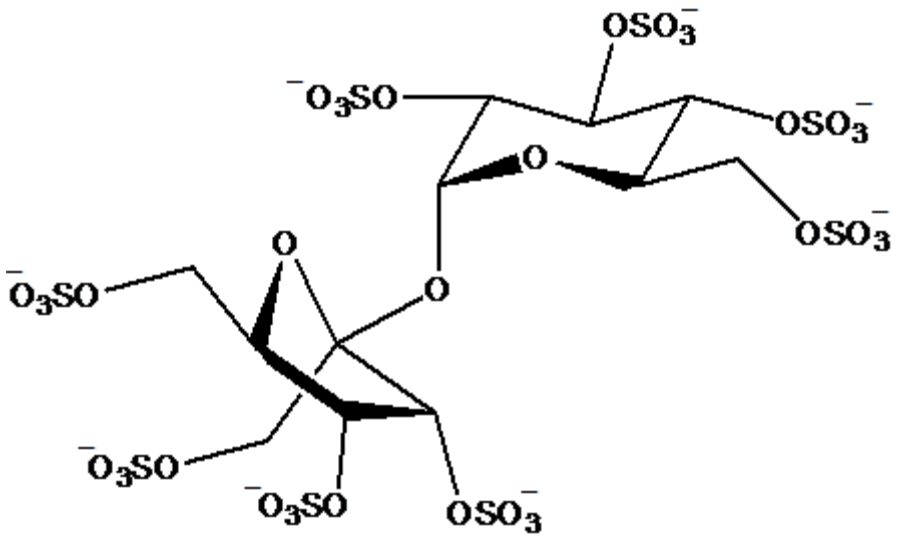

Figure 14. Structure of sucrose octasulfate.

Sucrose octasulfate (see **Figure 14**) has long been considered to be a heparin mimic, in that it can dimerize Fibroblast growth factors (FGFs) in a manner similar to heparin.[88-91] It has also been reported to bind and activate HC-II to a small degree.[92] However it has not been rigorously demonstrated to mimic heparins anticoagulant properties.

1.6 Interactions at the Na^+ Binding Site

The discovery that thrombin is a monovalent cation-activated enzyme was first reported by Orthner et. al. in a seminal paper of 1980.[93] The study showed that Na^+ and other monovalent cations like K^+ and Rb^+, but not $NH4^+$ or Li^+ increased the efficiency of cleavage (k_{cat}/K_m) of several chromogenic substrates by ~ 10 fold. The study also showed a Na^+ dependent decrease in the clotting time. The binding constant for thrombin was found to be 20mM at 30 □C. The binding o f Na^+ lead to a change in UV absorbance

difference spectra in the absorption range of Tyr residues. This was inferred to be due to a change in conformation of thrombin on Na^+ binding. The subsequent three decades of research on this topic has led to a tremendous amount of information to explain the role of Na^+ as an allosteric effector of thrombin. Most of the information is derived by exploiting three techniques: kinetics, mutagenesis and crystallography, and quite often, the inferences drawn from these studies are conflicting.

The exact location of Na^+ binding remained elusive until much after the discovery of the role of Na^+ as an allosteric effector inspite of several reported thrombin structures. This was due to the similarity in the observed electron density of Na^+ ion and water. In 1992 Tulinsky et. al. crystallographically identified the Na^+ binding site by exchanging Na^+ with Rb^+.[55] Subsequently, Na^+ was identified in several previously reported crystal structure where it was wrongly assigned to be an ordered water molecule.

Na^+ binding site is located in a narrow solvent filled cavity near Asp189 of the S1 pocket. The cavity is 8 Å × 18 Å in volume and is formed by four antiparalleβ -strands between Cys182-Cys191 and Val213-Tyr228. The cavity extends from the active site to the opposite surface of thrombin. The Na^+ ion is octahedrally coordinated with peptide carbonyl oxygen atoms of Arg221A and Lys224 and four conserved water molecules. This is further stabilized by interaction of the waters with side-chains of Asp189, Asp221 and main chain atoms of Gly223 and Tyr184A. (see **Figure 15**)

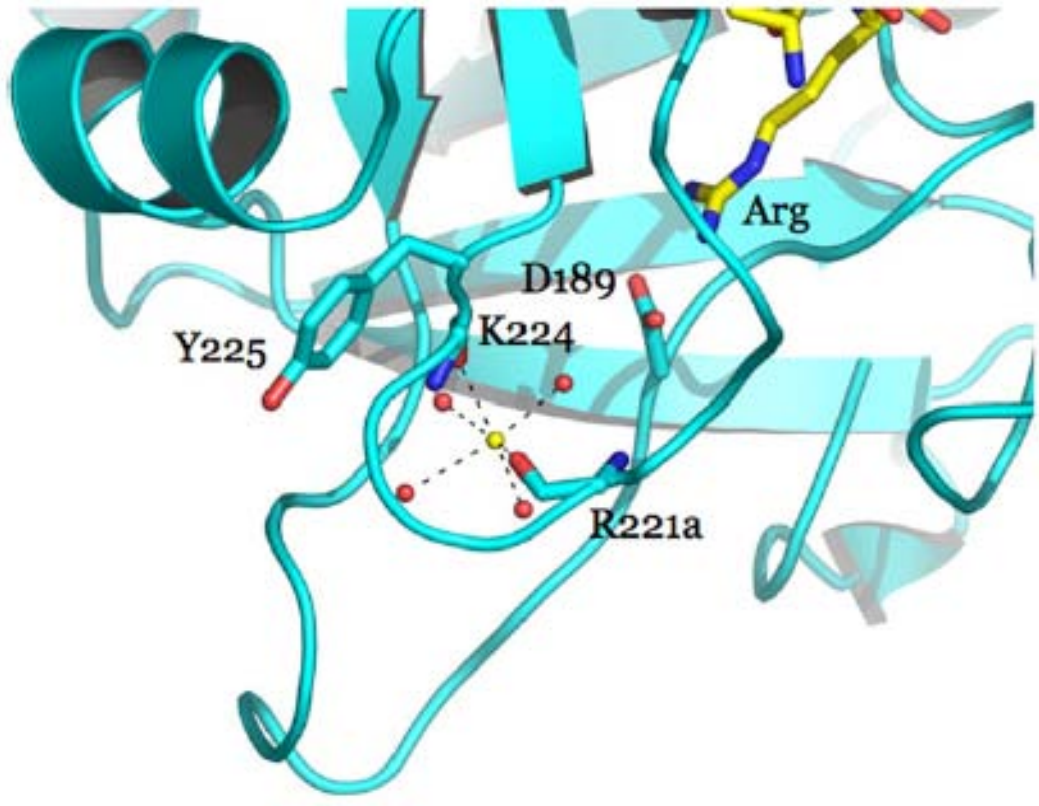

Figure 15. Molecular environment of Na^+ (yellow sphere) binding site in relation to S1 specificity pocket. Thrombin is shown in cartoon representation (light blue). Important residues interacting with Na^+ are shown in stick representation. Water molecules are shown as red spheres. P1 Arg side-chain of PPACK is shown in stick representation (yellow).

The effect of Na^+ on the physiological substrates of thrombin shows an increase in rate of release of fibrinopeptide A and B, and cleavage of PARs. On the other hand, binding of Na^+ decreases the specificity of thrombin for protein C activation. Since it was seen that binding of Na^+ to thrombin generally increased the rate of hydrolysis of substrates the Na^+ bound form was termed as "fast" form and the Na^+ free form was termed as "slow" form. The relevance of the two thrombin forms to blood coagulation is

still a contentious issue as Na^+ levels in blood are tightly regulated. Although, it has been reported that elevated and decreased levels of Na^+ can lead to thrombosis and bleeding respectively. The temperature dependence of K_D of Na^+ shows that at physiological temperature and Na^+ concentrations (143 mM) both slow and fast forms are equally populated.[20]

Apart from the change in UV absorbance difference spectrum reported by Orthner et. al., evidence of a global conformational change comes from circular dichroism studies, which show a loss of ellipticity in the far UV region, implying a change in packing of certain aromatic residues. Near UV CD spectra show evidence for change in local asymmetry of aromatic residues. The CD spectra of thrombin in absence and presence of Na^+ grossly overestimate the amount of secondary structure in thrombin, indicating the contribution of packing of aromatic side chains and disulphide bonds to the CD signal. It is likely instead, that binding of Na^+ to thrombin causes a conformational change of aromatic residue side-chains (and disulphide linkages) in loop regions of thrombin. Evidence that Trp residues are involved comes from the reported ~20% increase in intrinsic fluorescence of thrombin upon Na^+ binding.[94, 95]

Careful kinetic studies indicate that Na^+ binding increases the rate of association of substrate binding (k_1) and also the rate of deacylation (k_{cat}), which is the final step in the catalytic cycle. Form this study and from previous observations of a general trend for increase in K_m upon Na^+ binding, it was concluded that the conformational change induced upon Na^+ binding must be large enough to cause a general widening of the active

site cleft which remains in that configuration throughout the catalytic cycle of the enzyme. This effect is even more accentuated for substrates or inhibitors having significant interaction with the aryl binding pocket. This is exemplified by Y3A mutant of N-terminal peptide of hirudin. The Tyr3 residue occupies the aryl binding pocket of the active site and the wild type peptide binds with 35 fold higher preference for the Na+ bound form of thrombin. This preference is reduced to 1.3 fold in the Y3A mutant. This suggests that Na^+ binding especially leads to widening of the aryl binding pocket.[96]

Apart from its allosteric effect on the active site, Na^+ binding is linked to changes in the exosite-I as well. It has been observed that binding of C-terminus peptide of hirudin to the exosite-I exhibit the same changes to the kinetics of chromogenic substrate cleavage as does Na^+ binding. Thrombin bound with hirudin at exosite-I shows no further change in kinetic properties upon Na^+ binding. On the other hand, activity of Na^+ bound thrombin does not change upon hirudin binding. Furthermore, affinity of hirudin for the fast form of thrombin is higher than that for the slow form. All this evidence suggests an allosteric linkage between Na^+ binding site and exosite-I. Various residues energetically linked to Na^+ binding have been mapped by extensive mutagenesis studies. The domains linked to Na^+ binding are clustered in the Na^+ binding site, active site and exosite-I. This means that the conformational change linked to Na^+ binding must occur at specific regions and do not affect the secondary structure and global tertiary structure, as supported by the interpretation of UV and CD spectra. Finally, the residues at sites other

than the above stated ones might be involved in the allosteric communication between the active site, Na+ binding site and exosite I.[95, 97]

The structural evidence of thrombin slow↔fast allostery is complicated by several issues. Firstly, most of the previously published thrombin crystals were grown in solutions containing Na^+ as a part of the crystallization buffer. Secondly, irrespective of the presence or absence of Na^+ at the Na^+ binding site, the reported structures were always in the fast form as most of the structures were crystallized with an active site or exosite-I ligand. This is because of the well known communication among the three sites and the fact that binding of these ligands mimic the conformation of the fast form. Finally, crystal contacts themselves make a free energy contribution of ~3-6 kcal/mol, which is significantly higher than the energy difference between the two forms, implying that crystal contacts can mask any conformational changes due to slow↔fast allostery. Recently, several crystal structures of the slow form of wild-type or mutant thrombins have been published. By comparing the main chain RMSDs (Cα RMSD) of these structures with the PPACK thrombin structure published by Bode et. al. (PDB ID: 1PPB) two classes of structures emerge: a) Class I structures with Cα RMSDs comparable to the RMSDs of other published fast forms of thrombin (~0.4) and b) Class II structures with 3 fold higher Cα RMSDs compared to other published fast forms of thrombin (~1.25). (See **Table 2**) If we consider the average Cα RMSDs of all the fast forms (~0.4) as noise then the ratio of average Cα RMSDs of each residue of all the class I and

Table 2. Fast and slow structures submitted in the PDB and their respective Cα RMSD as compared to 1PPB

Structure PDB ID	Details	Cα RMSD vs. 1PPB
Fast forms		
1PPB	1.9 Å, PPACK inhibited	-
1HAH	2.3 Å, Na+ and hirugen bound	0.35
1HXF	2.1 Å, Hirugen bound, Na+ free	0.37
1SG8_B	2.3 Å, Na+ bound, R77aA	0.40
1SG8_E	2.3 Å, Na+ bound, R77aA	0.45
Putative slow forms		
Class I		
1SGI_B	2.3 Å, Na+ free from of 1SG8	0.40
1SGI_E	2.3 Å, Na+ free form of 1SG8	0.37
Class II		
2AFQ_B	1.9 Å , Na+ free, wild type	1.30
2GP9	1.9 Å, Salt-free, D102N	1.27
1RD3_B	2.5 Å, E217K	1.25
1RD3_D	2.5 Å, E217K	1.21

class II slow forms and average Cα RMSDs for each residue of all the fast forms of thrombin will give us a per residue Signal:Noise for all Cα RMSDs compared to the 1PPB control. This analysis shows that the class II structures show significant change in conformation which can be attributed to the slow form of thrombin. The class I structures

are conformationally indistinguishable from the Na^+ bound fast form. A close analysis of residues undergoing major conformational change reveals a positive correlation between residues with high conformational change and their implication of being involved in slow→fast allostery from kinetic and mutagenesis data. To no surprise, these residues are in the Na^+ binding site, active-site and exosite-I, strongly reinforcing the hypothesis of allosteric communication between the three sites.[98]

It is very difficult to identify which among the class II structures is cognate to the actual in-solution slow form, but inferences can be drawn from the structural commonalities among these structures. All these structures show the Na^+ binding loop shifts more towards the active site cleft. This blocks the S1 pocket in all the structures. Another feature is the reorganization of the aryl-binding pocket. In 1GP9 Trp215 is in a conformation which would block P2 and P4 interactions, whereas in 1RD3, Trp215 protrudes slightly into the S4 pocket. Finally, all the class II structures exhibit the destruction of the oxy-anion hole. The flipping of Gly193 leading to flipping of Glu192 results in a non-catalytic hydrogen bond with Ser195. All these observations explain the biochemical data of substrates and inhibitors, especially the effect on S1 and aryl binding site widening upon Na^+ binding. The class II structures thus represent the slow form of thrombin.

A corollary to the comparison between the slow and fast structures is the observation that the residues involved in the conformational change are not disordered but are stabilized by extensive but different hydrogen bonding interactions. It can be

inferred from this that the two forms represent energetic minima in solution. The observation of presence of catalytic activity even in absence of Na^+ leads to the hypothesis that there is a rapid and dynamic equilibrium between the catalytically inactive and active forms of thrombin and the role of Na^+ binding is to stabilize the active form. The evidence for this came from experiments by Shafer et. al.[71] which studies change of intrinsic fluorescence upon Na+ binding. It was observed that the binding profile was biphasic, with the fast phase within the dead time of the stop flow device and the slow phase of ~30 s^{-1} which is independent of Na^+ concentrations. The rate constant of the slow phase was found to be dependent on temperature. At higher temperature the binding profile is still biphasic but the ratio of fast:slow phase is similar to that obtained at 5 ^{0}C. The data fits the model of thrombin in two forms: one capable of Na^+ binding and the other incapable of Na^+ binding, the transitioning from the later to the former accounting for the temperature dependent slow phase. Gianni et. al. resolved a linear dependence of the fast phase on Na^+ concentration, implying that the conformational change reported by Shafer et. al. precedes Na^+ binding.[99] The mechanism can be described by the following equation:

$$\mathbf{E^* \leftrightarrow E \leftrightarrow E{:}Na^+}$$

Where E* is the thrombin conformer incapable of Na^+ binding and E is the conformer capable of Na^+ binding. This rationalizes the observed differences (and similarities) in fast, slow(class I) and slow(class II) structures to be attributed to each of these forms can be assigned to $E{:}Na^+$, E and E* allosteric states, respectively. Gianni et. al. show that the

ratio of E*:E is 1:1 in absence of Na^+ and Na^+ is simply acting to stabilize the E state.[99] These recent findings have also led to a re-thinking of the "slow-fast" nomenclature because E state, although it has no Na^+ coordinated, is still catalytically active.

1.7 Sulfated Dehydropolymers: Novel Allosteric Inhibitors of Thrombin Acting via Exosite-II

In the last five decades, heparins and Vitamin K epoxide reductase inhibitors have been the mainstay for anticoagulant therapy. These anticoagulants suffer several limitations. This anticoagulants inhibit thrombin activity by enhancing its inactivation by ATIII (see section **1.5.1**) or inhibiting thrombin biosynthesis. Vitamin K epoxide reductase inhibitors like warfarin suffer from several limitations like drug-drug interactions, drug-food interactions and high dose-response variability. Heparins on the other hand are ineffective in inactivating clot-bound thrombin. Further, unfractionated heparin (UFH) dose-response is highly variable due to its binding to plasma proteins. Because of the key role of thrombin in procoagulant pathways, direct thrombin inhibitors have recently received a lot of attention. Currently, only three DTI are approved by FDA viz. hirudin and its synthetic congener bivalirudin, and argatroban. In an effort to design new synthetic anticoagulants exploiting the template mechanism of heparin-induced thrombin inhibition, our laboratory discovered dehydro-polymers which display very interesting anticoagulant profile.

Dehydro-polymers are heterogeneous and polydisperse polymers of cinnamic acids which were synthesized by a two step chemo-enzymatic means in a two step protocol. In the first step coupling of cinnamic acid monomers is done using enzyme

horseradish peroxidase (HRP). Three cinnamic acid derivatives were chosen for homopolymerization viz. caffeic acid, ferulic acid and sinapic acid. Upon action of HRP, various radical intermediates form, that further undergoes chain extension. Key among these linkages are β-O-4 and β-O-5 linkage (although, β-β, 5-5 and 5-O-4 linkages are also a possibility). In the second step, the polymers are sulfated using trialkyl amine-sulfur trioxide complex. The resulting product is a heterogeneous and polydisperse mixture of sulfated dehydro-polymers of caffeic acid (CDs), ferulic acid (FDs) and sinapic acid (SDs) depending on the starting material used. (see **Figure 16**)

Prothrombin time (PT) and activated partial thromboplastin time (aPTT) measurement in presence of each of the DHPs indicated that they are potent anticoagulants. The DHPs were found to be 1.4 to 3.4 times more effective in prolonging PT, but 2.2 to 3.8 times less effective in prolonging aPTT, as compared to LMWH, with an overall higher effectiveness to prolong PT than aPTT. This implies that DHPs act on the intrinsic pathway more than on extrinsic pathway.

Among the DHPs, the anticoagulant potency follows the order: CDs>FDs>SDs. It is possible that there is a positive correlation between the degree of structural diversity and anticoagulant potency, CDs being the most diverse and SDs being least diverse.[100, 101]

Interestingly, direct and indirect enzyme inhibition studies revealed that the major mechanism of coagulation is a selective inhibition of thrombin and fXa. This was a surprise as these compounds were designed to mimic the template mechanism of ATIII mediated thrombin inhibition similar to heparins. FDs, CDs and SDs showed nM IC_{50} values for both thrombin and fXa in absence of ATIII. (see **Figure 17** and **Table 3**) Competitive inhibition studies for thrombin with heparins and C-terminal hirudin based peptide showed that CDs showed higher competition with heparins as compared to hirudin based peptide. This means that CDs have a preferentially bind to the exosite-II. Steady state kinetic studies with different concentrations of CDs showed that the V_{max} (and k_{cat}) decreased and the K_m increased slightly when the CDs concentration was increased. It was hypothesized based on this that CDs cause an allosteric disruption of catalytic triad.[102]

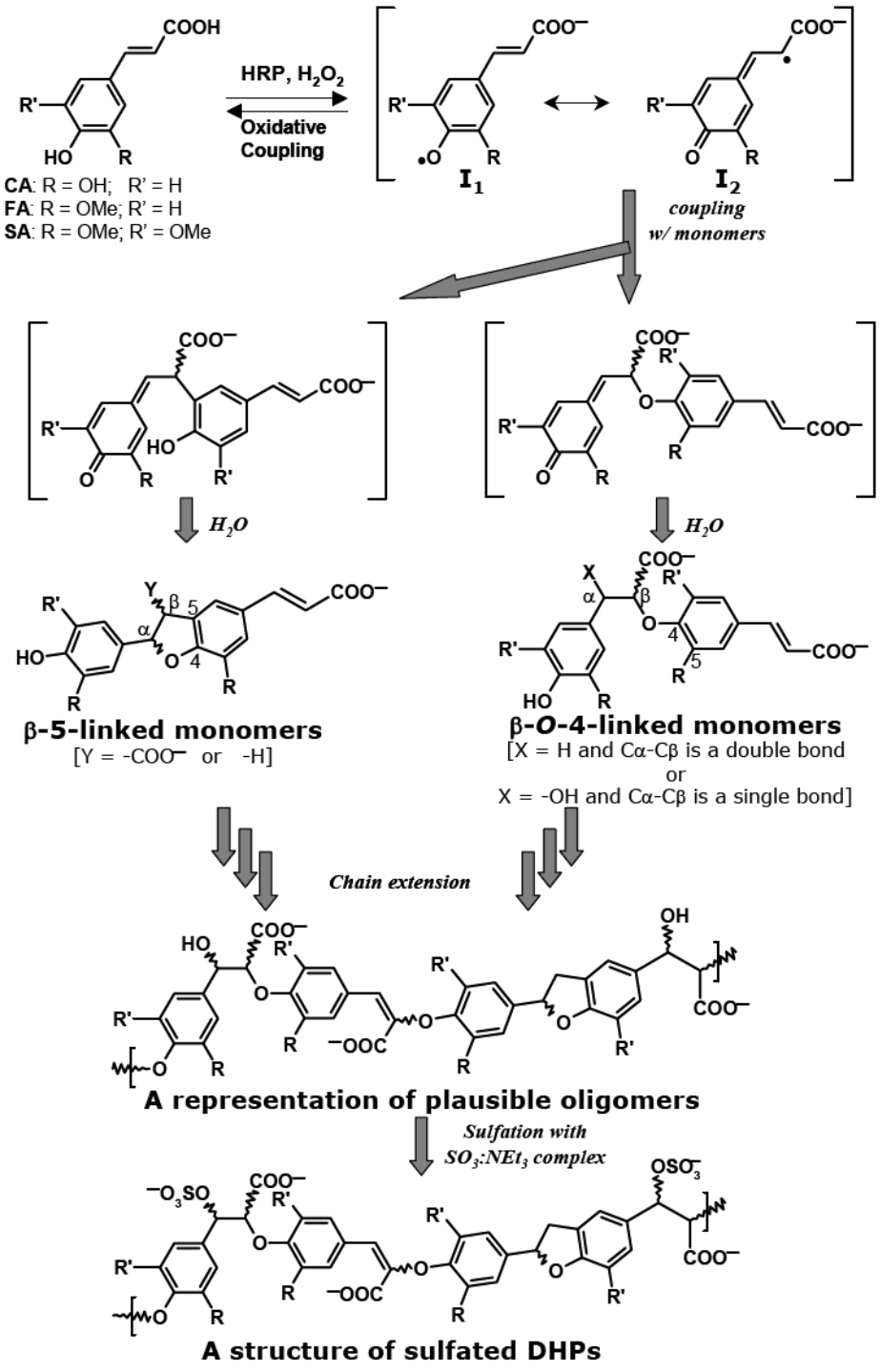

Figure 16. Chemoenzymatic synthesis of DHPs. CA, FA and SA stands for Caffeic acid, Ferulic acid and Synnapic acid respectively. This figure was taken from Reference 100.

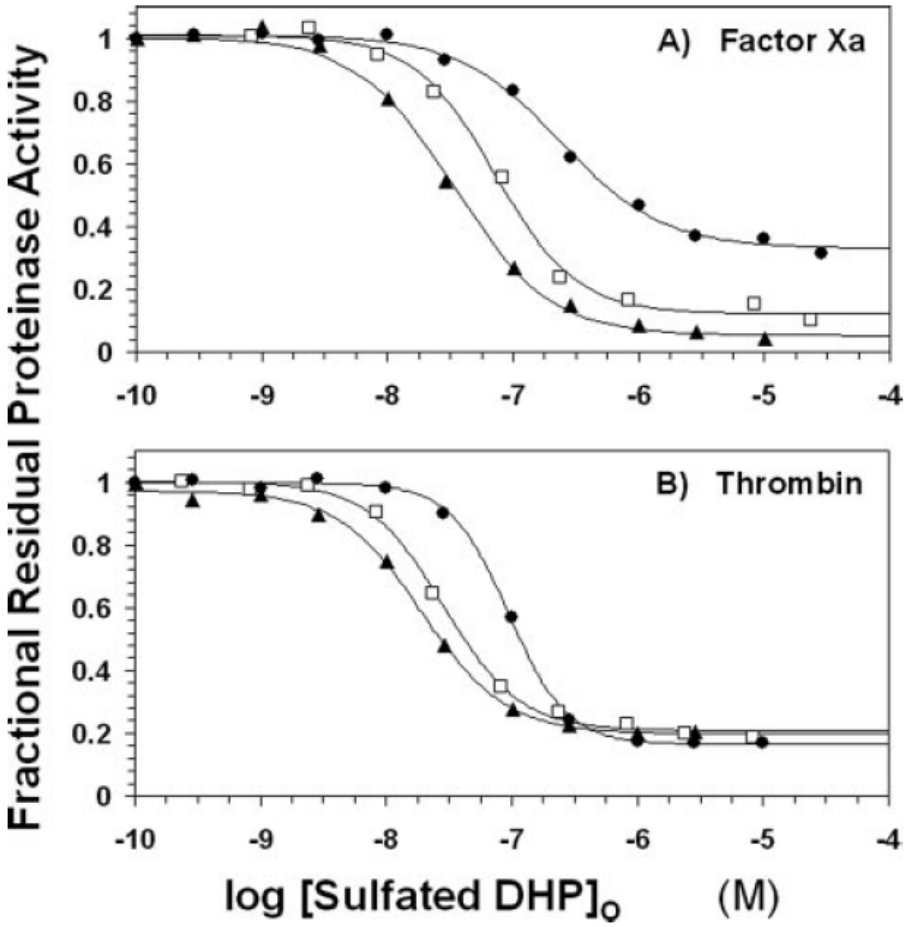

Figure 17. Direct inhibition of fXa and Thrombin by CDs (solid triagles), FDs (square) and CDs (solid dots). This figure was taken from Reference 102.

Table 3. IC_{50} values of inhibition of Thrombin, fXa, fIXa and fVIIa by various DHPs in presence (direct) and absence (Indirect) of Antithrombin-III. This table was taken from Reference 102.

	IC_{50} (nM)[a]							
	Thrombin		*Factor Xa*		*Factor IXa*		*Factor VIIa*	
	Direct	*Indirect*	*Direct*	*Indirect*	*Direct*	*Indirect*	*Direct*	*Indirect*
CDSO3	18 ± 2[b]	53 ± 6	34 ± 5	53 ± 4	3380 ± 64	4111 ± 446	>29,000[c]	>29,000
FDSO3	29 ± 2	71 ± 6	74 ± 8	133 ± 6	492 ± 16	593 ± 10	>23,640	>23,640
SDSO3	94 ± 4	45 ± 4	244 ± 28	97 ± 16	>28500	2004 ± 20	>28,500	356 ± 14

The structural basis for this mechanism remains to be found in order to gain a better understanding of this novel mechanism. One of the problems in doing this is the heterogeneity inherent in the DHPs. To resolve this problem the lab recently synthesized small molecules that represent the scaffold of one of the possible monomeric unit which could comprise the putative DHPs structure. The compounds showed inhibition of thrombin and fXa, with 4AS (see **Figure 18**) being the most active.

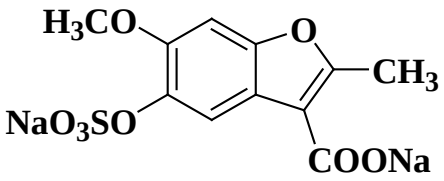

Figure 18. Structure of 4AS.

1.8 Specific Aims of the Research

A) To Understand the Structural Basis of DHP Inhibition Using X-ray Crystallography: Since 4AS represents one of the monomeric unit of DHPs, it is a good starting point for initiating structure-based drug design. Our aim is to solve the structure of 4AS complexed with thrombin. The minimum information that could be derived from the study is the location of binding site of 4AS on thrombin. Careful comparison of crystal structure of native enzyme and its isomorphous soaks may reveal the structural changes induced by the binding.

B) To Characterize Thrombin-Sucrose octasulfate Interaction by Biophysical and Biochemical Methods: Thrombin-heparin interaction has been extensively studied by fluorescence spectroscopy using active site fluorescent probe p-amino benzamidine. We propose to use the same method to characterize thrombin-SOS interaction. SOS and heparin have a sulfated sugar scaffold. Unlike heparin, sucrose octasulfate has higher charge density. The effect of sugar chain length has been characterized using different chain length heparins. We would like to determine the effect of charge density by studying this interaction.

CHAPTER 2 CRYSTALLOGRAPHIC ANALYSIS OF 4AS-SOAKED NATIVE BOVINE THROMBIN CRYSTALS AND HUMAN PPACK THROMBIN- 4AS CO-CRYSTALS

2.1 Introduction

2.1.1 Overview of Drug-Protein Crystallography

Protein crystallography is a biophysical method used to generate accurate models of proteins at atomic or near-atomic resolution. The wavelength of x-rays falls in the range (~1.5 Å) appropriate to deduce information about inter-atomic distances from diffraction scattering through interaction of the x-rays with the electrons of atoms. The method involves passing of an x-ray beam through a high quality protein crystal of appropriate size, and recording the diffraction pattern on an image plate or detector. By accurately measuring the position and intensity of each spot on the diffraction pattern, it is possible (with supplemental phase information) to construct a 3D map of electron density of the repeat unit of the crystal (the unit cell). Once the electron density map is generated, it is possible to build an accurate model of the molecule into this density.

The requirement of good quality protein crystals arises for two reasons: firstly, single molecules give weak diffraction, and secondly, in solution molecules are in constant motion which leads to a cancelling out diffracted x-rays. The repeated and periodic

arrangement of atoms in a crystal enhances the signal of each diffracted x-ray so that it is possible to measure its intensity with high statistical confidence levels.

Drug-protein crystallography adds an additional step in protein crystallography, in that, at some point during the experiment the drug needs to be incorporated, which can be done by adding appropriate concentrations of the drug in the crystallization buffer. This method is called co-crystallization. Alternatively, a preformed native protein crystal can be soaked in a solution that contains the drug. Unlike small molecule crystals, protein crystals contain between 40 to 70 % solvent. If given enough time, the drug can diffuse through the solvent channels and get incorporated into the crystal.[103, 104]

Drug-protein crystallography aids immensely to the process of structure-based drug discovery. It gives atomic level information about interactions made by the drug with the protein. Additionally, by comparing the structural differences in the drug-bound and unbound crystal forms it is possible to understand the structural basis of drug action. The information derived from the experiment can be further used to make modifications in the lead structure. It is also possible to use the information in virtual screening and docking studies of homologous series of compounds.[105]

2.1.2 Rationale for Specific Aim A

Since DHPs interact with thrombin at or near exosite-II it can be hypothesized that 4AS also would interact with that region. Since 4AS contains a sulfate and a carboxylate, it is likely that a sizable contribution to the binding energy would be ionic in nature. To avoid ionic screening effects, which could interfere in binding, it is necessary to screen for

crystallizing conditions having low ionic strength. In order to identify the allosteric changes induced by 4AS binding to thrombin, a native thrombin crystal has to be crystallized for comparison. Solving the structure of 4AS soaks of native thrombin crystal and comparing it with the native structure would unambiguously delineate the changes induced by 4AS binding. If the structural changes are small and the difference between the solution-form free energies of bound and unbound states are low, it is possible that the changes could be masked due to stabilizing crystal contacts in a pre-formed crystal. It is therefore also desirable to find a co-crystallizing condition for 4AS-thrombin complex.

It was surprising to find that among the ~550 thrombin structures deposited in the PDB not a single structure was that of unliganded wild-type thrombin (in fast form). Most of the information on thrombin structure has been derived from PPACK-thrombin and hirugen-thrombin structures. Recently, Iyaguchi. et. al. reported preliminary crystallization data of unliganded wild-type bovine thrombin.[106] But, the group has not reported the solved structure. It was proposed that these conditions be used for obtaining crystals for subsequent soaking. Both the native and derivative structure would be solved and compared. At the same time, small scale crystal trials to find co-crystallization conditions of thrombin-4AS complex were also proposed.

2.2 Results

2.2.1 Crystallization of Native Bovine thrombin and Human PPACK thrombin under co-crystallization conditions with 4-AS

The crystals of native bovine thrombin obtained under the reported conditions were of suboptimum size and unsuitable for diffraction experiments. (see **Figure 19**) This necessitated further screening and optimization of these conditions. As seen in the **Figure 19**, under the reported conditions, there was significant protein precipitation and also a high degree of nucleation. This leads to depletion of protein from the mother liquor by protein precipitates and simultaneously growing crystal nuclei, and as a result, the crystals fail to grow to larger dimensions. The goal of optimization was to achieve optimum size by decreasing the nucleation and precipitation. This was done by a carefully changing each condition variable, adding various additives and changing the experimental set-up (sitting-drop, micro-dialysis etc.) The crystals obtained after optimization are shown in **Figure 20.** The results of the optimization trials are summarized in **Table 4.**

Table 4. Result summary of optimization trials for native bovine thrombin crystals.

Condition Variable	Observation
PEG	PEG 3350 gave large crystals without any associated precipitates. Optimum concentration was 20 % w/v. Crystal formation under these conditions was so rapid that crystals could be seen immediately after the cover-slip was placed over the reservoir!
2-Propanol	Change in concentration did not affect the amount of nucleation considerably
pH	Optimum pH was 6.2 ± 0.2, pH lower than 5.8 lead to precipitation
Buffer concentration	Low concentrations of sodium citrate gave precipitates
Buffer substitution	MES, PIPES, Cacodylate and Bis-tris were used at pH 6.2 instead of sodium citrate. No crystals formed in any except in PIPES
Protein concentration	Optimum concentration was between 4.5 to 6.5 mg/ml
Drop Size	Larger drops gave larger crystals
Crystallization method **Sitting drop** **Sandwich drop** **Micro-dialysis**	Large amount of nucleation Same as hanging drop Large amount of nucleation
Other adjuvants **Calcium 1mM, 5 mM** **Glycerol 3, 5,10 % v/v**	Does not considerably affect the crystal size Increasing concentrations of glycerol gave decreasing amounts of nucleation

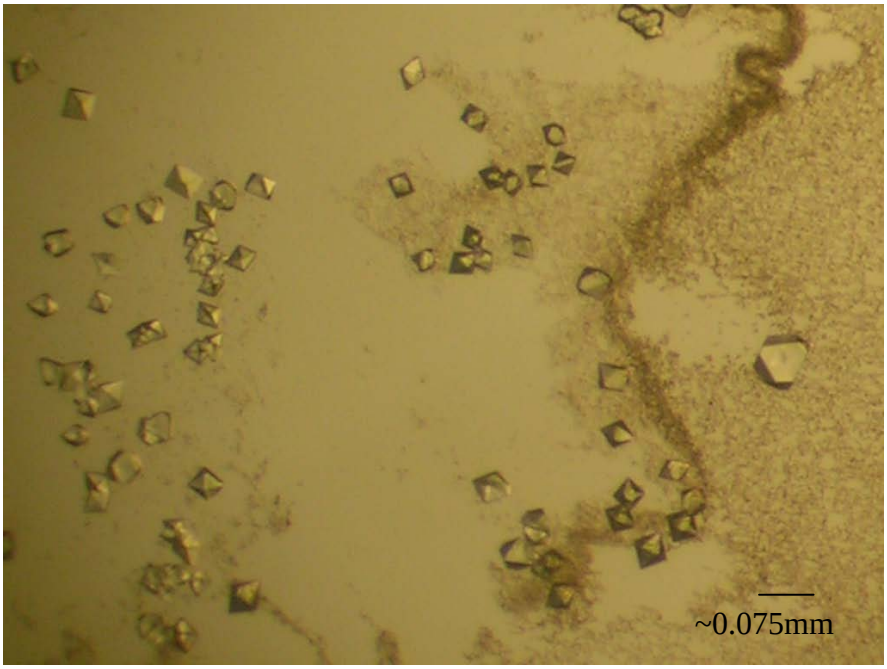

Figure 19. Crystals of native bovine thrombin under previously reported conditions.[106]

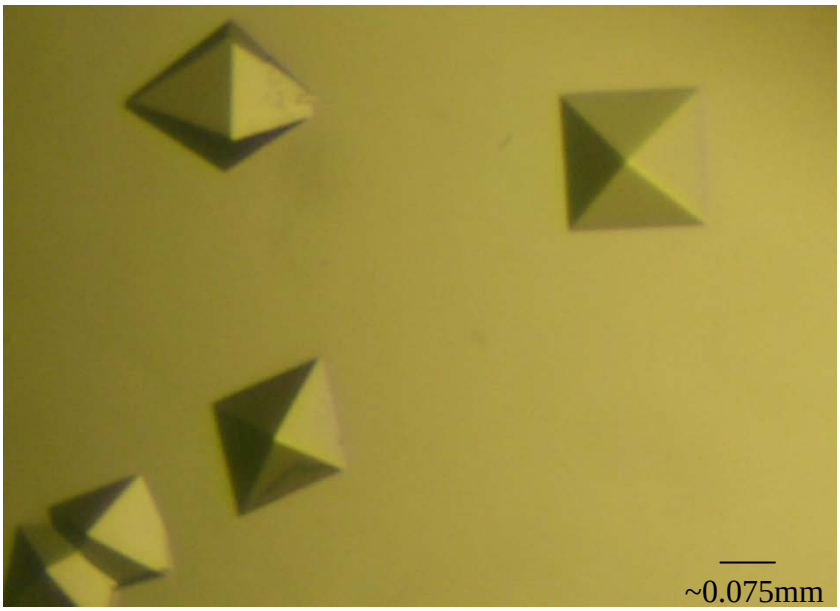

Figure 20. Crystals of native bovine thrombin obtained under optimized conditions.

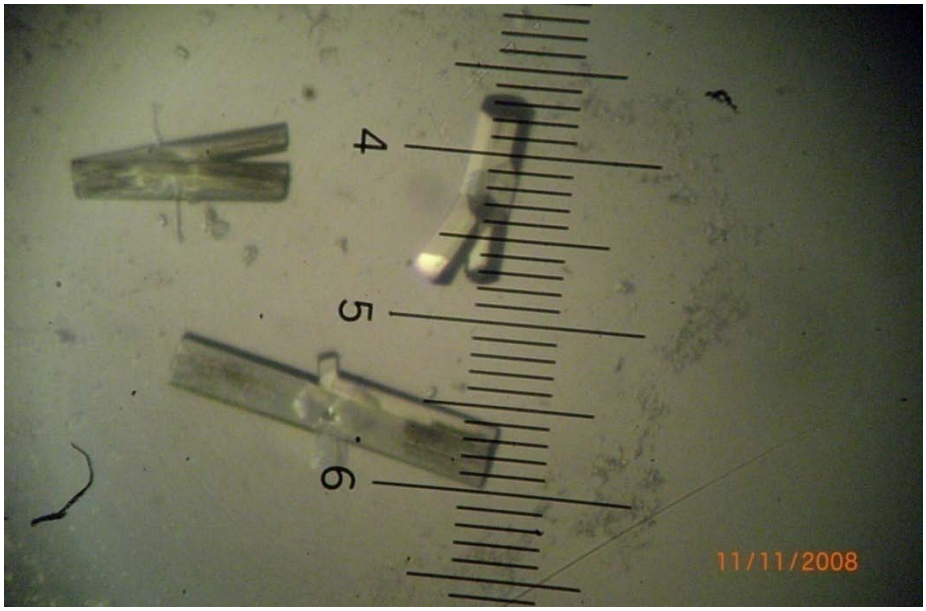

Figure 21. Human PPACK thrombin grown from crystallization buffer containing 4-AS. Each graduation is approximately equal to 0.05 mm.

Bovine thrombin crystals were grown under conditions where there was possibility of autolytic degradation. Since the crystals grew fairly quickly, autolytic degradation was not anticipated. This was confirmed with SDS-polyacrylamide gel electrophoresis under reducing conditions of the crystals which showed no signs of degradation. (see **Figure 22**) . In order to screen co-crystallization conditions for thrombin-4AS complex, human thrombin was covalently inhibited with PPACK. One such condition gave very large crystals. (Human ppack thrombin form-I) Although these crystals showed signs of epitaxial twinning at certain portions (see **Figure 21**), it was possible to perform the diffraction experiment by using parts of the crystal which seemed to have grown from a single nucleus.

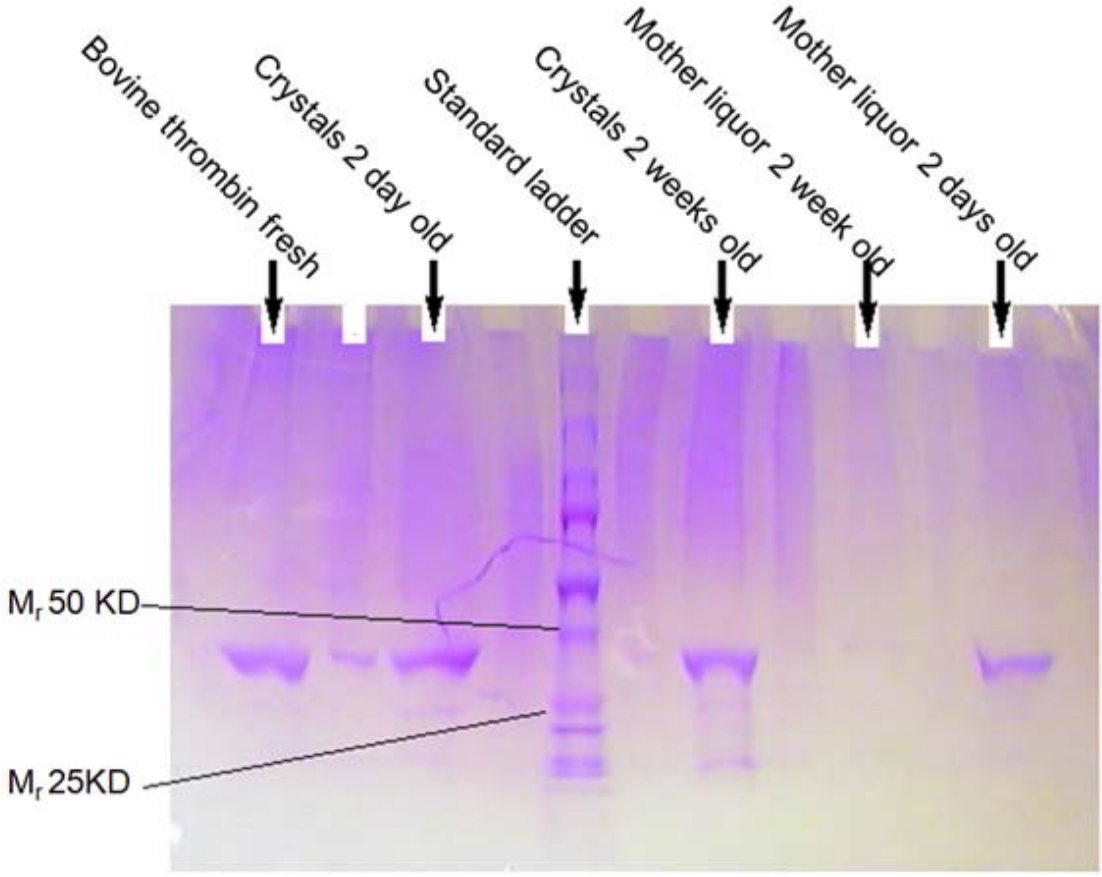

Figure 22. SDS polyacrylamide gel of native bovine thrombin crystals of different age and the corresponding mother liquor solution in which they were grown.

2.2.2 X-ray Diffraction Experiments

Complete data-sets of native bovine thrombin, bovine thrombin-4AS soaks and human ppack thrombin crystal form-I were collected for several crystals, out of which the best data was chosen for further analysis. Analysis of the systematic absences showed that the native bovine thrombin crystals and its 4AS derivatives belong to space-group $P4_32_12$ or $P4_12_12$ with unit cell parameters a = b = 87.64 Å, c = 194.51 Å; $\alpha = \beta = \gamma = 90^{o}$; and a = b = 87.64 Å, c = 195.99 Å, $\alpha = \beta = \gamma = 90^{o}$ respectively. The R_{merge} of the native and the

derivative was calculated to be 16.7 % and 15.3 % respectively. Human ppack thrombin crystal form-I belonged to orthorhombic space-group $P2_12_12_1$ having unit cell dimensions of a = 44.36 Å, b = 73.78 Å, c = 100.29 Å; α = β = γ = 90 °. The R_{merge} was 17 %. Preliminary diffraction data for the three crystals is summarized in the **Table 5.**

Table 5. Preliminary diffraction data of native bovine thrombin, bovine thrombin-4AS soak and human ppack thrombin form-I.

Parameter	**Native bovine thrombin**	**Bovine thrombin-5AS soak**	**Human-PPACK thrombin form-I**
Space group	$P4_32_12$ or $P4_12_12$	$P4_32_12$ or $P4_12_12$	$P2_12_12_1$
Unit cell parameters	a=b=87.64 , c=194.51 α=β=γ=90°	a=b= 87.64, c=195.99 α=β=γ=90°	a= 44.36, b= 73.78, c =100.29 α=β=γ=90°
Resolution (Å)	39.20-2.8 (2.9-2.8)	40-2.5 (2.59-2.5)	38.02 –2.7 (2.80 - 2.70)
Number of observed reflections	69882	133569	40521
Unique reflections	16696	27046	8843
Completeness(%)	85.9 (97.7)	99.1 (99.9)	92.5 (98.6)
R_{merge} (%)	16.7 (30.8)	15.3 (35.2)	17 (41.6)
Cell Volume (cubic Å)	1494137.3	1505275.75	328260.594

2.2.3 Structure determination

Models obtained from molecular replacement solution of native bovine thrombin, bovine thrombin-4AS soak and human PPACK thrombin crystal form-I, were refined to an R factor below 0.3. The refined model statistics for each structure, are given in **Table 6.** The Ramachandran plot for each of the structures is shown in **Figures 23-25 .** R factors and Ramachandran plot indicate that the models are consistent with the experimental data and allowed bonding geometries respectively. Moreover, examination of $2F_o$-F_c map

shows that most of the density is accounted for by the model. A detailed examination of the electron density map revealed no density for ligand in both bovine thrombin-4AS soaks as well as human PPACK thrombin crystal form-I.

Table 6. Refined model statistics for native bovine thrombin, bovine thrombin-4AS soak, and human PPACK thrombin crystal form-I structures.

	Native bovine thrombin	**Bovine thrombin soaks**	**Human PPACK thrombin**
R factor	0.23	0.24	0.27
R free	0.29	0.30	0.37
% reflections in test set	10	10	5
Bond length rmsd (Å)	0.007	0.012	0.009
Bond angles rmsd (deg)	1.027	1.48	1.26
Dihedral angles rmsd (deg.)	18.367	19.27	21.16
Planarity rmsd	0.004	0.006	0.006
Chirality rmsd	0.075	0.092	0.084

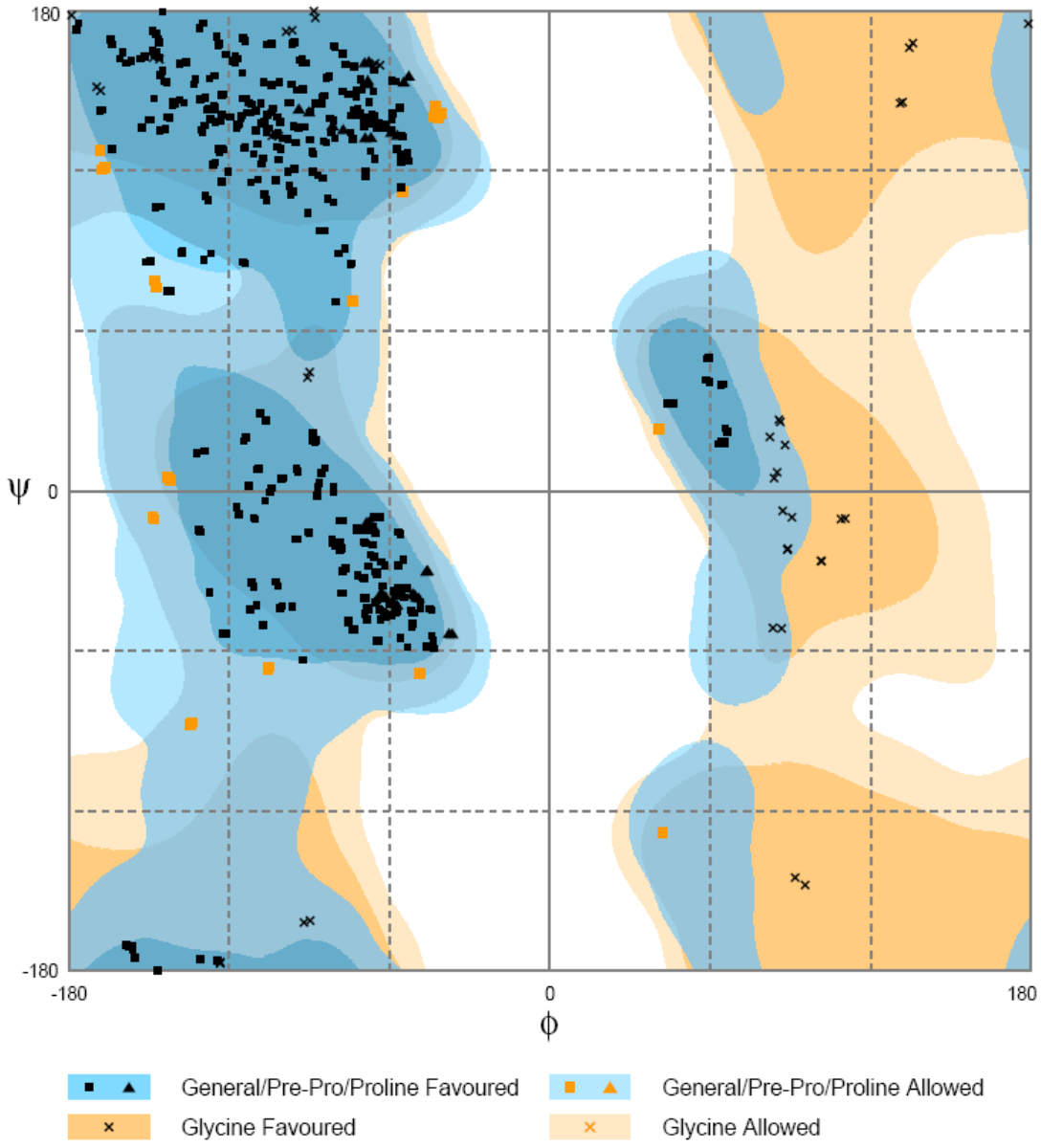

Number of residues in favoured region (~98.0% expected)	: 502 (95.4%)
Number of residues in allowed region (~2.0% expected)	: 24 (4.6%)
Number of residues in outlier region	: 0 (0.0%)

Figure 23. Ramachandran plot of refined native bovine thrombin structure. Plot was generated using RAMPAGE.[115]

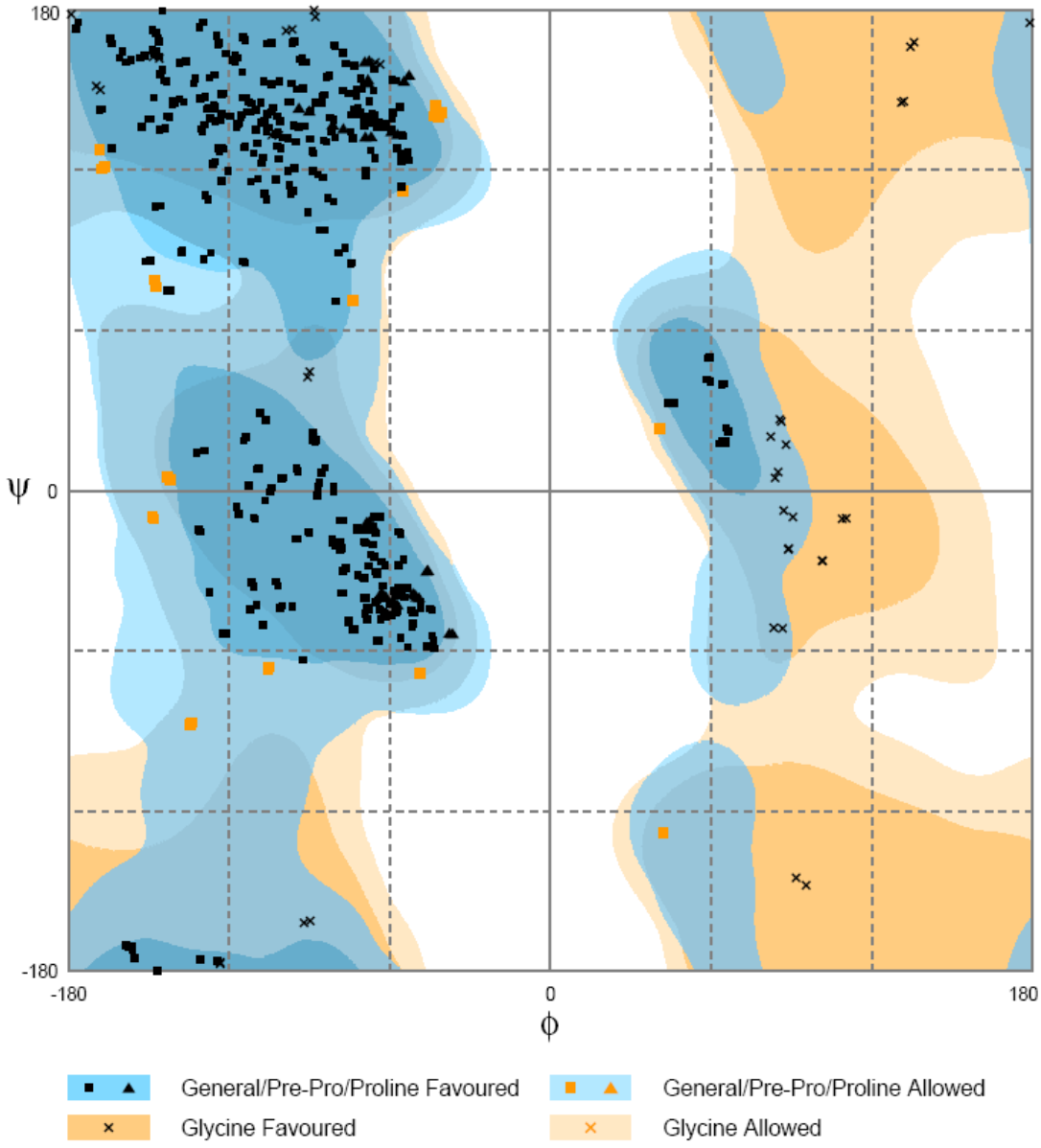

Number of residues in favoured region (~98.0% expected)	: 502 (95.4%)
Number of residues in allowed region (~2.0% expected)	: 24 (4.6%)
Number of residues in outlier region	: 0 (0.0%)

Figure 24. Ramachandran plot of refined bovine thrombin-4AS soak structure. Plot was generated using RAMPAGE.[115]

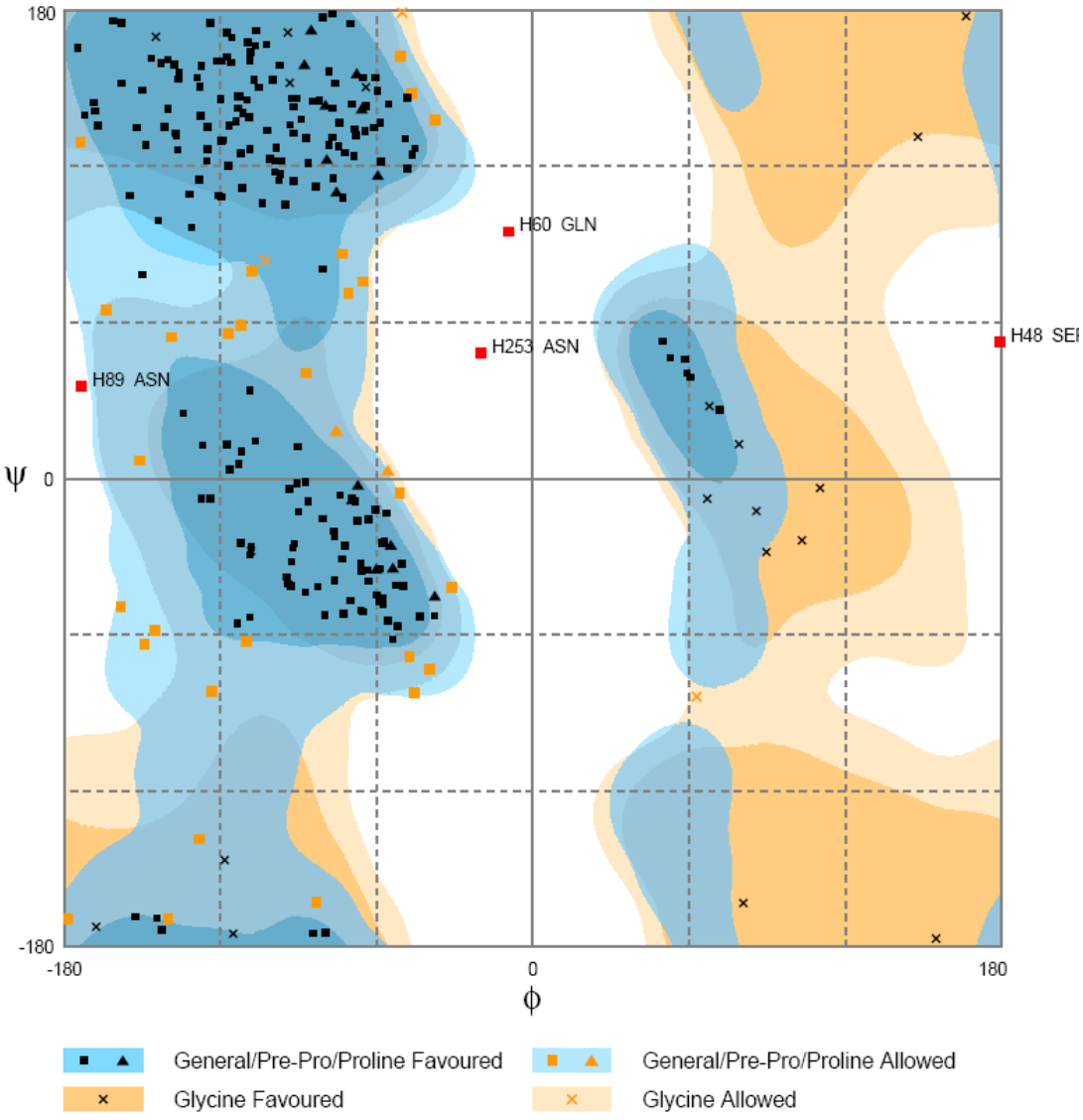

Number of residues in favoured region (~98.0% expected)	: 237 (86.5%)
Number of residues in allowed region (~2.0% expected)	: 33 (12.0%)
Number of residues in outlier region	: 4 (1.5%)

Figure 25. Ramachandran plot of refined human PPACK thrombin form-I. The plot was generated using RAMPAGE.[115]

2.3 Experimental

2.3.1 Crystallization of Native Bovine thrombin and Human PPACK thrombin-4AS co-crystals

Bovine thrombin and human thrombin were purchased from Haematologic Technologies Inc. (Essex Junction, VT). They were supplied in vials containing 10mg/ml thrombin in 50 % v/v glycerol solution. PPACK was purchased from BioMol Inc. Bovine thrombin was exchanged with 10 mM Tris-HCl, pH 8.0, and 50 mM NaCl using Amicon YM-10 ultracentrifugation tubes. The protein solution was stored in 10 µl aliquots at -80°C for future use. Human thrombin was diluted to 1 mg/ml using 0.2 M Phosphate buffer, pH 6.5, and incubated with a 10-fold molar excess of PPACK for 20 min at 20 °C. The solution was then exchanged with 2 mM MOPS buffer, pH 7, 0.1 M NaCl and 0.05 % w/v NaN_3. The solution was concentrated to 10 mg/ml concentration and stored at 4 °C.

Initial crystals of native bovine thrombin were obtained using the conditions reported by Iyaguchi et. al. by hanging drop vapor diffusion using 3 µl reservoir and 3 µl protein solution. The reservoir solution consisted 500 µl of 0.1 M sodium citrate, pH 5.6, 15 % w/v PEG 4000 and 20 % w/v 2-propanol. Tetragonal-bipyramidal crystals of dimensions 0.05 mm x 0.05 mm x 0.05 mm were obtained in two days at 25 °C.

Optimization of this condition was done by changing various parameters as listed in **Table 7.** Apart from the conditions listed in the table, crystallization was also tried with different crystallization methods like sitting-drop, sandwich drop and micro-dialysis and different pH conditions (5.5 to 7.0). Optimized crystals of 0.125 x 0.125 x 0.125 mm size

Table 7. Different conditions used to optimize the crystallization of native bovine thrombin crystals. pH under all conditions was 6.2.

Condition #	[Sodium Citrate] (M)	[2-Propanol] (v/v)	[PEG 3350] (w/v)	Other additive
1.	0.1	5	20	-
2.	0.1	10	20	-
3.	0.1	15	20	-
4.	0.1	20	20	-
5.	0.1	25	20	-
6.	0.1	15	19.5	-
7.	0.1	15	20.5	-
8.	0.1	15	20	5 mM $CaCl_2$
9.	0.1	15	20	1 mM $CaCl_2$
10.	0.1	15	20	3 % v/v Glycerol
11.	0.1	15	20	5 % v/v Glycerol
12.	0.1	15	20	10 % v/v Glycerol
13.	0.05	15	20	-
14.	0.1	15	20	3 % v/v MPD
15.	0.1	15	20	5 % v/v MPD
16.	0.1	-	20	10 % v/v MPD
17.	0.1	-	20	15 % v/v MPD
18.	-	15	20	0.1 M MES
19.	-	15	20	0.1 M Cacodylate
20.	-	15	20	0.1 M PIPES

were obtained by hanging-drop vapor diffusion using 3 µl reservoir and 3 µl protein solution in one and a half day at 25 ºC. The reservoir solution consisted of 500 µl of 0.1 M sodium citrate, pH 6.2, 20 % w/v PEG 3350 and 15 % v/v 2-propanol.

Human PPACK thrombin crystal form-I, was obtained using hanging-drop vapor diffusion method. 3 µl of solution containing 5 mg/ml human PPACK thrombin incubated overnight with a 10 fold molar excess of 4AS was mixed with 3 µl of reservoir solution. Reservoir consisted of 500 µl of 0.1 M Tris-HCl, pH 8.5 and 25 % v/v t-butanol. Large crystals of 0.25 mm x 0.25 mm x 1.5 mm were obtained in a week at 20 ºC.

2.3.2 Data Collection

Diffraction experiments were performed on Raxis IV (Rigaku Americas Co.) under cryo-cooling conditions at 100 K. Native bovine thrombin crystals grown as described in the previous section, were swiftly taken out from the mother liquor using a nylon loop and flash-frozen under a stream of liquid nitrogen on the goniometer head. The crystals did not require cryo-protection due to the presence of 2-propanol in the mother liquor, which acts as a cryo-protecting agent. Indexing of initial still frames indicated a tetragonal space group, which requires a minimum data of 45°. Since redundant data was desirable, the diffractometer was programmed to collect 0.5° oscillation frames from φ angles 0° to 180° at 0.5° intervals (360 frames) and an exposure time of 15 minutes and crystal-to-detector distance of 150 mm. Once the data collection was complete, the data was integrated using d*trek program under the CrystalClear software package (Rigaku Americas Co.). Complete data-sets were collected on several single crystals and the best data set was used for structure determination.

In order to prepare 4AS derivatives of native crystals, three hanging drops containing increasing concentrations of 4AS (with the highest concentration of 5mM 4AS) in the mother liquor were equilibrated against a reservoir solution for a day. The next day, native bovine thrombin crystals which were previously grown were consecutively transferred into the pre-equilibrated drops containing increasing concentrations of 4AS. The crystals were soaked in each drop for 2 hours. After the third soaking step, the crystals were mounted on the goniometer head as described for native bovine thrombin crystals.

0.5° oscillation frames were collected from φ angles 0 to 180° at intervals of 0.5° and exposure time of 10 minutes and crystal-to-detector distance of 150 mm. The data was integrated, scaled and merged using d*trek. Two data sets were collected using single crystals, the best of which was used for structure determination.

Initial diffraction experiments on Human PPACK thrombin crystal form-I showed that the crystals required cryo-protection. Cryo-protection was achieved by fast, consecutive transfers of the crystal in increasing concentrations of glycerol (10 % v/v, 15 % v/v, 20 % v/v) in mother liquor, using a nylon loop, after which the crystal was immediately mounted on goniometer head. 0.5° oscillation frames from 0° to 180° were collected using exposure time of 5 minutes and crystal to detector distance of 110 mm. The data was integrated, scaled and merged using d*trek. Several data sets were collected. Some of the crystals showed overlapping diffraction patterns indicating cracking of crystal or presence of epitaxial twinning. The best data-set was used for determining the structure. The data collection protocols for native bovine crystals, its 4AS derivatives and human PPACK thrombin crystal form-I are summarized in **Table 8.**

Merged reflections from d*trek are in the form of intensities. The intensities were converted to amplitudes using TRUNCATE program in CCP4 program suite 6.1.0.[107] In doing so, the program assumes negative intensities as zero and takes a square-root of the reflection intensities. Analysis of Matthew's coefficient probabilities[108] suggested two molecules of bovine thrombin per asymmetric unit and one molecule of human PPACK thrombin per asymmetric unit.

Table 8. Data collection protocol

Parameter	Native bovine thrombin	Bovine thrombin-4AS soaks	Human PPACK thrombin form-I
Cryo-protecting conditions	Not required	Not required	To 20 % glycerol in steps
Soaking conditions	-	5 mM β-5MSC in mother liquor	Crystal grown in 1 mM β-5MSC
Crystal to detector distance	150 mm	150 mm	110 mm
Exposure time	15 min	10 min	5 min
Start and end angle	0° – 180°	0° – 180°	0° - 180°

2.3.3 Structure determination

An automated molecular replacement (MR) search was done using PHASER 2.1 in the molecular replacement module of CCP4. The coordinates of L and H chains of 1MKX were used as a search model for native bovine thrombin and 4AS soak. Single solutions were obtained for space group $P4_32_12$ for native bovine thrombin and its 4AS derivative. High log likelihood gains (LLG) and translation function Z-scores (TFZ) indicated that the solution found were correct.

Previously solved structure of human PPACK thrombin (PDB ID: 1PPB) was used as a search model for MR for human PPACK thrombin from-I. Single solution was found in $P2_12_12_1$ space group. The summary of phasing by molecular replacement is shown in **Table 9.**

Table 9. Molecular replacement summary.

	Native bovine thrombin	**Bovine thrombin-5AS soaks**	**Human PPACK thrombin form-I**
Search model (PDB ID)	1MKX	1MKX	1PPB
Sequence identity	100%	100 %	100 %
Nmol/assymetric unit	2	2	1
RF Z	11.3	14.6	19.9
TFZ	50.3	19.5	33.7
LLG	2035	2034	1245

In order to remove phase bias from the models obtained from molecular replacement, initial cycle of refinement was done using simulated annealing in Phenix 1.4-3[109]. For human PPACK thrombin structure, simulated annealing in CNS 1.2 was used rather than phenix. This was because the human PPACK thrombin data is of relatively low resolution. At low resolution there is a higher parameter:observables ratio which can lead to over-refinement. Phenix.refine uses a cartesian coordinate refinement. This has higher number of refinement parameters, increasing the possibility of over-fitting at low resolution, as the number of observables is low relative to the parameters being refined.

The models obtained from simulated annealing were examined in Coot 0.5.2 against weighted $2F_o$-F_c (at 1σ contour level) and F_o-F_c (at 3σ contour level) difference maps.[110] The model was manually fit to $2F_o$-F_c density using utilities in Coot. This was followed by a restrained refinement in REFMAC 5.5. This cycle of manual fitting followed by restrained refinement was repeated until no further improvement in the model was observed. To guide this process the R and R_{free} were monitored throughout the process.

2.4 Discussion

Reasons for the absence of density to account for 4AS were investigated. One possible reason could be that the affinity of ligand is diminished in the crystallization buffer. But, since the two structures that were solved, were from crystal forms grown in significantly different buffer, pH and ionic strengths; the chances of this being the case is low and could point to a general low affinity of 4AS towards thrombin. The affinity of 4AS could not be determined using the fluorescent probe para amino-benzamidine due to a high amount of interference from 4AS. From the fluorescence experiments, it was also observed that 4AS did not give any change in fluorescence emission in presence or absence of thrombin. This precluded the determination of 4AS affinity using reverse titrations.

Another possibility could be that the crystallographic contacts might be blocking the binding site of 4AS. Examining the packing arrangement of the asymmetric unit and its neighboring symmetry related molecules, in both the structures, revealed a fully free and solvent exposed exosite-II. (see **Figure 26**) It is possible; however, that 4AS binds to a site other than exosite-II which might be unavailable for binding.

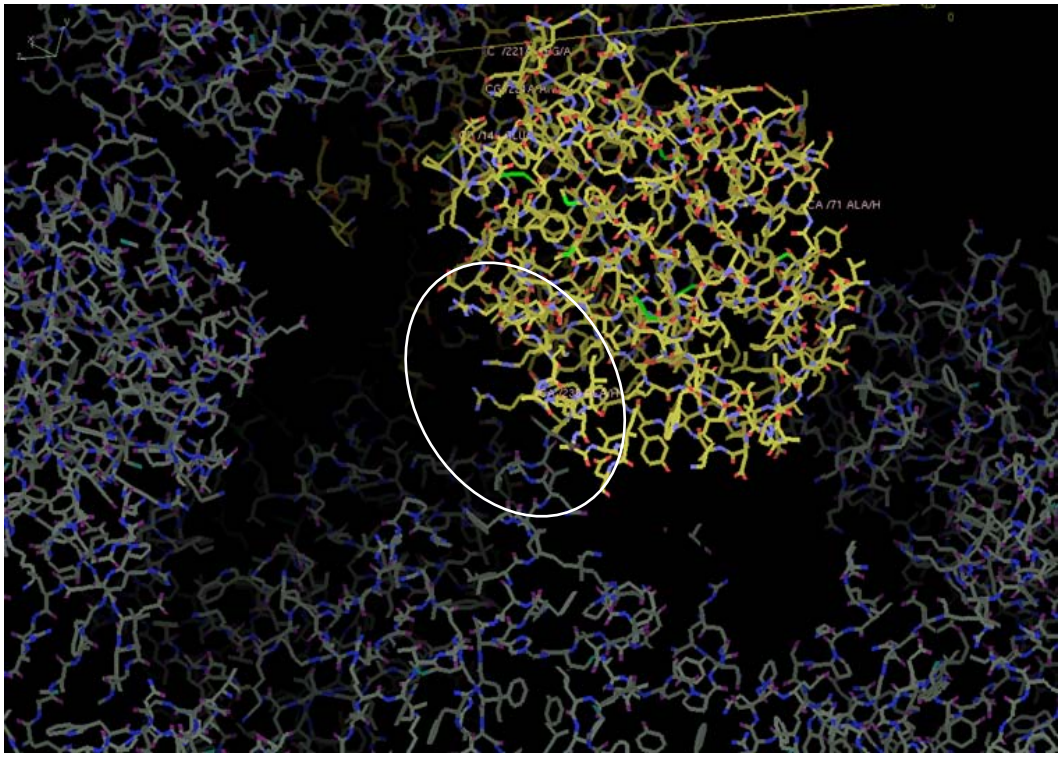

Figure 26. Asymmetric unit of bovine thrombin-4AS soak structure (green) shown along with neighboring symmetry related molecules (grey). The white circle shows unhindered, solvent-exposed exosite-II region.

If the occupancy of the 4AS is low, complete density may not show up. This could especially become problematic in the case where model has large difference between R and R_{free}, as in the case of the PPACK thrombin form-I. The quality of this model was determined by examining $2F_o$-F_c omit maps contoured at 1σ. Omit maps showed good density for all parts of the model (see **Figure 27**), except for the 149-loop which was disordered.

It was recently found (after the determination of both the crystal structures) that 4AS inhibited the hydrolysis of chromogenic substrate by thrombin very weakly (~20%

inhibition of thrombin hydrolysis of chromogenic substrate spectrozyme-TH) at milli molar concentrations.[111] This suggests a weak binding affinity of the ligand towards thrombin and can explain its absence in the electron density map solved by crystallography.

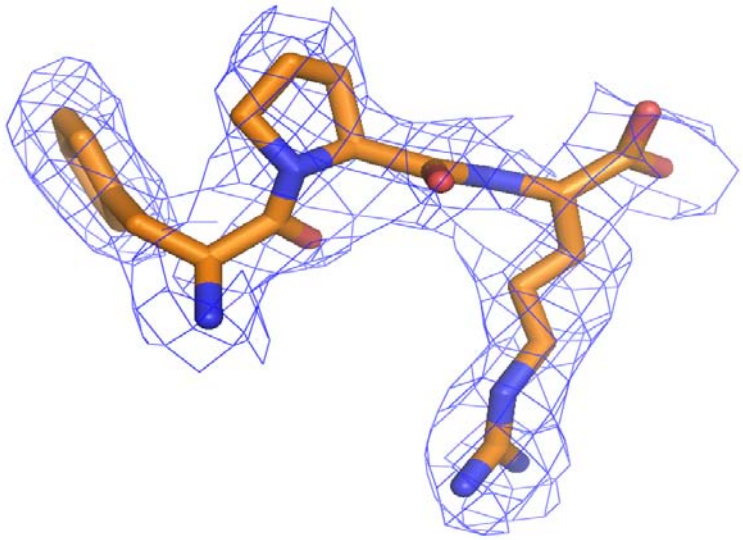

Figure 27. $2F_o$-F_c omit map contoured at 1σ overlaid on FPR fragment in human PPACK thrombin crystal form-I.

In the process of finding the structure of 4AS bound to thrombin, the crystal structure of unliganded native bovine thrombin was determined. The unliganded thrombin structure had not been previously reported due to the autolytic degradation of thrombin in the crystallization drop when stored for a long time. This did not happen under these conditions, possibly due to a rapid crystallization rate. Crystals attain maximum size within 3 days.

Although the structure was solved at a low resolution, several important aspects of the structure could be determined. The structure showed strong density for sodium at the sodium binding site indicating that both monomers in the asymmetric unit were sodium bound. Cα superposition of residues of the refined model on L and H chains of 1MKX shows an identical topology. (see **Figure 28**) Superposition of the active site catalytic triad is shown in **Figure 29.**

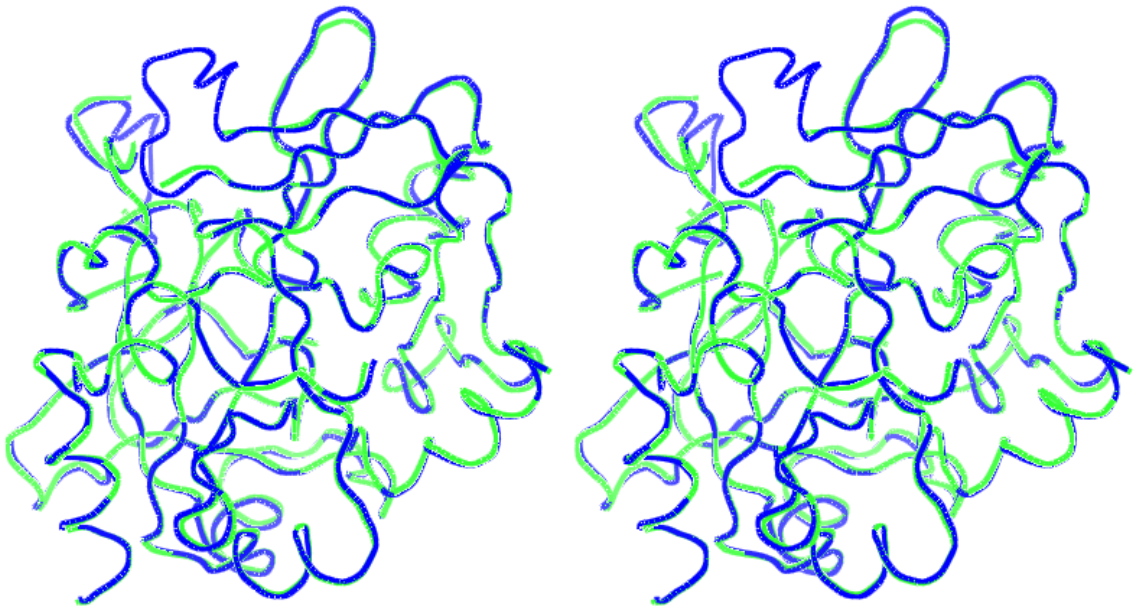

Figure 28. Overlay of protein backbone of bovine thrombin from 1MKX and solved structure

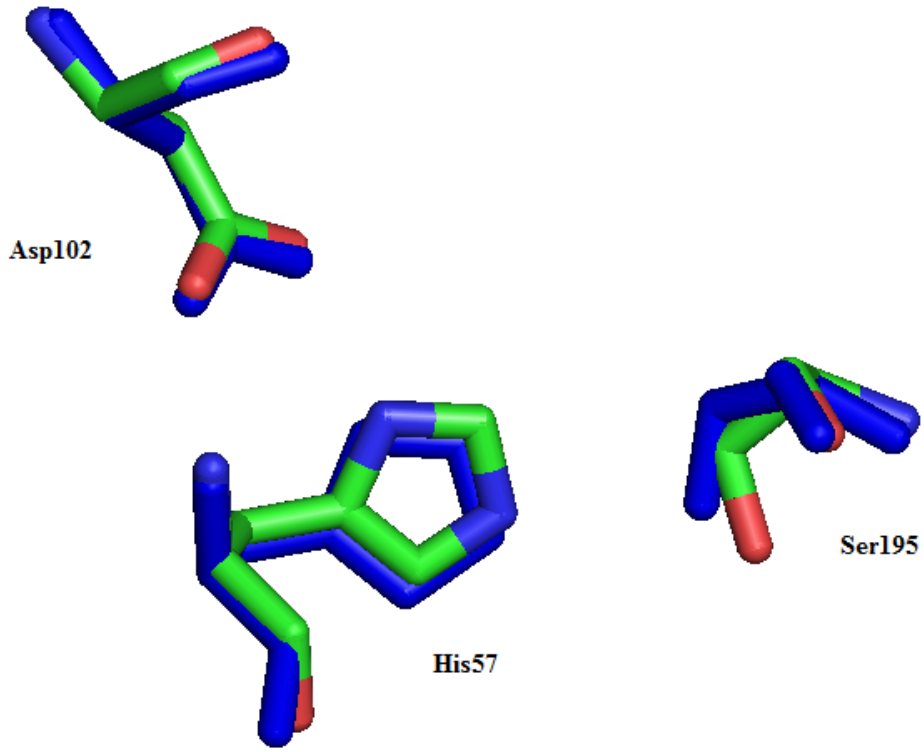

Figure 29. The catalytic triad of L and H chain of 1MKX (blue) superposed on the solved native bovine thrombin structure (green).

CHAPTER 3 BIOPHYSICAL AND BIOCHEMICAL CHARACTERIZATION OF THROMBIN-SUCROSE OCTASULFATE INTERACTION

3.1 Rationale for Specific Aim B

Thrombin-heparin interaction has been previously characterized by monitoring the change in fluorescence intensity of the active site fluorescent probe para-amino benzamidine (PABA). Sucrose octasulfate (SOS) has a sulfated sugar scaffold and would be expected to interact with thrombin in a manner similar to heparin. We propose to find the equilibrium dissociation constant of SOS using the fluorescent probe PABA. By determining the dissociation constant of SOS at different salt concentrations, it is possible to determine the ionic contribution to binding energy. By comparing the salt dependence of SOS-thrombin and heparin-thrombin interaction, which was previously reported,[112] the effect of high charge density of SOS on interaction with exosite-II can be understood.

Since SOS has no physiologically relevant anticoagulant property, the binding of SOS to exosite-II can be exploited to compete with inhibitors binding to exosite-II, and therefore can be envisioned as an antidote for such inhibitors. To explore this potential, competitive enzyme-inhibition experiments with DHPs were designed. Also, combined with the competitive enzyme inhibition experiments, indirect inference of the approximate site of DHP binding can be deduced by solving a crystal structure of thrombin complexed

with SOS. Conditions used to determine native bovine thrombin structure (see section **2.3**) can be used to obtain co-crystals of SOS complexed with thrombin.

3.2 Determination of Equilibrium Dissociation Constant (K_D) and Salt Dependence for Thrombin-Sucrose Octasulfate Interaction

3.2.1 Results

Fluorescence equilibrium binding titration of SOS with thrombin-PABA complex showed a concentration dependent and saturable change (quenching) of thrombin-PABA fluorescence which could be fitted to a quadratic binding isotherm as shown in the equation below:

$$\frac{\Delta F}{Fo} = \frac{\Delta F_{max}}{Fo} \times \frac{\{([P]_o + [L]_o + K_{Dobs}) - \sqrt{([P]_o + [L]_o + K_{Dobs})^2 - 4[P]_o[L]_o}\}}{2[P]_o}$$

where, $\Delta F/F_o$ is the fractional change in fluorescence emission as compared to initial fluorescence F_o where no ligand is present; $[P]_o$ is the protein concentration used; $[L]_o$ is the concentration of the ligand, SOS in this case; K_{Dobs} is the observed equilibrium dissociation constant and ΔF_{max} is the maximal change in fluorescence emission.

The binding isotherms for three different salt concentrations were fitted on the experimental data using Sigma-plot and are shown in **Figures 30-32**. The K_D value determined for each experiment is given in the **Table 10.**

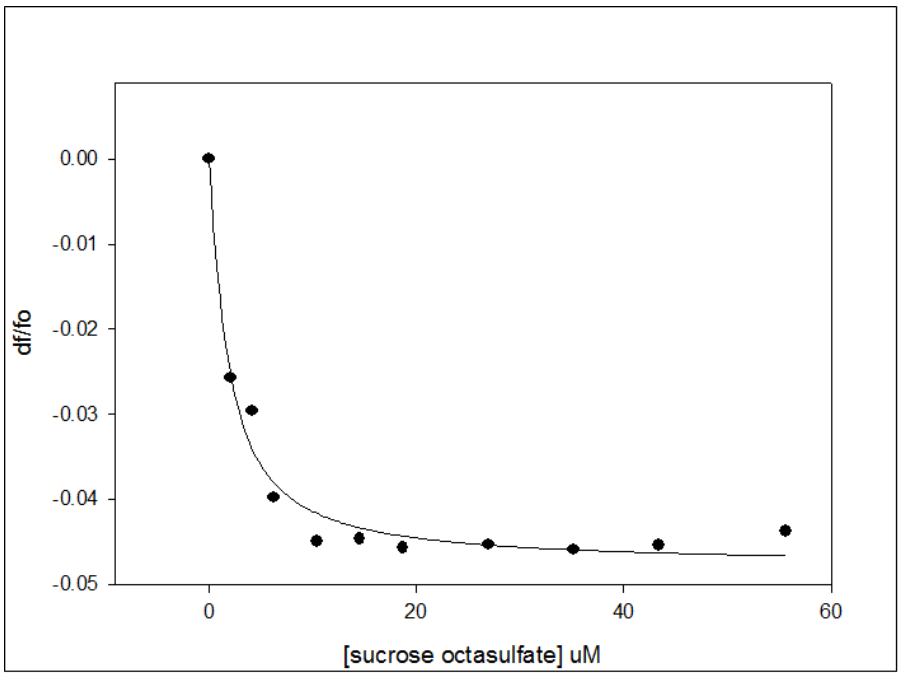

Figure 30. Binding isotherm of sucrose octasulfate for thrombin at 50 mM NaCl.

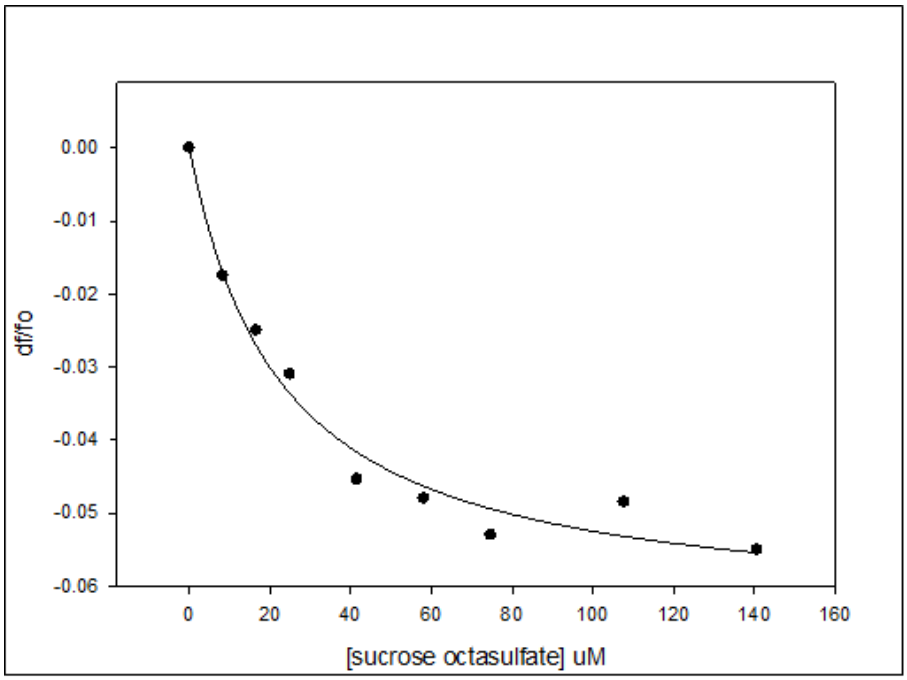

Figure 31. Binding isotherm of sucrose octasulfate for thrombin at 150 mM NaCl

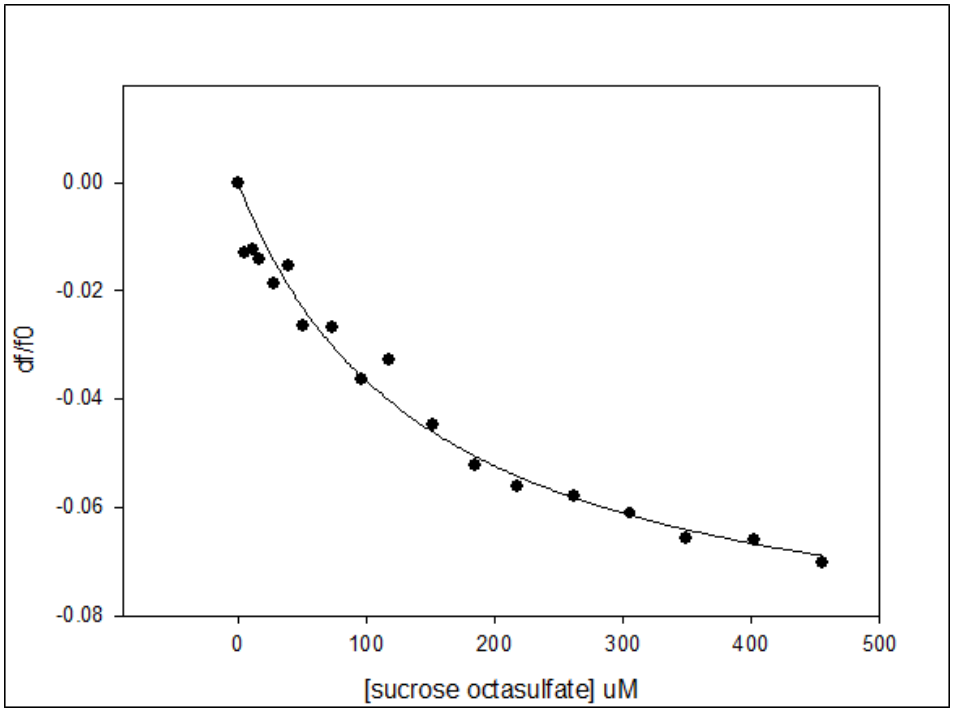

Figure 32. Binding isotherm of sucrose octasulfate for thrombin at 250 mM NaCl.

Table 10. K_{Dobs} values of sucrose octasulfate-thrombin interaction at different salt concentrations.

[NaCl] (M)	K_{Dobs} (μM)	ΔF_{max}
0.05	1.4 ± 0.3	-0.048 ± 0.001
0.15	22.1 ± 4.1	-0.064 ± 0.003
0.25	148.1 ± 24.7	-0.092 ± 0.006

3.2.2 Experimental

Human thrombin was purchased from Haematologic Technologies (Essex Junction, VT) and used as such. Para-amino benzamidine and sodium sucrose octasulfate was purchased from Sigma-Aldrich and BIOMOL international (Plymouth Meeting, PA).

Fluorescence binding titrations were performed in 20 mM Phosphate buffer, 0.1 mM EDTA and 0.1 % PEG 8000 and three different concentrations of NaCl (0.05 M, 0.15 M, and 0.25 M). Acrylic cuvettes coated with PEG 20,000 were used for this purpose. The QM-4 configuration in spectrofluorimeter (PTI ltd.) was used and the experiments were carried out at a constant temperature of 25 °C. The excitation and emission wavelengths of 345 nm and 370 nm respectively and excitation and emission band-pass of 4 nm and 8 nm respectively were selected for the experiments. Each reading was corrected for dilution and background fluorescence of PABA.

3.3 Competitive Enzyme Inhibition Assays of DHPs in Presence of Sucrose Octasulfate

3.3.1 Results

IC_{50} values of FDs in presence of increasing concentrations of SOS were determined using chromogenic substrate Spectrozyme-TH. Semi-logarithmic plots were fitted to the equation given below:

$$Y = Y_o + \frac{Y_M - Y_o}{1 + 10^{(\log [DHP]_o - \log IC_{50})HS}}$$

where, Y is the fractional residual proteinase activity in presence of inhibitor to its absence. Y_M and Y_o are the maximum and minimum possible values of the fractional residual proteinase activity, IC_{50} is the concentration of inhibitor that leads to a 50 % inhibition of enzyme activity and HS is the Hill slope.

The fitted plots showed characteristic sigmoidal shape seen in a standard dose-response curve. It was observed that the graph was shifted to the right as the concentration of SOS used in the experiment increased a characteristic behavior of competitive binding. (see **Figure 33**) However the extent to which the plot is shifted slowly diminishes as the concentration of SOS increases. The IC_{50} values are listed in **Table 11.**

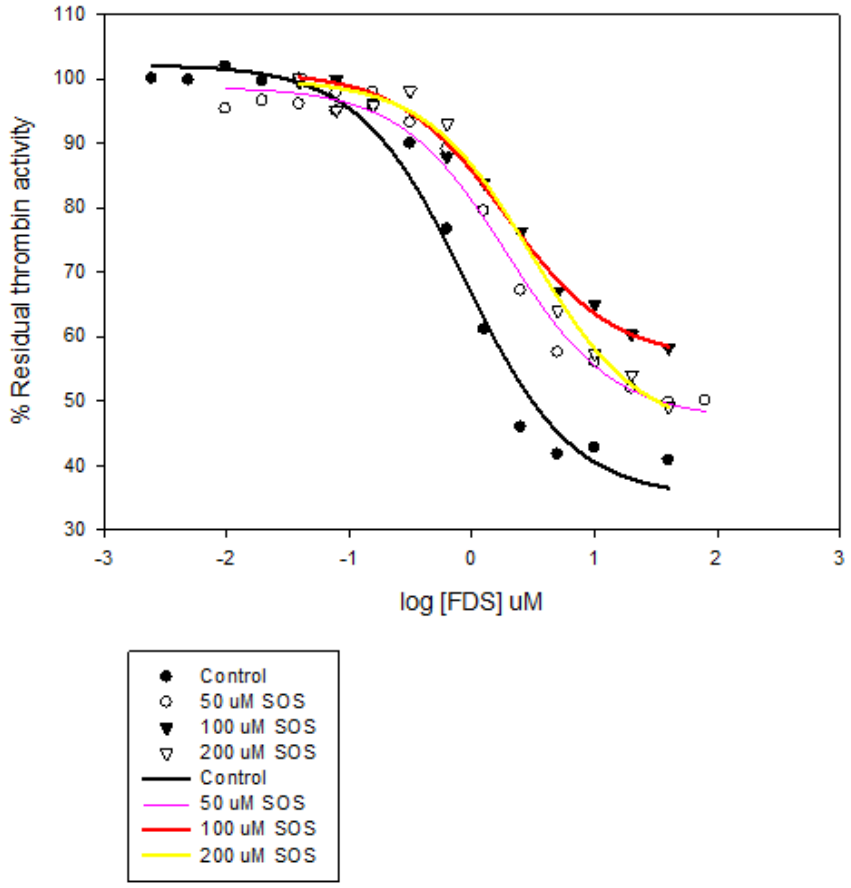

Figure 33. Inhibition of thrombin by FDs in absence and presence of SOS. Each data point is represented by different shaped symbols as shown in the legend. The fit is shown by different colored smooth lines.

Table 11. IC_{50} values of FDs for thrombin in the presence of various concentrations of SOS.

[SOS] (μM)	IC_{50}	Y_o	Y_M	HS
0	0.8	35.1	102.2	0.9
50	1.8	47.2	98.7	0.9
100	1.9	56.5	101.7	1.0
200	2.7	45.2	99.9	0.9

While measuring the residual thrombin activity of control which contained SOS but no DHPs, it was found that SOS itself inhibited thrombin, with the highest inhibition of ~12% seen at 200 μM. To investigate this behavior further, enzyme inhibition assay similar to that used for FDs was performed. The experiment showed that SOS inhibited thrombin with an IC_{50} of 3.8 μM with maximal inhibition of 12.8 %. A semi-logarithmic plot fitted according to the equation given above is shown in **Figure 34.**

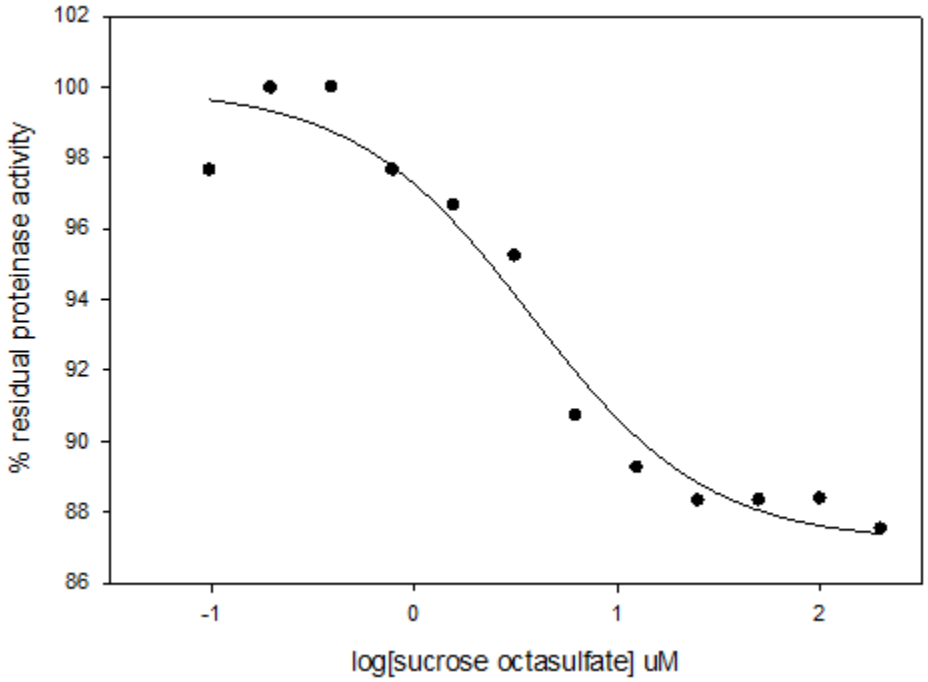

Figure 34. Inhibition of thrombin activity by SOS. Data points used to generate fit (smooth line) are shown by solid circles.

3.3.2 Experimental

Spectrozyme-TH was purchased from American Diagnostica (Greenwich, CT). FDs was synthesized in our lab by the protocol of Monien et. al.[100] Competitive assays of inhibition of thrombin proteinase activity by FDs were done in presence of three different concentrations of SOS (50 µM, 100 µM and 200 µM). An assay where no SOS was present served as control. 15 stock solutions at concentrations from 0.12 µM to 4 mM FDs (concentration calculated using an average molecular weight of 4120 Da) were prepared. 10 µl of each solution was added to 930 µl of phosphate buffer, pH 7.4, 0.1 mM EDTA, 0.1 % v/v PEG 8000 and 0.15 M NaCl in PEG 20,000 coated cuvettes to which 1 µl of

SOS stocks (which make appropriate final SOS concentration) was added. 10 µl of human thrombin (500 nM) was added to each cuvette and mixed. After 10 minutes of incubation, 30 µl of 1 mM Spectrozyme-TH was added successively to each cuvette, rapidly mixed and the residual enzyme activity was determined by measuring the initial rate of increase in absorbance at 405 nM. Residual proteinase activity relative to negative control where no FDs or SOS was present was calculated for each concentration of FDs. IC_{50} values for control, 50 µM SOS, 100 µM SOS and 200 µM SOS were measured by fitting the data from each of the respective experiment to the equation shown in section 3.4.1

Enzyme inhibition assays for determining IC_{50} of SOS were performed using the same procedure used to determine the IC_{50} of DHPs. Stock solutions containing different concentration of SOS ranging from 97 µM to 20 mM were used instead of FDs.

3.4 Crystal Structure Determination of Thrombin-Sucrose octasulfate Complex

3.4.1 Results

The preliminary data for SOS-bovine thrombin co-crystal is shown in the **Table 12**. After successful molecular replacement the structure was refined to an R and R_{free} value of 0.23 and 0.28 respectively. The Ramachandran plot of the refined model is shown in **Figure 35.**

Table 12. Preliminary diffraction data of bovine thrombin-SOS co-crystals

Parameter	Native bovine thrombin
Space group	$P4_32_12$
Unit cell parameters	a=b=87.56 , c=191.99 α=β=γ=90□
Resolution (Å)	27.92-2.2(2.28-2.2)
Number of observed reflections	304797
Unique reflections	38745
Completeness(%)	99.8 (100)
R_{merge}(%)	8.3 (31.1)
Cell Volume (cubic Å)	1472000.543

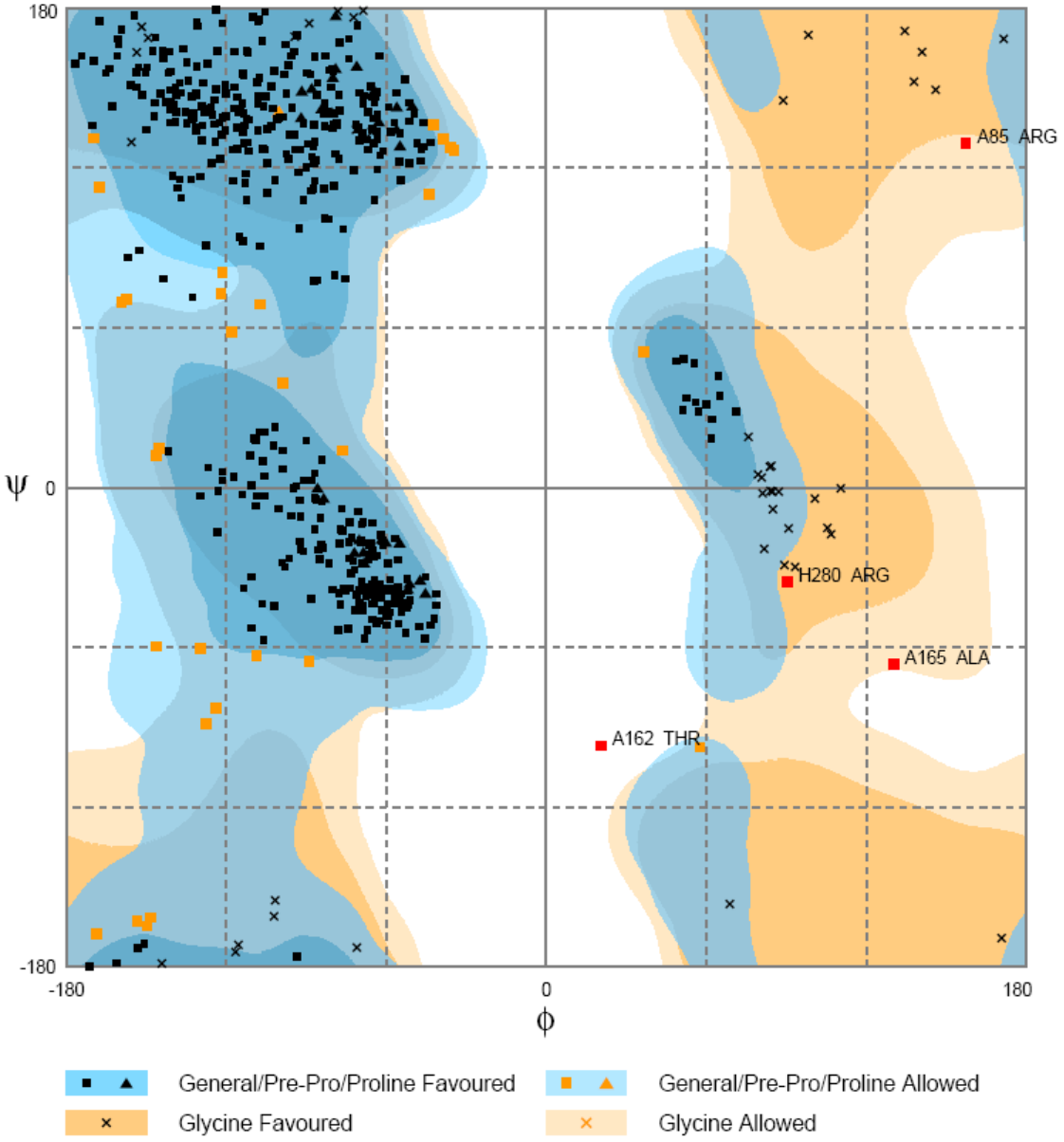

Number of residues in favoured region (~98.0% expected) : 523 (93.9%)
Number of residues in allowed region (~2.0% expected) : 30 (5.4%)
Number of residues in outlier region : 4 (0.7%)

Figure 35. Ramachandran plot of the refined structure of bovine thrombin-SOS co-crystals. The plot was generated using RAMPAGE.[115]

Examining the $2F_o$-F_c and F_o-F_c maps revealed clear density for Na^+ and various ordered water molecules in and around the Na^+ binding site. The two Na^+ ions were put into the model. At the same time, waters showing clear density in the $2F_o$-F_c map along with positive density in F_o-F_c and making at least one contact with the protein were also incorporated into the model. It was observed that there were two large blobs of density close to exosite-II showing up in both the $2F_o$-F_c and F_o-F_c maps. SOS was built into both these regions of densities. The sulfate groups on SOS were fit first followed by the sugar ring. After refinement, the $2F_o$-F_c map showed a good fit for both the SOS molecules. It should be noted that the density for SOS was weak and it was not possible to ascertain features like ring puckering and binding conformation for the two SOS molecules. In order to make sure that SOS was correctly fit, $2F_o$-F_c omit maps, contoured at 1σ were generated. The omit maps showed only broken density for the two sucrose octasulfate molecules, with missing density on the sugar backbone. Interestingly, the density seen in the omit maps was in the region of SOS that interacts with the protein, indicating these regions to be more ordered.

The two molecules of SOS (SRC1 and SRC2) interact with exosite-II of the two thrombin monomers (A and B) forming the asymmetric unit. SRC1 interacts with both the monomers, while SRC2 makes exclusive interactions with exosite-II of one of the monomers (A). (see **Figure 37**) Careful examination of electron density around the two SOS molecules shows that SCR2 makes an ionic hydrogen bond with His91(A) and electrostatic interaction with Lys236(A). Density for these interactions is also present in

the $2F_o$-F_c omit maps. The residues within interacting distance of the two SOS molecules are Arg93(A), Lys101(A), Lys126(B), Lys235(B), Arg240(A) Lys240 (A) and Arg244(A). (see **Figure 38**)

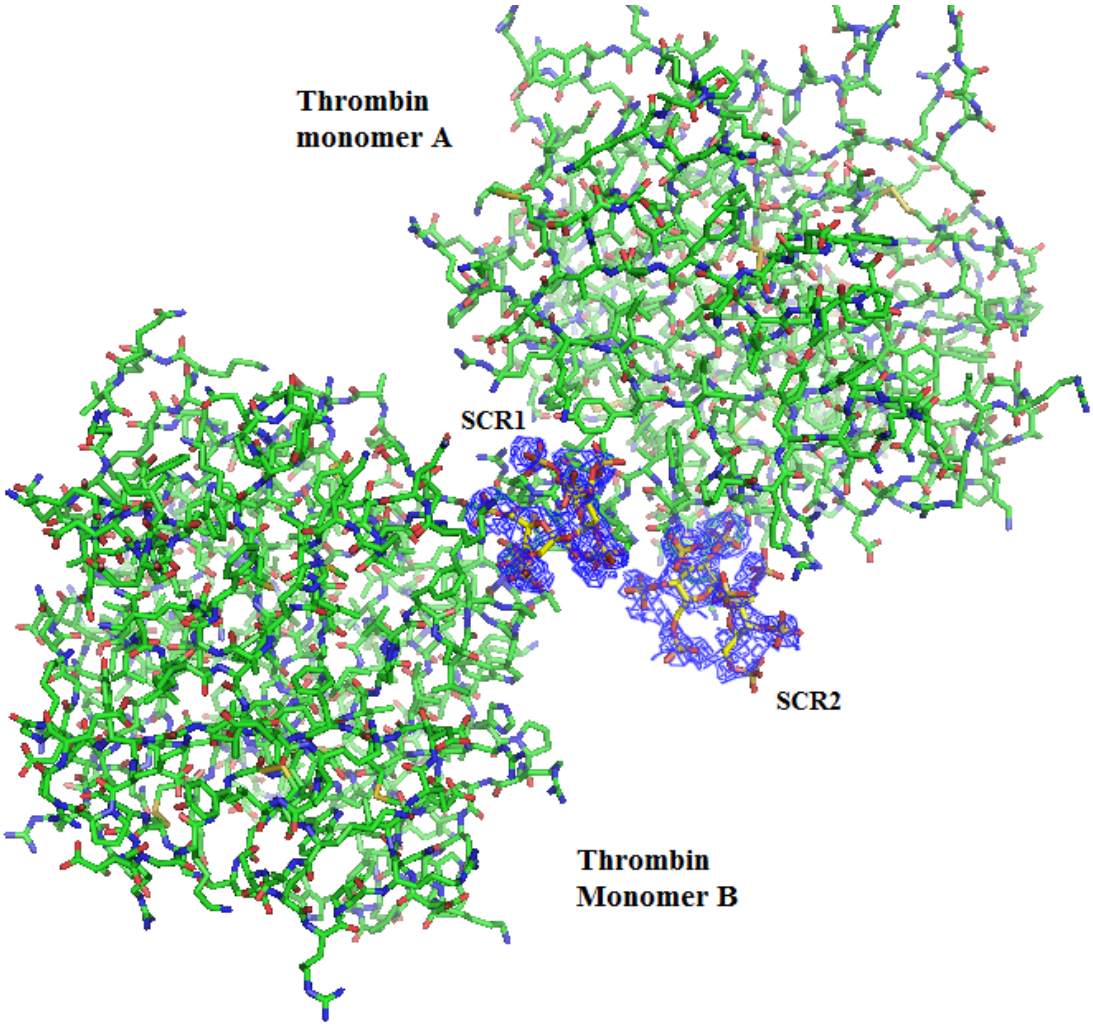

Figure 36. Interaction of two SOS molecules(SCR1 and SCR2) with two thrombin monomers (A and B) in the asymmetric unit. $2F_o$-F_c map contoured at 1σ is shown for SCR1 and SCR2.

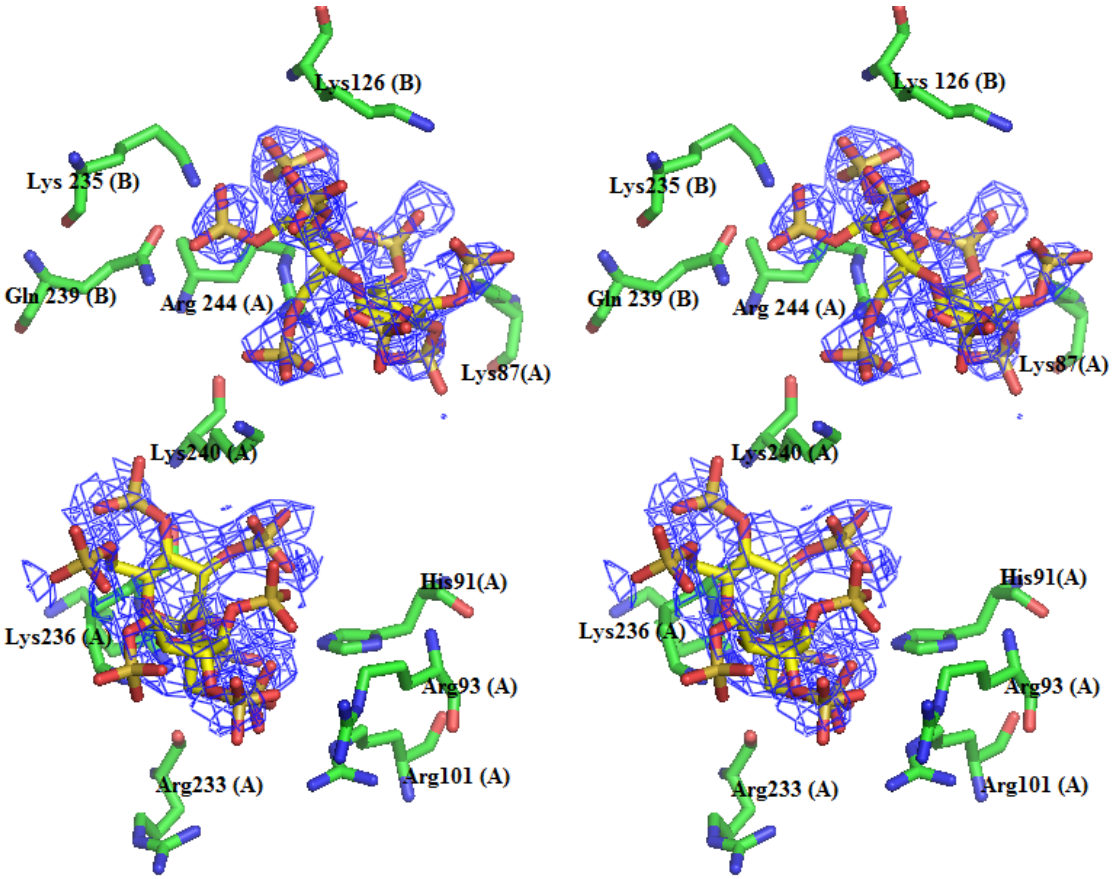

Figure 37. Thrombin residues in interaction distance of the two SOS molecules: SRC1 and SRC2 (shown in stick representation overlaid with 2Fo-Fc map contoured at 1 σ). The letter in parenthesis indicates the thrombin monomer to which each residue belongs.

Examination of the difference maps showed that the occupancy of the SOS molecules was below 1. This could be due to weak or non-specific binding. Since it was possible that citrate ions, present in the buffer, which has a moderately high charge-density might be interfering with binding. An additional data-set was collected in which the citrate was exchanged with cationic buffer bis-tris. Preliminary data for this crystal is given in **Table 13.** The model obtained from this data also showed two large electron density blobs

at the same location as that found in the previous structure. This strongly increases the confidence in the SOS molecules fit in the previous structure.

Table 13. Preliminary diffraction data for bovine thrombin-SOS co-crystals exchanged in bis-tris.

Parameter	
Space group	$P4_32_12$
Unit cell parameters	a=b=87.76 , c=190.62 $\alpha=\beta=\gamma=90^0$
Resolution (Å)	39.86 – 2.3 (2.38 – 2.3)
Number of observed reflections	408377
Unique reflections	33783
Completeness(%)	99.5 (100)
R_{merge}(%)	15.5 (37.7)

3.4.2 Experimental

Bovine thrombin obtained from Haematologic Technologies (Essex Junction, VT) and processed as described in section 2.3.1 was diluted to a concentration of 7 mg/ml using 0.01 M Tris-HCl, pH 8.0, 0.05 M NaCl. It was incubated for an hour with 20 mM SOS and this solution containing 20mM SOS and 7 mg/ml thrombin was used for crystallization under the optimized condition described to crystallize native bovine thrombin. (see section 3.2.1) Crystals of 0.5 mm x 0.5 mm x 0.5 mm dimensions grew at 25 ^{0}C, from hanging drops, containing 4 µl of thrombin-SOS mixture and 4ul of reservoir. Reservoir was composed of ingredients listed in condition # 3 of Table in section 3.2.1.

Frames from φ angles of 0 to 180^0, at 0.5^o intervals, were collected from a single crystal which diffracted beyond 2.2 Å resolution. The data were integrated, scaled and merged using d*trek. Preliminary analysis of the data showed a space group of $P4_32_12$ as

was the case with native bovine thrombin crystals. One of the unit cell dimensions (c) was considerably different as compared to native crystals and 4AS soaks.

The reflection intensities were converted to amplitudes using TRUNCATE[107] and the resulting file was used to perform molecular replacement using coordinates of 1MKX as search model, as described previously for native bovine thrombin crystals and 4AS derivatives. The search gave a single solution in $P4_32_12$ space group and two molecules per asymmetric unit. The model generated from molecular replacement was initially refined by simulated annealing in phenix.refine. The structure was further refined by cycles of manual refinement in Coot 0.5.2[110] using weighted difference maps and restrained refinement in REFMAC 5.2.

Another dataset was collected on SOS-bovine thrombin co-crystal grown under condition # 9 (**Table 7**), but before data collection, the citrate buffer was replaced by 0.05 M bis-tris (keeping all the other conditions including SOS concentration same) by gradual, step-wise exchange. The crystals diffracted to 2.4 Å resolution. The structure was solved and refined to an R factor and R_{free} of 0.24 and 0.30 respectively as described above.

3.5 Discussion

SOS at salt concentration of 150 mM, which is close to the physiological concentration of NaCl, has a K_D of ~ 22 μM. Comparing this with similar chain length heparin fragment shows that SOS interacts with far greater affinity than heparin. The closest heparin homolog in terms of chain length is a tetrasaccharide. Its K_D is reported to be 71±6 μM.[112] On an average there is 2 times higher charge density on SOS compared to

heparin which could be the reason for lower K_D. It has been previously reported that the presence of negatively charged groups on the ligands enhances the binding of ligand with exosite-I and exosite-II. This is due to the presence of a net dipole on these sites. It is possible that higher charge density on SOS leads to a faster associate rates (k_{on}). Although this may not have strong implications in designing better heparinoid mimetics, it adds one more piece of information to the understanding of the nonspecific interaction mechanism of ligands with thrombin exosite-II.

The interaction of polyanionic ligand with protein can be illustrated by the following equation:

$$\mathbf{P^{z+} + L = PL + Z\Psi M^{+}}$$

where P is the protein concentration, L is the polyanionic ligand concentration, Z the number of charged interactions made by the ligand with the protein, Ψ is the fraction of monovalent counterion bound per activator ionic charge that is released on protein binding and can be taken as 0.8. M^+ is the monovalent cation released when L binds to P. The K_D for such equilibrium can be described by the following equation:

$$\mathbf{K_{D(Non-ionic)} = \frac{[P^{z+}][L]}{[PL][M^+]^{Z\Psi}} = \frac{K_{D(obs)}}{[M^+]^{Z\Psi}}}$$

Rearranging this gives:

$$\mathbf{\log K_{D(obs)} = \log K_{D(Non\text{-}ionic)} + Z\Psi \log[Na^+]}$$

Plotting $\log K_{D(obs)}$ vs $\Psi \log[Na^+]$ gives a straight line with slope of Z and y-intercept of $\log K_{D(Non\text{-}ionic)}$. The above equation was used to determine the value of $K_{D(Non\text{-}ionic)}$ and Z (number of ionic interactions per number of ligand bound) for SOS interaction

with thrombin. Figure 38 shows the plot of $\log K_{Dobs}$ vs $\Psi\log[NaCl]$ for 50 mM, 150 mM and 250 mM NaCl. Fitting a straight line through the data-points gave a slope of 3.54 and a Y-intercept of -2.045. (see **Figure 38**) This means that the thrombin-SOS interaction has approximately 3.54 charged interactions and a $K_{D(Non\text{-}ionic)}$ of 6.2 mM.

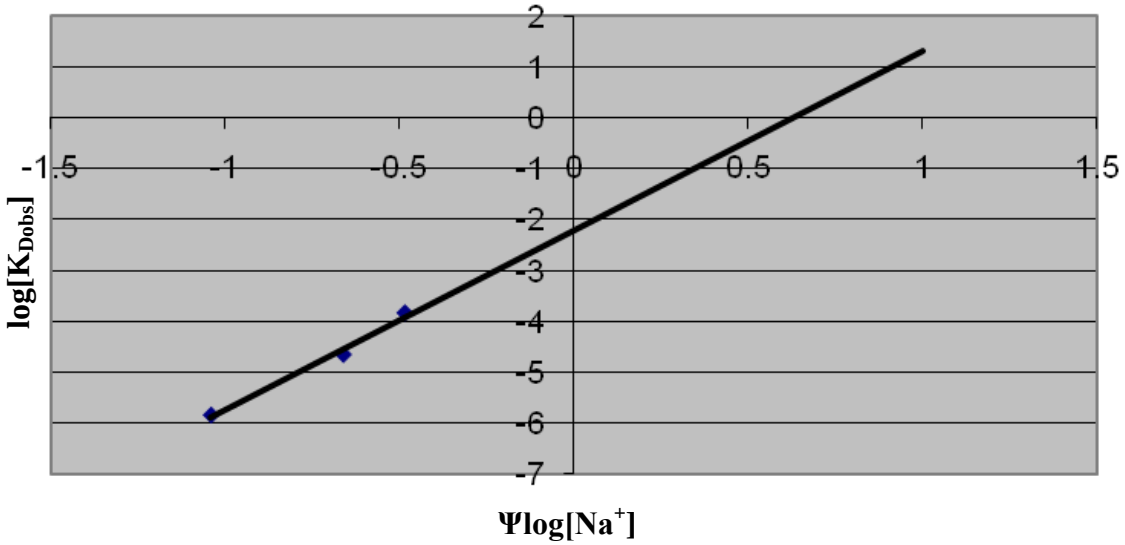

Figure 38. Salt dependence plot of thrombin-SOS interaction.

Competitive experiments with FDs described in section 3.4 can be quantitatively analyzed by the Dixon-Webb relationship given by the following equation:

$$IC_{50\,calc.} = IC_{50\,measured}\left(1 + \frac{[SOS]_o}{K_{D\,SOS}}\right)$$

A true competitor would shift the log dose-response curve to the right by a magnitude depending on the K_D and concentration of the competitor as described by this relationship. Using the K_D determined in section 3.1 and the experimental IC_{50} values measured at different concentrations of SOS we can calculate IC_{50calc}. **Table 14** shows IC_{50calc} values. A graphical representation of the representation of this is shown in **Figure 39**. Clearly SOS

is not a true competitor of FDs. The heterogeneous nature of FDs and the fact that SOS itself inhibits thrombin, further complicates this analysis.

Table 14. Comparision of $IC_{50measured}$ and IC_{50calc}.

[SOS] µM	IC_{50} measured (µM)	$IC_{50\ calc}$ (µM)
0	0.8	0.8
50	1.8	4.2
100	1.9	10.5
200	2.7	26.7

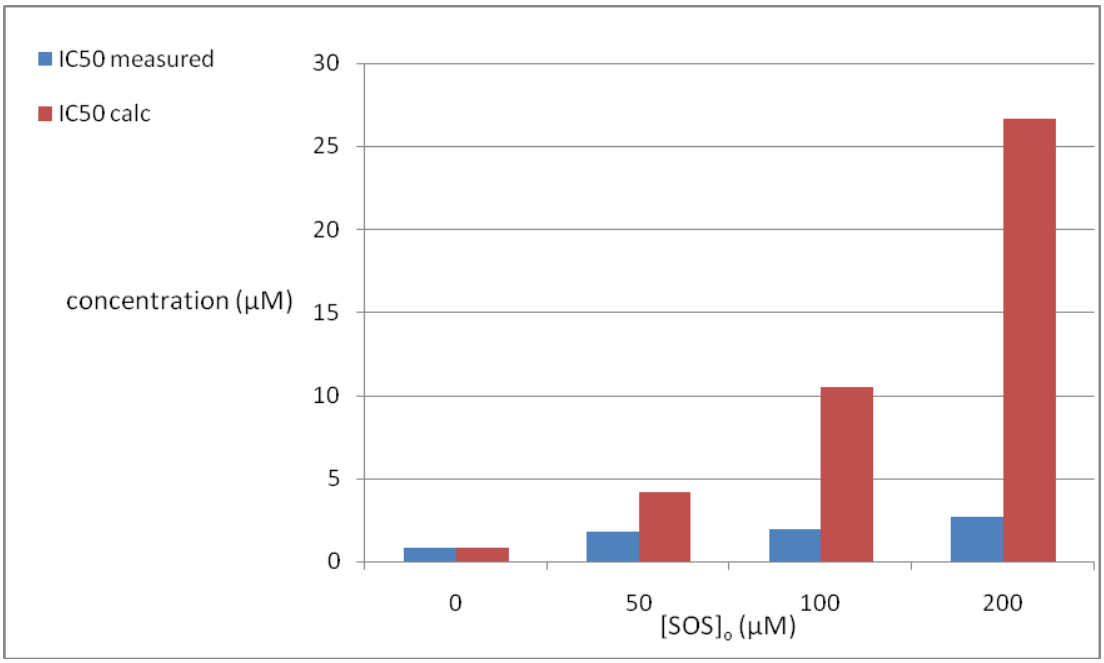

Figure 39. Graph of $IC_{50measured}$ measured experimentally at different concentrations of SOS(blue) and IC_{50calc} calculated using Dixon-Webb relationship.

Determination of the structure of bovine thrombin complexed with sucrose octasulfate shows two SOS molecules bound to thrombin. The additional structure solved without citrate, which was thought to interfere in the binding also revealed density for SOS at the same site as that solved in the previous structure. It should be noted that the density observed in the absence of citrate was not more well-defined than that observed with

citrate suggesting that the binding is still weak and possibly has multiple binding orientations.

Comparing the neighboring residues to the fitted SOS molecules, shows that SCR2 interacts only with thrombin monomer A and SCR1 interacts with exosite-II of both thrombin monomers (A and B). However, the interacting surface of SCR1 with monomer B is small compared to monomer A. It is possible that the interaction with thrombin monomer B is an artifact of crystal packing. SCR2 interacts with monomer A in a similar mode to the interaction of heparin octasaccharide with exosite-II. (see **Figure 40**)

In order to correlate the inhibition of thrombin cleavage of chromogenic substrate (section 3.4) with the structure results, the Cα residues of the refined structure was superposed on 1MKX. No significant difference was found except for the 149-loop. The 149-loop has been reported to be disordered in various structures previously published. In the current structure it was also found to be disordered. For most of its residues, density was only observed for the protein back-bone. No differences were found when the active site residues (His57, Asp102, and Ser195) were superposed on the corresponding residues of 1MKX.

It is possible that the conformational change may have been masked due to crystal packing in this crystal form. Many previously reported structures of thrombin bound to exosite ligands fail to show any conformational change, even when in-solution studies indicate an allosteric perturbation of structure.[47, 76, 113] In a recently reported structure of

thrombin complexed with suramin which was shown to inhibit thrombin by binding to exosite-II, the thrombin molecule did not show any significant conformational change.[85]

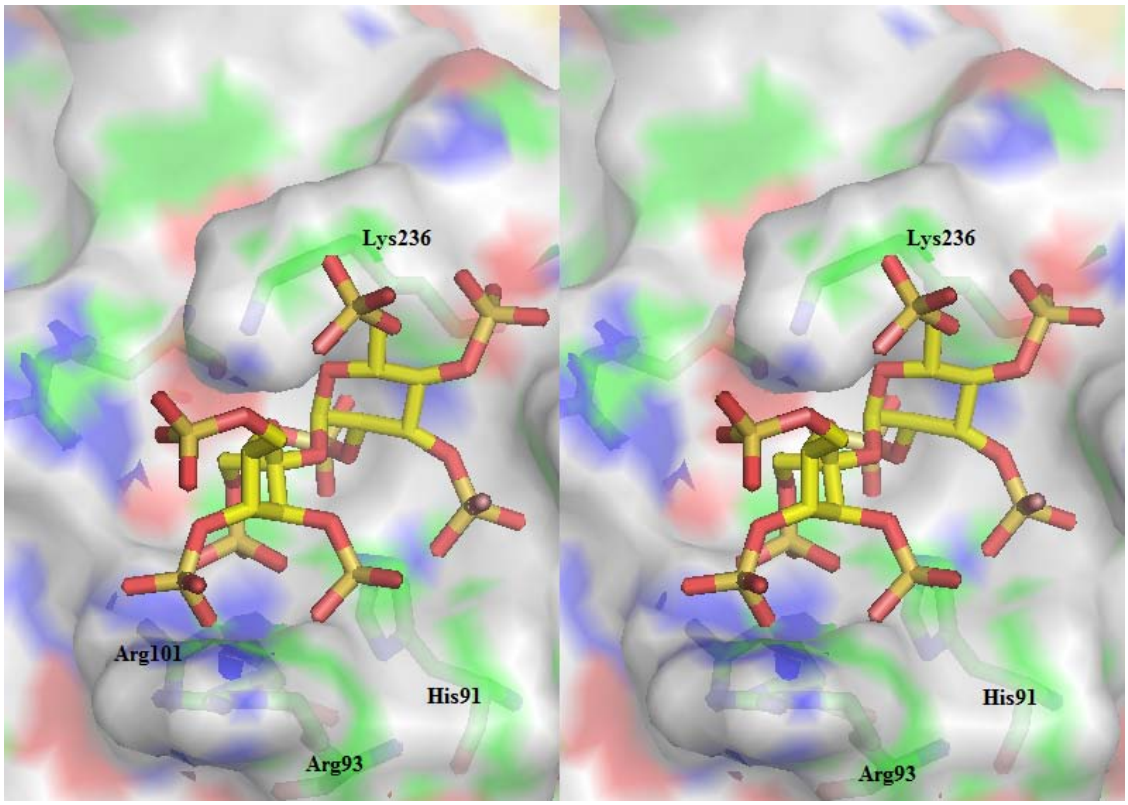

Figure 40. Interaction of sucrose octasulfate molecule SCR2 (stick representation) with thrombin monomer (semi-transparent electrostatic surface representation). Important thrombin residues are also shown in stick representation and are labeled.

3.6 Conclusion and Significance of Work

Refined structures of bovine thrombin-4AS soaks and human PPACK thrombin-4AS co-crystals were solved. The structure did not show any density for the ligand. In the process a new crystal form of native bovine thrombin in unliganded state was solved. This crystal form can be used to study thrombin-ligand interactions, especially for ligands binding to exosite-II, since it is not involved in any crystallographic contacts.

K_D of SOS for thrombin was determined using fluorescence spectroscopy with the secondary probe PABA. The K_D was significantly lower than heparin fragment of comparable size. The salt dependence of K_D revealed that a significant contribution to the binding energy is due to ionic forces. The number of charge interaction per molecule of SOS bound to thrombin was calculated to be 3.5. Competitive enzyme inhibition experiments of FDs using increasing concentrations of FDs were carried out. It was found that there was ~2-3 fold increase in the IC_{50} of FDs at the highest concentration of SOS used (200 μM). Based on the Dixon-Webb relationship it was found that SOS is not an ideal competitor for FDs.

The crystal structure of bovine thrombin cocrystallized with SOS showed two molecules of SOS bound to the two thrombin molecules in the asymmetric unit via exosite-II. One of the SOS molecules which was bound exclusively to one thrombin monomer showed interactions very similar to that made by heparin octasachharide. Key among the interactions are Lys236, His91, Arg93 and Arg101. Characterization of this interaction novel interaction mode of sucrose octasulfate adds to our current evidence of compounds binding to exosite-II like heparin, but unlike heparin showing direct inhibitory properties.

3.7 Future Direction

Recent studies have shown that 4AS is a more effective inhibitor for fXa than for thrombin. Crystallographic analysis of 4AS bound to fXa could be pursued. The optimized conditions for obtaining bovine thrombin crystals can be exploited for future soaking or co-crystallization experiments with tighter binding compounds based on the DHPs

scaffold. Apart from crystallography, in order to gain a better understanding of the allosteric mechanism of DHPs, a chromogenic substrate library can be used to identify changes in substrate specificity induced by the DHPs. Such work has been extensively reported by Vindigni et. al.[114] Since SOS was found to inhibit thrombin, steady state kinetic studies study could shed light on its mode of thrombin inhibition.

List of References

List of References

1. Davie, E. W. A brief historical review of the waterfall/cascade of blood coagulation. *J. Biol. Chem.* **2003**, *278*, 50819-50832.

2. Hougie, C. The waterfall-cascade and autoprothrombin hypotheses of blood coagulation: personal reflections from an observer. *J. Thromb. Haemost.* **2004**, *2*, 1225-1233.

3. Bloom, J. W.; Nesheim, M. E.; Mann, K. G. Phospholipid-binding properties of bovine factor V and factor Va. *Biochemistry* **1979**, *18*, 4419-4425.

4. Mann, K. G.; Nesheim, M. E.; Hibbard, L. S.; Tracy, P. B. The role of factor V in the assembly of the prothrombinase complex. *Ann. N. Y. Acad. Sci.* **1981**, *370*, 378-388.

5. Nesheim, M. E.; Mann, K. G. Thrombin-catalyzed activation of single chain bovine factor V. *J. Biol. Chem.* **1979**, *254*, 1326-1334.

6. Nesheim, M. E.; Taswell, J. B.; Mann, K. G. The contribution of bovine Factor V and Factor Va to the activity of prothrombinase. *J. Biol. Chem.* **1979**, *254*, 10952-10962.

7. Tracy, P. B.; Peterson, J. M.; Nesheim, M. E.; McDuffie, F. C.; Mann, K. G. Interaction of coagulation factor V and factor Va with platelets. *J. Biol. Chem.* **1979**, *254*, 10354-10361.

8. Fenton, J. W.,2nd; Fasco, M. J.; Stackrow, A. B. Human thrombins. Production, evaluation, and properties of alpha-thrombin. *J. Biol. Chem.* **1977**, *252*, 3587-3598.

9. Davie, E. W. Cloning of fibrinogen, prothrombin, and alpha 1-antitrypsin. *Harvey Lect.* **1981**, *77*, 1-21.

10. Degen, S. J.; Davie, E. W. Nucleotide sequence of the gene for human prothrombin. *Biochemistry* **1987**, *26*, 6165-6177.

11. Degen, S. J.; Davie, E. W. The prothrombin gene and serine proteinase evolution. *Ann. N. Y. Acad. Sci.* **1986**, *485*, 66-72.

12. Degen, S. J.; MacGillivray, R. T.; Davie, E. W. Characterization of the complementary deoxyribonucleic acid and gene coding for human prothrombin. *Biochemistry* **1983**, *22*, 2087-2097.

13. Hansson, K.; Stenflo, J. Post-translational modifications in proteins involved in blood coagulation. *J. Thromb. Haemost.* **2005**, *3*, 2633-2648.

14. MacGillivray, R. T.; Davie, E. W. Characterization of bovine prothrombin mRNA and its translation product. *Biochemistry* **1984**, *23*, 1626-1634.

15. Nelsestuen, G. L.; Zytkovicz, T. H.; Howard, J. B. The mode of action of vitamin K. Identification of gamma-carboxyglutamic acid as a component of prothrombin. *J. Biol. Chem.* **1974**, *249*, 6347-6350.

16. Bode, W. The structure of thrombin: a janus-headed proteinase. *Semin. Thromb. Hemost.* **2006**, *32 Suppl 1*, 16-31.

17. Bode, W. Structure and interaction modes of thrombin. *Blood Cells Mol. Dis.* **2006**, *36*, 122-130.

18. Davie, E. W.; Kulman, J. D. An overview of the structure and function of thrombin. *Semin. Thromb. Hemost.* **2006**, *32 Suppl 1*, 3-15.

19. De Cristofaro, R.; De Candia, E. Thrombin domains: structure, function and interaction with platelet receptors. *J. Thromb. Thrombolysis* **2003**, *15*, 151-163.

20. Wells, C. M.; Di Cera, E. Thrombin is a Na(+)-activated enzyme. *Biochemistry* **1992**, *31*, 11721-11730.

21. Bajzar, L.; Manuel, R.; Nesheim, M. E. Purification and characterization of TAFI, a thrombin-activable fibrinolysis inhibitor. *J. Biol. Chem.* **1995**, *270*, 14477-14484.

22. Nesheim, M.; Bajzar, L. The discovery of TAFI. *J. Thromb. Haemost.* **2005**, *3*, 2139-2146.

23. Nesheim, M.; Wang, W.; Boffa, M.; Nagashima, M.; Morser, J.; Bajzar, L. Thrombin, thrombomodulin and TAFI in the molecular link between coagulation and fibrinolysis. *Thromb. Haemost.* **1997**, *78*, 386-391.

24. Esmon, C. T. The subunit structure of thrombin-activated factor V. Isolation of activated factor V, separation of subunits, and reconstitution of biological activity. *J. Biol. Chem.* **1979**, *254*, 964-973.

25. Kurachi, K.; Fujikawa, K.; Davie, E. W. Mechanism of activation of bovine factor XI by factor XII and factor XIIa. *Biochemistry* **1980**, *19*, 1330-1338.

26. Legaz, M. E.; Schmer, G.; Counts, R. B.; Davie, E. W. Isolation and characterization of human Factor VIII (antihemophilic factor). *J. Biol. Chem.* **1973**, *248*, 3946-3955.

27. Naito, K.; Fujikawa, K. Activation of human blood coagulation factor XI independent of factor XII. Factor XI is activated by thrombin and factor XIa in the presence of negatively charged surfaces. *J. Biol. Chem.* **1991**, *266*, 7353-7358.

28. Schmer, G.; Kirby, E. P.; Teller, D. C.; Davie, E. W. The isolation nd characterization of bovine factor VIII (antihemophilic factor). *J. Biol. Chem.* **1972**, *247*, 2512-2521.

29. Coughlin, S. R.; Scarborough, R. M.; Vu, T. K.; Hung, D. T. Thrombin receptor structure and function. *Cold Spring Harb. Symp. Quant. Biol.* **1992**, *57*, 149-154.

30. Coughlin, S. R.; Vu, T. K.; Hung, D. T.; Wheaton, V. I. Expression cloning and characterization of a functional thrombin receptor reveals a novel proteolytic mechanism of receptor activation. *Semin. Thromb. Hemost.* **1992**, *18*, 161-166.

31. Xu, W. F.; Andersen, H.; Whitmore, T. E.; Presnell, S. R.; Yee, D. P.; Ching, A.; Gilbert, T.; Davie, E. W.; Foster, D. C. Cloning and characterization of human protease-activated receptor 4. *Proc. Natl. Acad. Sci. U. S. A.* **1998**, *95*, 6642-6646.

32. Andersen, H.; Greenberg, D. L.; Fujikawa, K.; Xu, W.; Chung, D. W.; Davie, E. W. Protease-activated receptor 1 is the primary mediator of thrombin-stimulated platelet procoagulant activity. *Proc. Natl. Acad. Sci. U. S. A.* **1999**, *96*, 11189-11193.

33. De Candia, E.; Hall, S. W.; Rutella, S.; Landolfi, R.; Andrews, R. K.; De Cristofaro, R. Binding of thrombin to glycoprotein Ib accelerates the hydrolysis of Par-1 on intact platelets. *J. Biol. Chem.* **2001**, *276*, 4692-4698.

34. Esmon, C. T. The roles of protein C and thrombomodulin in the regulation of blood coagulation. *J. Biol. Chem.* **1989**, *264*, 4743-4746.

35. Esmon, C. T.; Owen, W. G. The discovery of thrombomodulin. *J. Thromb. Haemost.* **2004**, *2*, 209-213.

36. Damus, P. S.; Rosenberg, R. D. Antithrombin-heparin cofactor. *Methods Enzymol.* **1976**, *45*, 653-669.

37. Rosenberg, R. D.; Damus, P. S. The purification and mechanism of action of human antithrombin-heparin cofactor. *J. Biol. Chem.* **1973**, *248*, 6490-6505.

38. Tollefsen, D. M.; Majerus, D. W.; Blank, M. K. Heparin cofactor II. Purification and properties of a heparin-dependent inhibitor of thrombin in human plasma. *J. Biol. Chem.* **1982**, *257*, 2162-2169.

39. Rawlings, N. D.; Tolle, D. P.; Barrett, A. J. MEROPS: the peptidase database. *Nucleic Acids Res.* **2004**, *32*, D160-4.

40. Page, M. J.; Di Cera, E. Evolution of peptidase diversity. *J. Biol. Chem.* **2008**, *283*, 30010-30014.

41. Di Cera, E. Thrombin interactions. *Chest* **2003**, *124*, 11S-7S.

42. Page, M. J.; Di Cera, E. Serine peptidases: classification, structure and function. *Cell Mol. Life Sci.* **2008**, *65*, 1220-1236.

43. Nesheim, M. E.; Mann, K. G. The kinetics and cofactor dependence of the two cleavages involved in prothrombin activation. *J. Biol. Chem.* **1983**, *258*, 5386-5391.

44. Malkowski, M. G.; Martin, P. D.; Guzik, J. C.; Edwards, B. F. The co-crystal structure of unliganded bovine alpha-thrombin and prethrombin-2: movement of the Tyr-Pro-Pro-Trp segment and active site residues upon ligand binding. *Protein Sci.* **1997**, *6*, 1438-1448.

45. Bode, W.; Turk, D.; Karshikov, A. The refined 1.9-A X-ray crystal structure of D-Phe-Pro-Arg chloromethylketone-inhibited human alpha-thrombin: structure analysis, overall structure, electrostatic properties, detailed active-site geometry, and structure-function relationships. *Protein Sci.* **1992**, *1*, 426-471.

46. Birktoft, J. J.; Blow, D. M. Structure of crystalline -chymotrypsin. V. The atomic structure of tosyl- -chymotrypsin at 2 A resolution. *J. Mol. Biol.* **1972**, *68*, 187-240.

47. Vijayalakshmi, J.; Padmanabhan, K. P.; Mann, K. G.; Tulinsky, A. The isomorphous structures of prethrombin2, hirugen-, and PPACK-thrombin: changes accompanying activation and exosite binding to thrombin. *Protein Sci.* **1994**, *3*, 2254-2271.

48. Papaconstantinou, M. E.; Bah, A.; Di Cera, E. Role of the A chain in thrombin function. *Cell Mol. Life Sci.* **2008**, *65*, 1943-1947.

49. Braun, P. J.; Hofsteenge, J.; Chang, J. Y.; Stone, S. R. Preparation and characterization of proteolyzed forms of human alpha-thrombin. *Thromb. Res.* **1988**, *50*, 273-283.

50. Pechik, I.; Madrazo, J.; Mosesson, M. W.; Hernandez, I.; Gilliland, G. L.; Medved, L. Crystal structure of the complex between thrombin and the central "E" region of fibrin. *Proc. Natl. Acad. Sci. U. S. A.* **2004**, *101*, 2718-2723.

51. Carter, W. J.; Cama, E.; Huntington, J. A. Crystal structure of thrombin bound to heparin. *J. Biol. Chem.* **2005**, *280*, 2745-2749.

52. Di Cera, E. Thrombin as procoagulant and anticoagulant. *J. Thromb. Haemost.* **2007**, *5 Suppl 1*, 196-202.

53. Huntington, J. A. Slow thrombin in solution. *Biochem. J.* **2005**, *390*, e1-3.
54. Johnson, D. J.; Adams, T. E.; Li, W.; Huntington, J. A. Crystal structure of wild-type human thrombin in the Na+-free state. *Biochem. J.* **2005**, *392*, 21-28.

55. Zhang, E.; Tulinsky, A. The molecular environment of the Na+ binding site of thrombin. *Biophys. Chem.* **1997**, *63*, 185-200.

56. Huntington, J. A.; Esmon, C. T. The molecular basis of thrombin allostery revealed by a 1.8 A structure of the "slow" form. *Structure* **2003**, *11*, 469-479.

57. Di Cera, E.; Guinto, E. R.; Vindigni, A.; Dang, Q. D.; Ayala, Y. M.; Wuyi, M.; Tulinsky, A. The Na+ binding site of thrombin. *J. Biol. Chem.* **1995**, *270*, 22089-22092.

58. Martin, P. D.; Robertson, W.; Turk, D.; Huber, R.; Bode, W.; Edwards, B. F. The structure of residues 7-16 of the A alpha-chain of human fibrinogen bound to bovine thrombin at 2.3-A resolution. *J. Biol. Chem.* **1992**, *267*, 7911-7920.

59. Qiu, X.; Padmanabhan, K. P.; Carperos, V. E.; Tulinsky, A.; Kline, T.; Maraganore, J. M.; Fenton, J. W.,2nd Structure of the hirulog 3-thrombin complex and nature of the S' subsites of substrates and inhibitors. *Biochemistry* **1992**, *31*, 11689-11697.

60. Brandstetter, H.; Turk, D.; Hoeffken, H. W.; Grosse, D.; Sturzebecher, J.; Martin, P. D.; Edwards, B. F.; Bode, W. Refined 2.3 A X-ray crystal structure of bovine thrombin complexes formed with the benzamidine and arginine-based thrombin inhibitors NAPAP, 4-TAPAP and MQPA. A starting point for improving antithrombotics. *J. Mol. Biol.* **1992**, *226*, 1085-1099.
61. Shaw, E. Synthetic irreversible inhibitors of coagulation enzymes. *Folia Haematol. Int. Mag. Klin. Morphol. Blutforsch.* **1982**, *109*, 33-42.

62. Blomback, B. The N-terminal disulphide knot of human fibrinogen. *Br. J. Haematol.* **1969**, *17*, 145-157.

63. Eaton, D.; Rodriguez, H.; Vehar, G. A. Proteolytic processing of human factor VIII. Correlation of specific cleavages by thrombin, factor Xa, and activated protein C with activation and inactivation of factor VIII coagulant activity. *Biochemistry* **1986**, *25*, 505-512.

64. Foster, D.; Davie, E. W. Characterization of a cDNA coding for human protein C. *Proc. Natl. Acad. Sci. U. S. A.* **1984**, *81*, 4766-4770.

65. Iwanaga, S.; Wallen, P.; Grondahl, N. J.; Henschen, A.; Blomback, B. On the primary structure of human fibrinogen. Isolation and characterization of N-terminal fragments from plasmic digests. *Eur. J. Biochem.* **1969**, *8*, 189-199.

66. Mann, K. G.; Jenny, R. J.; Krishnaswamy, S. Cofactor proteins in the assembly and expression of blood clotting enzyme complexes. *Annu. Rev. Biochem.* **1988**, *57*, 915-956.

67. Takagi, T.; Doolittle, R. F. Amino acid sequence studies on factor XIII and the peptide released during its activation by thrombin. *Biochemistry* **1974**, *13*, 750-756.

68. Bode, W.; Schwager, P. The refined crystal structure of bovine beta-trypsin at 1.8 A resolution. II. Crystallographic refinement, calcium binding site, benzamidine binding site and active site at pH 7.0. *J. Mol. Biol.* **1975**, *98*, 693-717.

69. Bode, W.; Mayr, I.; Baumann, U.; Huber, R.; Stone, S. R.; Hofsteenge, J. The refined 1.9 A crystal structure of human alpha-thrombin: interaction with D-Phe-Pro-Arg chloromethylketone and significance of the Tyr-Pro-Pro-Trp insertion segment. *EMBO J.* **1989**, *8*, 3467-3475.

70. Friedrich, R.; Panizzi, P.; Kawabata, S.; Bode, W.; Bock, P. E.; Fuentes-Prior, P. Structural basis for reduced staphylocoagulase-mediated bovine prothrombin activation. *J. Biol. Chem.* **2006**, *281*, 1188-1195.

71. Vindigni, A.; Di Cera, E. Release of fibrinopeptides by the slow and fast forms of thrombin. *Biochemistry* **1996**, *35*, 4417-4426.

72. Ascenzi, P.; Amiconi, G.; Bode, W.; Bolognesi, M.; Coletta, M.; Menegatti, E. Proteinase inhibitors from the European medicinal leech Hirudo medicinalis: structural, functional and biomedical aspects. *Mol. Aspects Med.* **1995**, *16*, 215-313.

73. Ascenzi, P.; Amiconi, G.; Coletta, M.; Lupidi, G.; Menegatti, E.; Onesti, S.; Bolognesi, M. Binding of hirudin to human alpha, beta and gamma-thrombin. A comparative kinetic and thermodynamic study. *J. Mol. Biol.* **1992**, *225*, 177-184.

74. Rydel, T. J.; Tulinsky, A.; Bode, W.; Huber, R. Refined structure of the hirudin-thrombin complex. *J. Mol. Biol.* **1991**, *221,* 583-601.

75. Vitali, J.; Martin, P. D.; Malkowski, M. G.; Robertson, W. D.; Lazar, J. B.; Winant, R. C.; Johnson, P. H.; Edwards, B. F. The structure of a complex of bovine alpha-thrombin and recombinant hirudin at 2.8-A resolution. *J. Biol. Chem.* **1992**, *267,* 17670-17678.

76. Vitali, J.; Martin, P. D.; Malkowski, M. G.; Olsen, C. M.; Johnson, P. H.; Edwards, B. F. Structure of a bovine thrombin-hirudin51-65 complex determined by a combination of molecular replacement and graphics. Incorporation of known structural information in molecular replacement. *Acta Crystallogr. D Biol. Crystallogr.* **1996**, *52,* 453-464.

77. Betz, A.; Hofsteenge, J.; Stone, S. R. Interaction of the N-terminal region of hirudin with the active-site cleft of thrombin. *Biochemistry* **1992**, *31,* 4557-4562.

78. Braun, P. J.; Dennis, S.; Hofsteenge, J.; Stone, S. R. Use of site-directed mutagenesis to investigate the basis for the specificity of hirudin. *Biochemistry* **1988**, *27,* 6517-6522.

79. Szyperski, T.; Guntert, P.; Stone, S. R.; Wuthrich, K. Nuclear magnetic resonance solution structure of hirudin(1-51) and comparison with corresponding three-dimensional structures determined using the complete 65-residue hirudin polypeptide chain. *J. Mol. Biol.* **1992**, *228,* 1193-1205.

80. Szyperski, T.; Antuch, W.; Schick, M.; Betz, A.; Stone, S. R.; Wuthrich, K. Transient hydrogen bonds identified on the surface of the NMR solution structure of Hirudin. *Biochemistry* **1994**, *33,* 9303-9310.

81. Jackman, M. P.; Parry, M. A.; Hofsteenge, J.; Stone, S. R. Intrinsic fluorescence changes and rapid kinetics of the reaction of thrombin with hirudin. *J. Biol. Chem.* **1992**, *267,* 15375-15383.

82. Stone, S. R.; Hofsteenge, J. Kinetics of the inhibition of thrombin by hirudin. *Biochemistry* **1986**, *25,* 4622-4628.

83. Padmanabhan, K.; Padmanabhan, K. P.; Ferrara, J. D.; Sadler, J. E.; Tulinsky, A. The structure of alpha-thrombin inhibited by a 15-mer single-stranded DNA aptamer. *J. Biol. Chem.* **1993**, *268,* 17651-17654.

84. Long, S. B.; Long, M. B.; White, R. R.; Sullenger, B. A. Crystal structure of an RNA aptamer bound to thrombin. *RNA* **2008**, *14,* 2504-2512.

85. Lima, L. M.; Becker, C. F.; Giesel, G. M.; Marques, A. F.; Cargnelutti, M. T.; de Oliveira Neto, M.; Queiroz Monteiro, R.; Verli, H.; Polikarpov, I. Structural and thermodynamic analysis of thrombin:suramin interaction in solution and crystal phases. *Biochim. Biophys. Acta* **2009**, *1794*, 873-881.

86. Dementiev, A.; Petitou, M.; Herbert, J. M.; Gettins, P. G. The ternary complex of antithrombin-anhydrothrombin-heparin reveals the basis of inhibitor specificity. *Nat. Struct. Mol. Biol.* **2004**, *11*, 863-867.

87. Li, W.; Johnson, D. J.; Esmon, C. T.; Huntington, J. A. Structure of the antithrombin-thrombin-heparin ternary complex reveals the antithrombotic mechanism of heparin. *Nat. Struct. Mol. Biol.* **2004**, *11*, 857-862.

88. Kulahin, N.; Kiselyov, V.; Kochoyan, A.; Kristensen, O.; Kastrup, J. S.; Berezin, V.; Bock, E.; Gajhede, M. Dimerization effect of sucrose octasulfate on rat FGF1. *Acta Crystallogr. Sect. F. Struct. Biol. Cryst. Commun.* **2008**, *64*, 448-452.

89. Hung, K. W.; Kumar, T. K.; Kathir, K. M.; Xu, P.; Ni, F.; Ji, H. H.; Chen, M. C.; Yang, C. C.; Lin, F. P.; Chiu, I. M.; Yu, C. Solution structure of the ligand binding domain of the fibroblast growth factor receptor: role of heparin in the activation of the receptor. *Biochemistry* **2005**, *44*, 15787-15798.

90. Yeh, B. K.; Eliseenkova, A. V.; Plotnikov, A. N.; Green, D.; Pinnell, J.; Polat, T.; Gritli-Linde, A.; Linhardt, R. J.; Mohammadi, M. Structural basis for activation of fibroblast growth factor signaling by sucrose octasulfate. *Mol. Cell. Biol.* **2002**, *22*, 7184-7192.

91. Zhu, X.; Hsu, B. T.; Rees, D. C. Structural studies of the binding of the anti-ulcer drug sucrose octasulfate to acidic fibroblast growth factor. *Structure* **1993**, *1*, 27-34.

92. Wall, D.; Douglas, S.; Ferro, V.; Cowden, W.; Parish, C. Characterisation of the anticoagulant properties of a range of structurally diverse sulfated oligosaccharides. *Thromb. Res.* **2001**, *103*, 325-335.

93. Orthner, C. L.; Kosow, D. P. Evidence that human alpha-thrombin is a monovalent cation-activated enzyme. *Arch. Biochem. Biophys.* **1980**, *202*, 63-75.

94. Villanueva, G. B.; Perret, V. Effects of sodium and lithium salts on the conformation of human alpha-thrombin. *Thromb. Res.* **1983**, *29*, 489-498.

95. Ayala, Y.; Di Cera, E. Molecular recognition by thrombin. Role of the slow-->fast transition, site-specific ion binding energetics and thermodynamic mapping of structural components. *J. Mol. Biol.* **1994**, *235*, 733-746.

96. De Filippis, V.; De Dea, E.; Lucatello, F.; Frasson, R. Effect of Na+ binding on the conformation, stability and molecular recognition properties of thrombin. *Biochem. J.* **2005**, *390*, 485-492.

97. Guinto, E. R.; Vindigni, A.; Ayala, Y. M.; Dang, Q. D.; Di Cera, E. Identification of residues linked to the slow-->fast transition of thrombin. *Proc. Natl. Acad. Sci. U. S. A.* **1995**, *92*, 11185-11189.

98. Huntington, J. A. How Na+ activates thrombin--a review of the functional and structural data. *Biol. Chem.* **2008**, *389*, 1025-1035.

99. Gianni, S.; Ivarsson, Y.; Bah, A.; Bush-Pelc, L. A.; Di Cera, E. Mechanism of Na(+) binding to thrombin resolved by ultra-rapid kinetics. *Biophys. Chem.* **2007**, *131*, 111-114.

100. Monien, B. H.; Henry, B. L.; Raghuraman, A.; Hindle, M.; Desai, U. R. Novel chemo-enzymatic oligomers of cinnamic acids as direct and indirect inhibitors of coagulation proteinases. *Bioorg. Med. Chem.* **2006**, *14*, 7988-7998.

101. Henry, B. L.; Connell, J.; Liang, A.; Krishnasamy, C.; Desai, U. R. Interaction of antithrombin with sulfated, low molecular weight lignins: Opportunities for potent, selective modulation of antithrombin function. *J. Biol. Chem.* **2009**, .

102. Henry, B. L.; Monien, B. H.; Bock, P. E.; Desai, U. R. A novel allosteric pathway of thrombin inhibition: Exosite II mediated potent inhibition of thrombin by chemo-enzymatic, sulfated dehydropolymers of 4-hydroxycinnamic acids. *J. Biol. Chem.* **2007**, *282*, 31891-31899.

103. Drenth, J.; Mesters, J. *Principles of protein X-Ray crystallography;* Springer: New York, 2007; , pp 332.

104. McPherson, A. *Introduction to macromolecular crystallography;* Wiley-Liss: Hoboken, N.J., 2003; , pp 237.

105. Royal Society of Chemistry; Hubbard, R. E. *Structure-based drug discovery : an overview;* RSC Publishing: Cambridge, UK, 2006; , pp 261.

106. Iyaguchi, D.; Yao, M.; Watanabe, N.; Tanaka, I.; Toyota, E. Crystallization and preliminary x-ray studies of the unliganded wild-type bovine thrombin. *Protein Pept. Lett.* **2007**, *14*, 923-924.

107. Collaborative Computational Project, Number 4 The CCP4 suite: programs for protein crystallography. *Acta Crystallogr. D Biol. Crystallogr.* **1994**, *50*, 760-763.

108. Matthews, B. W. Solvent content of protein crystals. *J. Mol. Biol.* **1968**, *33*, 491-497.

109. Adams, P. D.; Grosse-Kunstleve, R. W.; Hung, L. W.; Ioerger, T. R.; McCoy, A. J.; Moriarty, N. W.; Read, R. J.; Sacchettini, J. C.; Sauter, N. K.; Terwilliger, T. C. PHENIX: building new software for automated crystallographic structure determination. *Acta Crystallogr. D Biol. Crystallogr.* **2002**, *58*, 1948-1954.

110. Emsley, P.; Cowtan, K. Coot: model-building tools for molecular graphics. *Acta Crystallogr. D Biol. Crystallogr.* **2004**, *60*, 2126-2132.

111. Verghese, J.; Liang, A.; Sidhu, P. P.; Hindle, M.; Zhou, Q.; Desai, U. R. First steps in the direction of synthetic, allosteric, direct inhibitors of thrombin and factor Xa. *Bioorg. Med. Chem. Lett.* **2009**, .

112. Olson, S. T.; Halvorson, H. R.; Bjork, I. Quantitative characterization of the thrombin-heparin interaction. Discrimination between specific and nonspecific binding models. *J. Biol. Chem.* **1991**, *266*, 6342-6352.

113. Fuentes-Prior, P.; Iwanaga, Y.; Huber, R.; Pagila, R.; Rumennik, G.; Seto, M.; Morser, J.; Light, D. R.; Bode, W. Structural basis for the anticoagulant activity of the thrombin-thrombomodulin complex. *Nature* **2000**, *404*, 518-525.

114. Vindigni, A.; Dang, Q. D.; Di Cera, E. Site-specific dissection of substrate recognition by thrombin. *Nat. Biotechnol.* **1997**, *15*, 891-895.

115. Lovell,S.C.; Davis, I.W.; Arendall III, W.B.; de Bakker, P.I.W.; Word, J.M.; Prisant, M.G.; Richardson, J.S.; Richardson, D.C. Structure validation by Cα geometry: φ/ψ and Cβ deviation. *Proteins: Structure, Function & Genetics.* **2002**, 50, 437-450.